Kinetic Analysis of Fcγ Receptor and T Cell Receptor Interacting with Respective Ligands

A Thesis
Presented to
The Academic Faculty

by

Ning Jiang

In Partial Fulfillment
of the Requirement of the Degree
Doctor of Philosophy
in Bioengineering

Georgia Institute of Technology
December 2005

KINETIC ANALYSIS OF FCγ RECEPTOR AND T CELL RECEPTOR INTERACTING WITH RESPECTIVE LIGANDS

Approved by:

Dr. Cheng Zhu, Advisor
School of Biomedical Engineering
Georgia Institute of Technology

Dr. Andres J. Garcia
School of Mechanical Engineering
Georgia Institute of Technology

Dr. Julia E. Babensee
School of Biomedical Engineering
Georgia Institute of Technology

Dr. Hanjoong Jo
School of Biomedical Engineering
Georgia Institute of Technology
School of Medicine
Emory University

Dr. Michael L. Dustin
School of Medicine
New York University

Dr. P. Anton van der Merwe
School of Pathology
University of Oxford

Date Approved: Nov 28, 2005

ACKNOWLEDGEMENTS

My heartfelt gratitude and appreciation goes to my advisor Dr. Cheng Zhu. I thank him for his invaluable support, his wisdom on the presented project, and his encouragement during my school years at Georgia Tech. I would like to thank Drs. Julia E. Babensee, Michael L. Dustin, Andres J. Garcia, Hanjoong Jo, P. Anton van der Merwe as thesis committee members, for their helpful suggestions and comments during my thesis work.

I would like to thank Dr. Periasamy Selvaraj for his suggestions, comments and generous supply of reagents on the work of Fc receptor. I would also like to thank Dr. Brian Evavold and Dr. Suryaprakash Sambhara for their suggestions on the work of T cell receptor. I especially would like to thank Dr. Julie Plowden for her continuous supply of spleen of F5 TCR transgenic mice during my thesis work.

Pursuing my Ph.D program at the School of Bioengineering, Georgia Institute of Technology, has been a valuable learning experience. It has been my pleasure to work with all my colleagues and friends in my lab. Especially, I would like to thank Dr. Yan Zhang for his help in some of the T cell receptor experiments and Mr. Fang Kong for his help in some of the data analysis. I would also like to thank Ms. Fang Zhang for sharing micropipette instrument.

Special thanks go to student health center of Georgia Institute of Technology for their blood draw and NIH tetramer facility in Emory University for supplying F5 pMHC monoers and tetramers.

Finally, I would like to thank my husband, my parents and my grandmother for their support and believe during the years. Especially my father, Dr. Zonglai Jiang, influenced me when I was little to pursue Ph.D. in life science.

TABLE OF CONTENTS

LIST OF TABLES

LIST OF FIGURES

SUMMARY

Low affinity Fcγ receptor III (FcγRIII, CD16) triggers a variety of cellular events upon binding to the Fc portion of IgG. A real-time flow cytometry method was developed to measure the affinity and kinetics of such low affinity receptor/ligand interactions, which was shown as an easily operated yet powerful tool. Results revealed an unusual temperature dependence of reverse rate of CD16a^{TM} dissociating from IgG. Except for a few studies using mammalian cell CD16s, most kinetics analyses use purified aglycosylated extracellular portion of the molecules, making it impossible to assess the importance of the receptor anchor and glycosylation on ligand binding. We used a micropipette adhesion frequency assay to demonstrate that the anchor length affects the forward rate and affinity of CD16s for IgG in a species specific manner, most likely through conformational changes. Receptor glycosylation dramatically reduced ligand binding by 100 folds.

T cell receptor (TCR) is arguably the most important receptor in the adaptive human immune system. Together with coreceptor CD4 or CD8, TCR can discriminate different antigen peptides complexed with major histocompatibility complex (MHC) molecule (pMHC), which differ by as few as only one amino acid, and trigger different T cell responses. When T cell signaling was suppressed, TCR had similar affinity and kinetics for agonist and antagonist pMHC whose binding to CD8 was undetectable. TCR on activated T cell had a higher affinity for pMHCs, suggesting that TCRs organize themselves differently on activated T cells than on naïve T cells. In the absence of inhibitors for signaling, TCR binds agonist pMHC with several orders of magnitude higher affinity than antagonist pMHC. In addition, engagement of TCR by pMHC signals an upregulation of CD8 binding to pMHC, which is much stronger than the TCR-pMHC binding. The transition from weak TCR binding to the strong CD8 binding takes place around 0.75 second after TCR in contact with pMHC and can be reduced by several inhibitors of tyrosine and lipid phosphorylation, membrane rafts, and actin cytoskeleton. These results provide new insights to understanding T cell discrimination.

CHAPTER I

SPECIFIC AIMS

Low affinity Fcγ receptor III (FcγRIII, CD16) and T cell receptor (TCR) are two important receptors in the human immune system. Upon binding to the Fc portion of an IgG in an immune complex, FcγRIIIs trigger different immune responses due to different cell types on which they are expressed. By comparison, TCR recognizes peptide ligands that associated with major histocompatibility complex (MHC) molecule (pMHC). For a given TCR, the pMHC ligands may act as agonist, partial agonist, antagonist and null based on their ability to induce T cell activation. Although differing in only a few amino acids, FcγRIII isoforms bind to IgG with distinct kinetic rates and affinities. In contrast to FcγRIII that binds to a conserved ligand (Fc portion of IgG), TCR together with its coreceptor, CD8, can discriminate peptides on an antigen presenting cell (APC) differing as few as only one amino acid to result in different outcomes for T cell activation. In this thesis, two aspects of the structure-function relationship of FcγRIII-IgG binding was characterized and the kinetics/affinities bases of TCR antigenic peptide discrimination were explored. Specifically, the following aims were pursued.

I. To measure ligand-binding properties of Fcγ receptor III in real-time flow cytometry.
II. To quantify the effects of membrane anchor and glycosylation of Fcγ receptor III on ligand binding affinity and kinetics.
III. To dissect signaling independent TCR-pMHC binding kinetics.
IV. To investigate TCR-triggered signaling-dependent rapid transition to CD8-mediated strong adhesion.

Data generated from this thesis has provided new insights to understanding T cell discrimination.

CHAPTER II

INTRODUCTION

CD16 is a low affinity Fcγ receptor compared to Fcγ receptor I (CD64) and has an even lower affinity to soluble IgG. Several groups have studied the affinity and kinetics of different FcγRIII isoforms using different methods, surface plasmon resonance (SPR, 3D), competitive inhibition assay (CI, 3D), micropipette (MP, 3D), and fluorescent recovery after photobleach method (FRAP, 2D). Different methods utilize different forms of receptors, for example, aglycosylated extracellular portion of a protein in SPR and cell expressed molecules in other three assays. Different methods also has their capability in estimate kinetics parameters, for example, CI can only estimated affinity where other three assays can report affinity as well as kinetics information. Therefore, developing a 3D method that will generate both the affinity and kinetics information for a specific receptor ligand interaction is in need. In specific aim I, a real-time flow cytometry method for measuring affinity and kinetics of CD16 molecules interacting with IgG was developed. Two protocols were developed, association and dissociation, and their application on $CD16a^{TM}$, $CD16b^{NA2}$ were compared. Real-time flow cytometry was also used to study temperature effect on receptor/ligand binding. Results show that real-time flow cytometry is an easy operated yet powerful protocol in studying low affinity receptor/ligand binding. The affinity and kinetics parameters we acquired are in good agreement with other measurements.

As discussed above, most published data regarding CD16 ligand binding measured in 3D neglect the effect of protein anchor and glycosylation. Previously it has been shown in micropipette assay that cell expressed CD16s with different membrane anchors bind ligand with different affinities regardless of the same extracellular sequence. Molecules with different anchors may have different diffusion rate on cell membrane, which may influence kinetic measurement. Therefore, to compare the anchor effect in a cleaner background, we now show that soluble CD16s (sCD16) isotypes with different anchor truncation of bind to human IgG1 (hIgG1) with different affinity and they are correlated with anchoring length in specific aim II. This trend is inversed when the ligand

is changed from hIgG1 to mouse IgG2a (mIgG2a). Resulted data suggest a conformational change on receptor anchor, which is distal to ligand binding epitope, could affect ligand binding and this effect varied with different ligand used. Effect of receptor glycosylation was also studied by comparing affinities of glycosylated CHO CD16 and aglycosylated CHO CD16 isotypes (aglycosylated receptor was generated by supplementing culture medium with tunicamycin to block the synthesis of N-glycosylation) binding to hIgG1. Results show that receptor glycosylation will dramatically inhibit ligand binding by 100 folds suggesting sugar moieties close to ligand binding pocket will destabilize ligand binding and resulted a much smaller affinity compared to aglycosylated receptor.

TCR/pMHC interaction is another type of weak adhesion. Their affinity and kinetics measurement were impossible until the merge of SPR. In SPR measurement, it is required that either purified receptor or ligand was immobilized on sensor chip. However, experiments have shown that activated T cells react to pMHC better than naïve T cells. This difference could result from that TCRs organize them differently on activated T cells than naïve T cells. Micropipette adhesion assay using receptors reside in their native environment and it allows us explore this difference. In specific aim III, TCR on both activated T cells and naïve T cells interacting with four different pMHC were tested. Their affinity and kinetics were compared. Results show that TCR on activated T cell has a higher affinity toward pMHC. Though trigger different biological out comes, agonist pMHC and antagonist pMHC have similar affinity and kinetics.

Upon engagement to pMHC, TCR recognize different antigenic peptides that incorporated to MHC and generate distinct signal. Together with its coreceptor and other accessory molecules, they will orchestrate different response to antigen. Over the past several years, significant advances have been made in elucidating the molecular details of signal cascades upon TCR activation. Recent discovery of immunological synapse and applications of different fluorescent microscopic technology have brought us colorful and live pictures of what is happening on the T cell/APC contact. However, due to the tempera resolution, event that happens in the first several seconds after T cell in contact with an APC is still not well defined. In specific aim IV, we use micropipette adhesion assay to explore the initial contact of a T cell and a pMHC decorated RBC. In

physiological condition, results show that T cell will develop aggravated adhesion towards agonist-MHC on RBC but not other pMHCs. This adhesion is mediated by TCR-CD8/pMHC only and is independent of other molecules. We further show that, this change in adhesion mode happens around 0.75 second after TCR in contact with pMHC and can be completely blocked by CD8 blocking antibody and can be reduced by inhibiting protein tyrosine kinase (PTK) activation and disrupting actin polymerization.

CHAPTER III

BACKGROUND

Cell-cell interaction is a very important step in many biological processes, including embryo development, wound healing, immune response and many other aspects of maintaining a healthy living being. This interaction is mostly initiated by a group of specialized proteins on the cell membrane, called receptors, interact with another group of proteins, called ligands. Ligands can be either soluble proteins secreted by other cells or proteins on another cell membrane. Like other proteins, each receptor and its ligand have a unique structure that dictates their recognition between them to be very specific. Once a receptor recognizes its ligand from a pool of proteins, it usually generates a signal to alert cell to response to the outside environment. Take human immune system as an example; many cells have the ability to launch a killing sequence based on the signals sent by their surface receptors. In the innate immune system, ligand binding to Toll-like receptors (TLR) on macrophages and dendritic cells can direct host the cell to engulf pathogens. Ligand binding to Fcγ receptors (FcγR) on neutrophils can coordinate the cell to phagocytose immune complexes (IC). In the adaptive immune system, ligation of T cell receptors (TCR) on cytotoxic T cell with its ligand enables T cell to directly secrete toxic molecules to its target cell. In this thesis, the kinetics of FcγRIII and TCR binding to their respective ligands were analyzed.

Fcγ Receptors

Fc receptors (FcRs) recognize the Fc portion of antibodies either in soluble state or as part of an immune complex. Five different types of FcRs recognize different immunoglobulins (Ig) [1-3]. Fcγ receptors (FcγRs) recognize Fc portion of the IgG. They are expressed on almost all the hematopoietic cells. Multivalent binding of FcγR to IgG in immune complex or opsonized particles triggers different cellular reactions depending on the Fcγ receptors class and isotype as well as the cells on which they expressed. There

are three subclasses of FcγRs, Fcγ receptor I (FcγRI, CD64), Fcγ receptor II (FcγRII, CD32), and Fcγ receptor III (FcγRIII, CD16). CD64 is a high affinity Fcγ receptor ($K_A \sim 10^{-9}M^{-1}$), whereas CD32 and CD16 are low affinity Fcγ receptors ($K_A \sim 10^{-6}M^{-1}$) [4, 5]. For the phagocyte, the activation of FcγRs can trigger a spectrum of integrated cell programs including oxidative burst, secretion of intracellular granule contents, cellular cytotoxicity, gene activation with new protein synthesis, and release of various cytokines [6]. The FcγRs on B lymphocytes can provide negative regulatory signals, and in the context of autoimmunity, modulation of B cell hyperactivity stands out as a potential therapeutic target [7]. FcγRs are also found on some γ/δ T cells and are transiently expressed during thymic development [7]. FcγRs on natural killer (NK) cells mediate antibody-dependent cellular cytotoxicity [8].

Structures and Functions of FcγRIII

CD16 is encoded by two genes, gene A and gene B, which give two different protein products, CD16a and CD16b. CD16a is expressed on macrophages, mast cells, and natural killer cells as a transmembrane receptor. However, it does not contain any signal motif. As compensation, it associates with a hemo- or hetero-dimeric γ and/or ζ chains, which contain immunoreceptor tyrosine-based activation motif (ITAM) [9, 10] that is rich in tyrosine phosphorylation sites in its cytoplasma domaim. The absence of γ and ζ leads to the loss of surface expression of CD16a [11]. Present exclusively on neutrophils, CD16b is the only Fc receptor anchored by a glycosyl-phosphatidylinositol (GPI) linker to the plasma membrane. CD16b has two alleles, $CD16b^{NA1}$ and $CD16b^{NA2}$. Despite the lack of a signaling component, CD16b plays an active role in triggering Ca^{2+} mobilization and neutrophil degranulation [12, 13]. In addition, in conjunction with FcγRIIa, FcγRIIIb activates phagocytosis, degranulation, and oxidative burst, which lead to the clearance of opsonized pathogens by neutrophils. Recently, a soluble form of FcγRIIIb was reported to activate the complement receptor CR3-dependent inflammatory process [14].

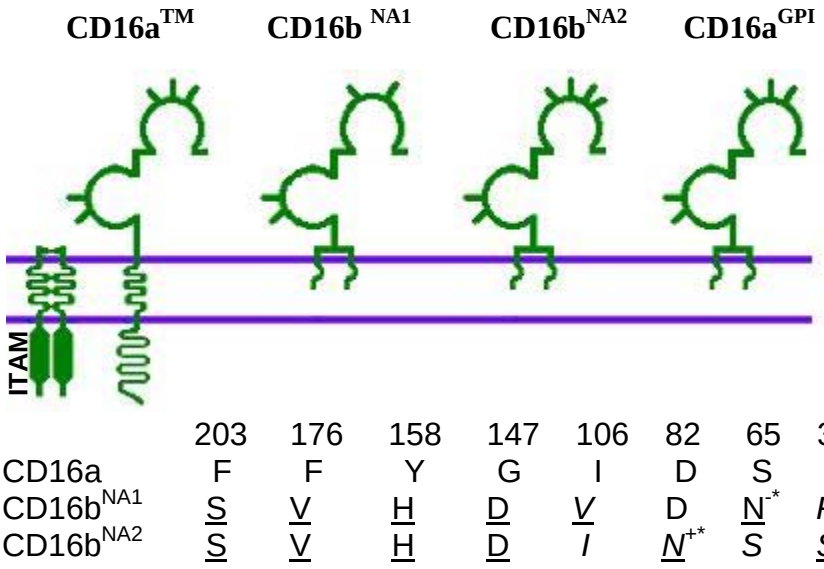

Figure 3-1. Structure differences within CD16a^{WT}, CD16b^{NA1}and CD16b^{NA2}.

Figure 3-1 shows one mutant CD16a^{GPI} that has a GPI anchor instead of a transmembrane domain and the three different wild types CD16 molecules, CD16a^{TM} that is associated with γ and ζ chains, CD16b^{NA1} and CD16b^{NA2} that have GPI anchors and do not associate with γ and ζ chains. All these CD16 molecules are composed of two Ig-like globules with the glycosylation sites shown as sticks. The extracellular domain amino acids that differ among the three CD16 isoforms are listed. Compared to those on CD16a, the different amino acids on CD16b are underlined, while the differences between the two CD16b alleles are shown in italic. Early experiments using fusion proteins, single-residue mutation and antibody mapping, show that the ligand binding site of CD16 is located at the second, membrane-proximal, Ig-like globule [15-18]. In addition, studies suggested mutants with amino acids Q143-Y150 replaced by alanine one by one greatly decreased IgG binding, except for mutant D147A, which increased the binding by more than twofold [16].

The first crystal structure of FcγRIIIb was solved in 2000 [19]. An acute interdomain hinge angle of approximately 50° was observed. The putative Fc binding region of the receptor carries a net positive charge complementary to the negative-charged receptor binding regions on Fc. Later, crystal structures of FcγRIIIb in complex with human IgG Fc were published by two groups independently [20, 21]. Although the crystals obtained by the two groups have different space group symmetried, the

superposition of two structures resulted in a root mean square (r.m.s.) deviation of 0.5 Å for all Cα atoms. Both groups found that sFcγRIIIb has the characteristic heart-shaped domain arrangement described for sFcγRIIb and other sFcRs. Compared with the stand alone structure, the sFcγRIIIb molecule displays an opening of its interdomain angle for 10° where it is in complex with hIgG1 Fc. The horseshoe shaped hFc1 molecule also opens. The contact interface between sFcγRIIIb and hFc1 consists mainly of van der Waals interaction on Cγ2-A (Cγ2-B in P. Sun's paper) of Fc and hydrogen bonds and salt bridges on Cγ2-B (Cγ2-A in P. Sun's paper) of Fc. Such binding breaks down the symmetry of the Fc, creating an asymmetric interface whereby the identical residues from Hinge-A and Hinge-B interact with different, unrelated surfaces of the receptor.

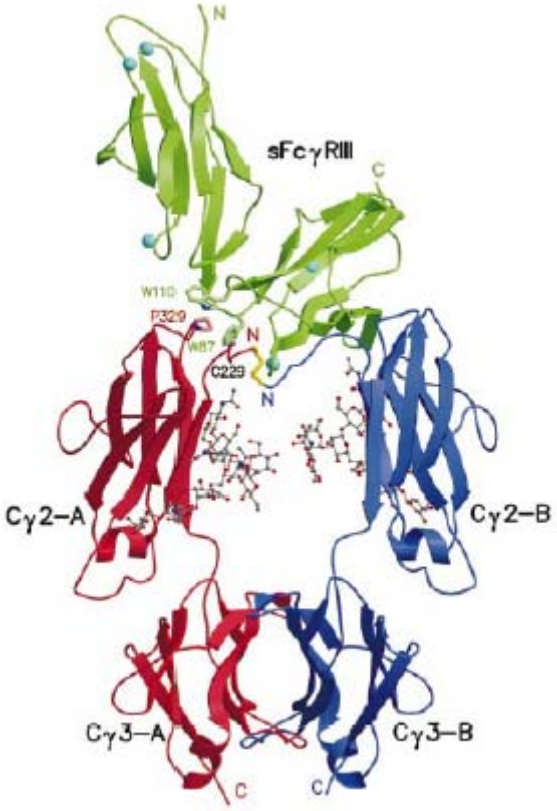

Figure 3-2. The overall structure of the sFcγRIII-hFc1 complex (adapted from Sondermann P., et al, Nature, 2000).

In order to characterize the IgG binding of FcγRIIIs, aglycosylated soluble CD16s produced by E. coli. have used to measure their affinities and kinetics using surface plasma resonance (SPR, for example, with the commonly used instrument BIAcore®).

SPR technique measures the mass concentration of proteins (refractive index) in close proximity to a specially prepared surface. It requires immobilization of one of the interacting molecules onto a sensor surface allowing the other binder molecules to flow over it; in this way, the real-time binding is detected. Proteins synthesized by E. coli. do not have sugar moiety attached to their amino residues due to the lack of post-translational enzymes. However, Jeffrey C. Edberg and colleagues have shown that CD16a molecules expressed on NK cell and monocyte have different affinities to their ligand due to differential cell type-specific glycosylation, although they have identical protein cores. These results indicate that natural glycoforms of FcγRIIIa (cell type-specific glycosylation variants) bind ligand differently, conferring a lower affinity on monocyte/macrophage FcγRIIIa, which makes the receptor ideal for initial immune complex capture and sensitive to moderate changes in serum IgG levels [22]. More recent mutagenesis results have shown that monomeric IgG bound to N163Q transfectants with higher affinity than to other transfectantas, suggesting that (N)-linked glycosylation in asparagines 163, which is located in ligand binding pocket, influences the affinity of CD16 for its ligand. In addition, preincubatyion of wild-type CD16 transfected cells with Tunicamycin (an inhibitor of N-glycosylation) resulted in an increased binding of monomeric IgG whereas N163Q-CD16-transfected cells remained unaffected. Therefore, glycosylation in N163 is a mechanism of regulation for affinity of FcγRIII for its ligand IgG. [23]. The importance of post-translation process is also observed in other molecular system, such as CD8, where non-sialylated glycoforms are present in immature thymocytes but are virtually absent in mature thymocytes. This glycosylation difference is linked to ligand binding affinity difference between CD8 on mature and immature thymocytes [24].

Chesla et al. have previously reported kinetic rates and affinity on human CD16s expressed on CHO cells, CD16a-TM, $CD16b^{NA1}$, $CD16b^{NA2}$, and $CD16a^{GPI}$ (figure 3-1) [25]. The results showed that anchor influenced kinetics and affinity. Compared with $CD16a^{TM}$, $CD16a^{GPI}$ bound faster with higher affinity to human and rabbit IgGs but slower with lower affinity to murine IgG2a. It was suggested that the membrane anchor influenced ligand binding of CD16 by conformational change. However, the anchor effect has not been well appreciated in receptor-ligand binding partly because affinity and

kinetics measurement of such a weak interaction, like FcγRIII, is not available until recent application of the SPR technology. Almost all SPR measurements used molecules that are produced by E. Coli, which can be used to produce milligram quantity to satisfy the instrumentation requirement. However, molecules that generated this way only contain receptor's extracellular domain, which has been a limitation in exploring the anchor effect on ligand binding kinetics of a molecule. Another reason of slow progress in this area is the lacks of molecular structure of transmembrane and GPI anchors. Again, almost all X-ray crystal structures of membrane proteins only contain the extracellular domain because it is very difficult to purify milligram quantity of membrane protein from mammalian cells and it is even harder to crystallize proteins with their nature anchor. However, anchoring effect in ligand binding has been seen on another receptor. Thy-1 protein, a member of the Ig superfamily, is bound to the cell membrane by a GPI anchor. It has been shown that following anchor cleavage by phospholipase C, the reactivity of the solubilized Thy-1 with several mAbs is lost, and its reactivity with polyclonal anti-Thy-1 Abs is markedly decreased. These results suggest that the marked decrease in Thy-1 immunoreactivity following delipidation is due to conformational changes in the Thy-1 protein after anchor truncation [26].

T Cells

T lymphocytes are one of the most important cells in the human immune system responsible for the adaptive immune response. They originate from bone marrow and mature in the thymus, and hence acquire the name T cell. When T cells mature, they differentiate into two distinct lineages that can be distinguished by their expression of CD4 or CD8 membrane molecules. Helper T (T_H) cells are usually identified by the presence of the cell-surface molecules CD4. Cytotoxic T (T_C) cells express CD8 molecules. As their name indicated, T_H cells help B cells and other T cells to multiply into large clones and carry out their role in the immune response. T_H cells enhance B cell antibody production, macrophage activation, and T_C cell differentiation. T_C cells are responsible for killing virus-infected cells, transplanted tissue, and cancer cells. T_C cells kill a target cell either by latching onto the target cell's surface and injecting a membrane-disrupting agent perforin or by a mechanism involving the engagement of the

Fas cell-surface molecules, which leads to apoptosis of the target cell. The present project focuses on T_C cells.

TCR, MHC Molecules and Co-receptors

Unlike B cells which use cell bound antibody (B cell antigen receptor, BCR) to recognize an antigen in its intact protein state, T cells can recognize an antigen only after the antigen has been broken down from protein to a small peptide (8-15 amino acid in length) and presented by a major histocompatibility complex (MHC) molecule. Virtually every cell in the body expresses MHC molecules. Three MHC genes encode three classes of molecules that are essential for T cell functions. Class I region genes encode MHC class I (MHC-I) molecules, which are expressed on the surface of almost all nucleated cells and which present peptide antigen to T_C cells. Class II region genes encode MHC class II (MHC-II) molecules, which are expressed primarily on antigen-presenting cells (APCs; macrophages, dendritic cells, B cells, Langerhans cells of the skin, and human endothelial cells) and which present peptide antigen to T_H cells. Class III (MHC-III) region genes encode class III molecules, the complement proteins, and other proteins unrelated to MHC class I and class II molecules [27]. MHC-I molecules are the focus of the present project.

The antigenic peptide presented by MHC molecules is recognized by TCR. TCR is a heterodimeric molecule composed of either α and β or γ and δ chains. These two chains are held together by a disulfide bond; they are built with the Ig fold as their backbone structure. TCR is also non-covalently associated with two ζ chains and CD3 which contains ε, δ, γ and η chains [28]. Similar to FcγR, the absence of CD3 and ζ chains leads to the loss of surface expression of TCR [29]. CD3 and ζ chains contain ITAM, which will transmit signals after TCR ligantion with antigen. This requires TCR/peptide-MHC (pMHC) interaction as well as co-receptors, CD4 or CD8.

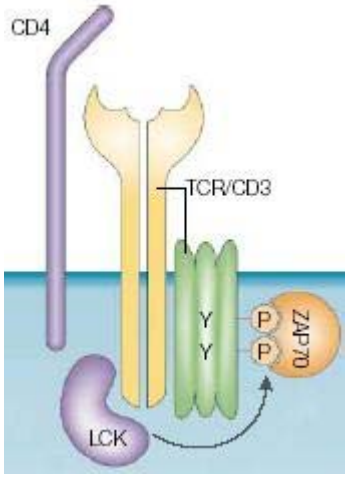

Figure 3-3. Schematic drawing of early signaling events in T cells (adapted from Okkenhaug et al., Nat. Rev. Immunol., 2003).

Another molecule that also recognizes class I MHC is the coreceptor CD8 that is expressed on the T_C cell surface as either an αα homodimer or an αβ heterodimer. Either α or β chain of CD8 consists of four discrete functional domains that can be related to the primary sequence as follows: the Ig-like extracellular domain, the membrane proximal stalk (hinge) region, the transmembrane domain and the cytoplasmic domain. Recently available crystal structure shows that the Ig-like domain is involved in the binding to pMHC [30, 31]. Fewer studies have focused on the interaction between coreceptors and pMHC than those between TCR and pMHC binding. Significant discrepancies exist among the in vitro data generated in different studies using soluble molecules [32].

There are more than half a dozen crystal structures of αβ TCRs complexed to their cognate antigenic pMHC ligands. Those include both class I [33-36] and class II complexes [37, 38]. These data in general support a common docking mode of TCRs towards the pMHC complex [39-42]. The overall topology of the docking mode is such that the Vα domain of the TCR is closest to the N-terminal residues of the antigenic peptide whereas the Vβ domain of the TCR is closest to the C-terminal segment of the peptide. This conservation also mandates that the TCR Vβ domain contacts the MHC α1 domain, while the TCR Vα domain interacts with the other domain of the MHC antigen-resenting platform (α2 for MHC-I or β1 for MHC-II).

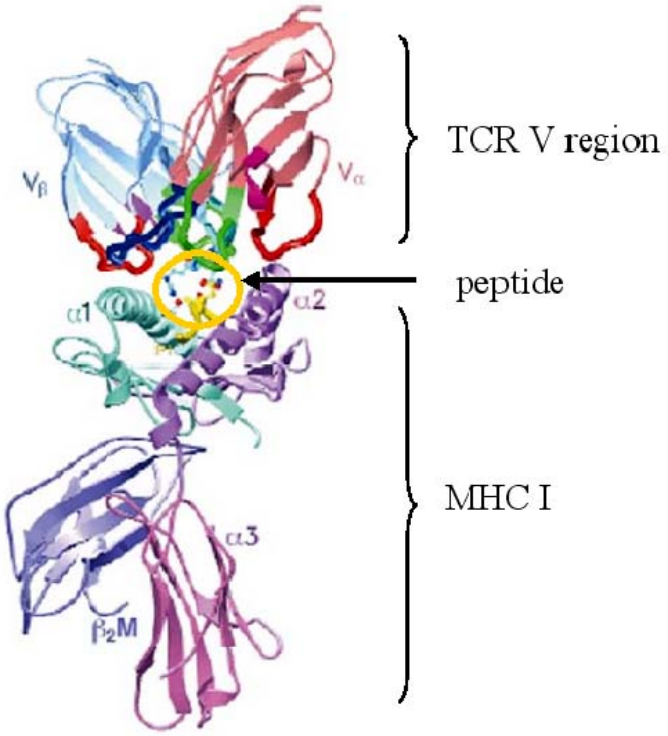

Figure 3-4. Structure of the BM3.3 TCR–pBM1–H-2K^b complex (adapted from Reisei et al., Nat Immunol, 2000).

How TCR and the co-receptor coordinate this bidentate interaction and subsequent downstream signaling is of particular interest. Structures of the interacting ectodomains of both CD8 [43] and CD4 [44-46] are known. In addition, the binary complex structures of the CD8αα homodimeric Ig-like domains bound to pMHC-I for human and mouse have been defined [30, 31]. Very recently the crystal structure of a CD4 two domain (D1D2) fragment complexed to a pMHC-II has also been determined [47]. Unexpectedly, the way CD4 binds to pMHC-II is quite different from that of CD8 to pMHC-I. CD8αα binds to the pMHC-I molecule in a manner analogous to the way in which an antibody interacts with antigen using its CDR-like loops. In fact, in the CD8αα–pMHC-I interaction, all six CDR-like loops from the two CD8 monomers clamp down onto the protruding CD loop of the MHC-I molecule's α_3 domain. Additional contacts with MHC-I α_3 itself, β_2-microglobulin (β_2M) and, to a small extent, MHC-I α_2 have been defined [31]. By contrast, CD4 uses its N-terminal domain's "top corner" to reach the domain junction between MHC-II α_2 and β_2 domains without directly

contacting the corresponding CD loop on the β_2M. The CD4 binding does not seem to cause noticeable conformational change of pMHC-II, as if the α_2 and β_2 domains of MHCII were pre-configured for CD4 binding. This situation contrasts with that of CD8–pMHC-I ligation, which is associated with a swing of the α_3 domain of pMHC-I upon CD8 binding [30, 31]. To date, the biological significance of the α_3 domain movement is unresolved.

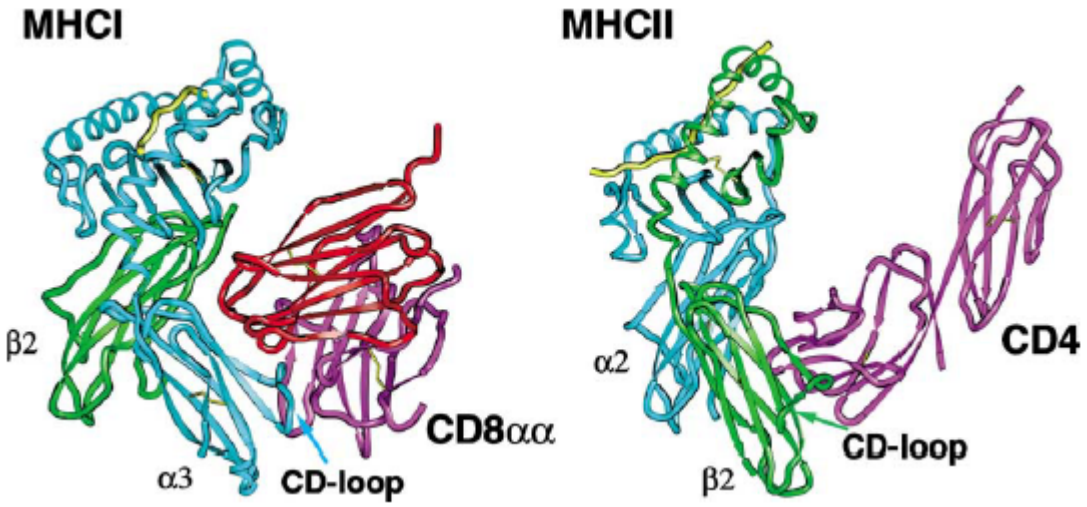

Figure 3-5. Comparative ribbon drawings of the complex structures between an MHC molecule and its respective co-receptor. Left, the CD8αα homodimer (in red and magenta) complexed to murine MHC-I H-2K^b (cyan for α chain and green for β2 chain) is shown. Right, the CD4 first two domain (in magenta) is shown complexed to murine MHCII I-A^k (cyan for α chain and green for β chain). Note how the CD8 dimer clamps down on the CD loop of MHC's α3 domain, whereas CD4 uses its top corner to reach the domain junction between MHC's α2 and β2 (adapted from Wang, J.H., et al., Proc Natl Acad Sci U S A, 2001).

Signal Transduction in TCR

TCR does not have signaling motif itself and has to associate with ITAM containing proteins, such as CD3 and ζ chains. TCR initiates signaling by recruiting and activating protein tyrosine kinases (PTK) of the Src, Syk and Tec families [48-50]. Immunoreceptor tyrosine-based activation motifs (ITAM) of the signal transducing antigen receptor subunits (CD3 and ζ) are phosphorylated by Src PTK (probably Lck in T cells) thus allowing the Syk family PTK ZAP70 to bind to the ITAM via its tandem Src-homology 2 (SH2) domains. ITAM-bound ZAP70 is then tyrosine phosphorylated and

activated, leading to the phosphorylation of ZAP70 substrates such as the adaptors SLP76 (SH2 domain containing lymphocyte protein of 76,000 MW) and LAT (linker of activated T cells) [50-52]. These adapters form scaffolds to assemble signal tranduction molecules in the correct intracellular location for them to execute their effector function either directly or after allosteric regulation by co-assembled regulatory proteins. Tyrosine phosphorylation of adaptors links antigen receptors to a cascade of signaling pathways during T-cell activation; the key ones are the activation of Ras and Rho-family GTPases, MAPK cascades [53-55], phosphatidylinositol 3 kinase (PI-3 kinase) [56-59], PKCθ [60, 61], and the NF-κB pathway [62-64]. In addition, TCR ligation leads to the phosphorylation and activation of PLC-γ1, which initiates inositolphospholipid (IP) turnover and intracellular free ionized calcium ($[Ca^{2+}]_i$) flux [65-68]. A summation of these effects leads to transcriptional activation of biologically important genes.

Phosphoinositide 3-kinases

Phosphoinositide 3-kinases (PI3Ks) regulate numerous biological processes, including cell growth, differentiation, survival, proliferation, migration and metabolism. Based on structure similarities, the PI3K family can be subdivided into three classes — class I, class II and class III. The class I PI3Ks are subdivided into two groups — the class IA and class IB PI3Ks. The class IA PI3Ks are activated by tyrosine-kinase-associated receptors, including antigen, co-stimulatory and cytokine receptors. The class IB PI3K, PI3Kγ, is activated by G-protein-coupled receptors (GPCRs) — a large family of receptor proteins that includes the chemokine receptors. Little is known about the role of class II and class III PI3Ks in lymphocytes [69, 70]. The class IA PI3Ks are the focus of this thesis.

Class IA PI3Ks are heterodimeric enzymes consisting of a regulatory subunit (p85α, p85β or p85γ) and a catalytic subunit (p110α, p110β or p110δ). Each of the catalytic subunits can associate with all of the regulatory subunits. The function of class I PI3Ks is to phosphorylate the D-3 position of the inositol head group of the phosphatidylinositol-(4,5)-bisphosphate (PtdIns(4,5)P_2) to produce phosphatidylinositol-(3,4,5)-trisphosphate (PtdIns(3,4,5)P_3) at the inner leaflet of the plasma membrane. PtdIns(3,4,5)P_3 binds to numerous intracellular enzymes that contain pleckstrin-

homology domains (PH domains) [71, 72] and reported to occur in response to ligation of several surface molecules involved in T-cell activation and proliferation, including the T-cell receptor [56], CD28 [73], CTLA-4 [74], CD2 [56] and CD4 [57, 75], which modulate the early events in T-cell activation. Use of the pharmacological PI3K inhibitors wortmannin and LY294002, gene knockout and many other methods has identified that PI3K products interact with many different types of signaling products. They are the TEC family of tyrosine kinases which include Itk, Tec and Btk [76, 77], GTPases which include Rac and Rho [78, 79], and perhaps the most important of these is the serine/threonine kinase AKT/PKB, which has an important role in cell proliferation, growth, survival and metabolism in many cell types, and the role of which is conserved through evolution [80-82]. Recently, Harriague et al. used mouse CD4 T cell hybridoma and human peripheral resting CD4 T cells to show that as early as 100 second after placing T cells and APC in contact, Akt was highly enriched at the contact zone. Neither the formation of conjugates between T cells and APCs nor signaling events such as phosphotyrosine accumulation and calcium increase changed substantially when PI3K was inhibited. They also found that PIP_3 accumulated at the T cell-APC synapse as well as in the rest of the T cell plasma membrane [59]. About the same time, Costello et al. used mouse transgenic CD8 naïve T cells, P14 and F5, to show that production of PtdIns(3,4,5)P_3 was dynamically sustained for hours as T cells responded to antigen. In addition, sustained elevation of PtdIns(3,4,5)P_3 was essential for T cell proliferation. They also found that PtdIns(3,4,5)P_3 accumulation in the T cell-APC contact zone as well as at the antipodal pole of the cell. The immunue synapse is thus not the sole site of sustained signal transduction in activated T cells [58].

Mechanism of TCR Triggering

TCR Repertoires Diversity

By gene rearrangement, TCR diversity greatly exceeds Ig diversity. Each T cell expresses only one clone of TCR. Not only can TCR tell self peptides from nonself peptides, but it can also discriminate agonist (strong activating), partial agonist (weak activating), null (nonresponsive) and antagonist (inhibitory) peptides within nonself

peptides [83]. All these four peptides have the same amino acid length and differ as little as only one residual. Furthermore, TCR recognizes an antigenic peptide from a sea of self peptides presented by the same MHC molecules at the same time on the same target cell surface. Studies have shown that as low as few tens of specific peptide-MHCs are enough to fully activate the T cell [84-86]. Exactly how TCR is activated is still a hotly debated issue in immunology.

Models for TCR Antigenic Peptide Recognition

Soon after the TCR was discovered, researchers started to propose models and tried to elucidate the mechanism for TCR antigenic peptide discrimination. These include affinity model [87], conformational change model [88, 89], dimerization or oligomerization model [90, 91], kinetic proof-reading [92] or kinetic discrimination model [93], and kinetic/segregation model [94, 95] etc. Conformational change is commonly seen in enzyme-substrate interaction. But no evidence has been found from crystallographic studies to support the conformational change model for TCR. Dimerization or oligomerization is a common strategy used by numerous growth factor receptors, cytokine receptors and FcγR, but using chemically cross-linked MHC molecules to induce oligomerization of TCR either on cell surface or in solution only provides indirect evidence. In two studies, direct evidence has been reported that TCR also uses dimerization or oligomerization as signaling method. But when Baker and Wiley tried to repeat this experiment, they could not obtain the same results[96]. The affinity model argues that TCR-pMHC binding affinity is the key parameter that regulates the TCR activation. It is hard to envision how a little variation of affinity among the different peptide-MHCs interacting with the same TCR may give rise to a huge variation in cellular responses. Kinetic proof-reading and kinetic discrimination models suggested that kinetics, especially the dissociation rate constant, which differs a lot among variant peptide-MHC interacting with the same TCR, is the key regulator. The kinetic/segregation model further extends the kinetic proof-reading or kinetic discrimination model. It proposes that the segregation induced by kinetic difference between TCR and different peptide-MHC is the determinant for TCR triggering. Recent emerged peptide stability model highlight the interaction between peptide and MHC as an

important factor in determining the outcome of TCR. In this model, partial agonist can be generated through changing peptide affinity for MHC [97]. All these arguments are focused on the affinity and kinetics of TCR binding to peptide-MHC. Therefore, studying the TCR/peptide-MHC/CD8 interaction, especially the 2D kinetics, will provide useful information for the understanding of the mechanism of T cell antigenic peptide discrimination. This is the main approach of the present thesis.

Role of CD8 in T cell activation

Unlike FcγRs which can induce full cell response by its own, the full activation of a T cell cannot be fulfilled by the interaction of TCR with peptide-MHC alone. Other molecular interactions, such as co-receptor CD4 and CD8 binding to MHC, adhesion molecule CD2 binding to its counter receptor CD58 (CD48 in mouse) [94, 98, 99], costimulatory molecules CD28 interacting with CD80/CD86 [100] are actively involved in this process (Figure 3-6).

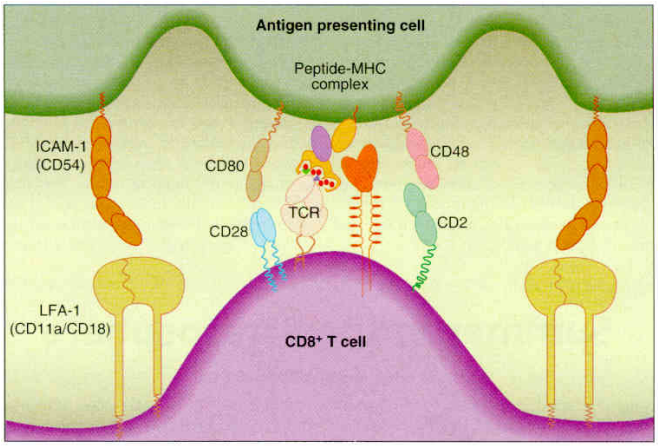

Figure 3-6. TCR and accessory molecules interacting with counterpart ligands on APC in immune synapse. [101]

Kinetics and Affinities of CD8-pMHC Interactions

The binding of CD8aa to pMHC was initially demonstrated by using cell–cell adhesion assays [102-104]. In recent years, SPR has proved to be a reliable method for measuring the affinity and kinetics of very weak protein–protein interactions such as CD8–pMHC and TCR–pMHC [98]. The binding of CD8 to pMHC is extremely weak [Kd = 90–220 μM [105]; 11–40 μM [106]; 22–86 μM [107]; 100 μM [108] and 140-200

μM [109]], with significantly lower affinities than those characterizing TCR–pMHC interactions (1–50 μM at 25°C) [110] or those characterizing typical adhesion molecule interactions (for example, CD2 and CD48, 30–50 μM at 25°C) [98]. However, the most striking feature of the CD8–pMHC interaction is its extremely fast kinetics (dissociation rate constant, $k_{off} \geq 18\ s^{-1}$ [105]) compared with TCR–pMHC interactions (k_{off} ranging from 0.01–0.1 s^{-1} for agonist peptide pMHC [110]). It is so fast that the direct measurement of the association rate constant (k_{on}) is impossible. These extremely fast kinetics have been observed in both the human and mouse CD8–pMHC complex interactions [105]. These results indicate that the affinity of CD8-pMHC interaction is only slightly dependent on species or allele type. The transient nature of the CD8–pMHC interaction supports the notion that T-cell activation involves binding of CD8 and TCR to the same pMHC molecules (with the TCR dominating the interaction).

Cooperativity in pMHC Binding between CD8 and TCR

Experiments involving soluble mouse CD8, TCR and MHC molecules have suggested that CD8 enhances binding of TCR to the pMHC complex through a reduced "off" rate and this effect is independent of haplotype and peptide content. However, using human proteins, Wyer et al. have revealed that the TCR binding and dissociation time-course were independent of the presence of CD8 molecules in the reaction mixture. Based on these observations the authors concluded that there is no cooperativity in CD8 and TCR interactions with their pMHC ligand, i.e., CD8-pMHC interaction does not affect the affinity of the TCR-pMHC interaction, and CD8 and TCR bind the antigen independently. This however does dot exclude the possibility of CD8 involvement in pMHC binding on the cell-surface that can influence the process in a different way.

CD8 Modulation of TCR-pMHC Interaction on Live Cells

Mescher's group has shown that upon the addition of anti-TCR mAb in solution (fluid-phase), where only bivalent cross-linking of the TCR is presumed to occur, CTL are stimulated to undergo CD8-dependent adhesion to class I MHC. CTL binding to irrelevant class I MHC could also be achieved by this TCR cross-linking method and can

be blocked by CD8 antibody too [111]. They further show that this CD8-dependent adhesion of CTL to Class I MHC is sensitive to cytoskeleton disruption agents cytochalasin D and E and colchicines [112]. Furthermore, fluid phase anti-TCR mAb is not a sufficient stimulus to initiate PI hydrolysis or cause and increase in $[Ca^{2+}]_j$, but these events are activated when cells undergo CD8-dependent adhesion to class I MHC [111, 113, 114]. TCR-dependent activation of CD8 requires protein tyrosine phosphorylation, as shown by the ability of herbimycin A and genistein to inhibit triggered adhesion to class I MHC [114]. Recently the same group used wortmannin, a potent PI3 kinase inhibitor, blocks TCR-signaled activation of CD8-mediated adhesion to class I MHC protein [115]. Other groups also found that TCR-ligand interaction on CTL is greatly strengthened by CD8. Using $CD8^+$ and $CD8^-$ CTL clones, Luescher et al. found that monomeric K^d molecules photoaffinity labels better on $CD8^+$ cells than $CD8^-$ cells and the differential binding can be reduced by over 95% in the presence of anti-CD8 antibody. Substitution of K^d Asp 227 with Lys in the soluble ligand resulted in a more than 80% reduction of the TCR labeling on $CD8^+$ cells but had no detectable effect on the labeling of $CD8^-$ cells [116]. Similar results have been obtained using monomeric pMHC as a ligand. Under this condition, Ca^{2+} responses can only be observed in CD8+ cells, not when either the CD8:MHC or CD8:Lck interactions are prevented. This demonstrates that an intact CD8 coreceptor is necessary for effective TCR signaling in response to monomeric peptide-MHC molecules [117].

CHAPTER IV

MATERIALS AND METHODS

Cell

CHO cells transfected to express CD16a^{TM}, CD16a^{GPI}, CD16b^{NA2} and B7-1-CD59, as well as nontransfected CHO cells, were kind gifts of Dr. P. Selvaraj, Emory University School of Medicine. Macrophages from Tap knockout mice and naïve F5 T cells purified from spleen of F5 transgenic mice were kindly provided by Dr. S. Sambhara from CDC. Naïve and activated 2C T cells were provided by Dr. Jonathan Schneck of the Johns Hopkins University. Erythrocytes were isolated from the whole blood of normal healthy volunteers.

Antibodies

The murine monoclonal antibody 214.1 (anti-CD16, capture antibody) was provided by Dr. Selvaraj. mAB 3G8 (anti-CD16, blocking antibody), mAB 8c/6-39 (anti-hIgG1), IgG2a from murine myeloma, and all FITC labeled secondary antibodies were purchased from Sigma-Aldrich (S. Louis, MO). Human IgG1 from myeloma cell culture were provided by Dr. A. Whitty from Biogen. FITC labeled mAB R19-15 (anti-mIgG2a), PE labeled mAB RR3-15 (anti- TCR Vβ 11), PE labeled mAB 145-2C11 (anti-CD3ε chain), and PE labeled mAB 53-6.7 (anti-CD8α (Ly-2)) were purchased from BD Biosciences Pharmingen (San Jose, CA). Purified mAB 5H10 (CD8 blocking antibody) was purchased from Caltag (Burlingame, CA).

Peptide

The nonamer peptides NP68 (ASNENMDAM) (agonist), P4Q (ASNQNMDAM) (partial agonist), P7E (ASNENMEAM) (antagonist), P8T (ASNENMDTM) and HIV gag (SQVTNPANI) (null) were custom synthesized and purified by RP-HPLC.

MHC Monomers and Tetramers

Biotinylated H-2D^{b} monomers and tetramers incorporated with different peptide were provided by NIH Tetramer Facility (Bethesda, MD).

Other Materials

Carboxylated-modified microspheres, diameter 7.75 μm, and fluorescein microbeads standards were purchased from Bangs Laboratories (Fishers, IN). Carbodiimide kit for carboxylated-modified beads was obtained from Polysciences (Warrington, PA). Streptavidin, biotin-X-NHS kit, PP2, genistein, PD98059, BAPTA-AM, latrunculin A, wortmannin were obtained from Calbiochem (La Jolla, CA). Sephadex G-200 was purchased from Pharmacia (Piscataway, NJ). Gel filtration column, gel filtration standard and fraction collector were obtained from Biorad (Hercules, CA). dimethylformamide was purchased from Pierce Biotechnology (Rockford, IL). Essential IgG free BSA, boric acid, phosphatidyl-inositol specific phospholipase C (PIPLC), tunicamycin, cytochalasin D, colchicine, methyl-β-cyclodextrin, and α-cyclodextrin were purchased from Sigma-Aldrich (S. Louis, MO).

Cell Culture

General Culture of CHO Cells

CHO cells were cultured in RPMI with 10% FBS, 2mM L-glutamine, 1mM sodium pyruvate and 1% Penicillin/streptomycin according to standard practices. CD16a^{TM} and B7-1-CD59 transfectant cell lines were supplemented with 400 μg/ml G-418, while CD16a^{GPI}, CD16b^{NA2} transfectant cell lines were supplemented with 400 μg/ml hygromycin B as the selection agent.

Naïve T cell Purification and T cell Activation

F5 Transgenic T cells were purified from spleenocytes using murine T cell CD8 subset column kit (R&D Systems Inc., Minneapolis, MN). A portion of the naïve F5 T cells were than activated in vitro with macrophage which were retrieved from Tap$^{-/-}$

mouse and loaded with specific peptide. The ratio of naïve T cells to macrophages used was in the range 1.5-2.0. Both naïve and activated cells were cultured in complete RPMI media supplemented with 10% FBS, 5 x 10^{-5} M mercaptoethanol and 100U/ml IL-2.

Covalently Couple 214.1 to Microspheres

After washing by 2 x 1 ml carbonate buffer, 0.5 ml of 2.5% suspension of carboxylated microparticles were resuspended phosphate buffer (pH4.5) and washed three times in phosphate buffer. Pellet was resuspended in 0.02 M phosphate buffer, pH 4.5. To the redispersed pellet, carbodiimide solution was added dropwise to reach a concentration of 4% and mixed for 3-4 hours at room temperature. Then the microspheres were washed 3 times in phosphate buffer to get rid of unreacted carbodiimide. Next, 200 – 400 μg of capture antibody 214.1 was added to microspheres and incubated for overnight at room temperature with mixing. Microparticles were collected and supernatant was tested by BCA to estimate the efficiency of coupling. The pellet was resuspended in 0.2 M borate buffer and 50μl of 0.1 M methanolamine was added and mixed gently for 30 minutes at room temperature to block unreacted sites on the microparticles. Microspheres were then collected again and resuspended in 1 ml of 10 mg/ml BSA solution and mixed gently for 30 minutes at room temperature. Repeat the last step once, but shorten the mixing time to 5 minutes. Finally microspheres were collected and stored in PBS with 1% BSA at 4°C until use.

Chromium Chloride Coupling of IgG to RBCs

Human IgG and mouse IgG2a were covalently coupled to the membranes of RBCs by means of a chromium chloride (CrCl3) method previously described [118]. 1% CrCl3 solution was prepared, properly aged at pH 5, and diluted in 20 mM acetate-buffered saline, pH 5.5, at varies ratio (ranging from 1:100 to 1:800). Fresh red blood cells were washed 5X in saline and resuspended to 2% hct. IgG was added to each 250 ml sample and mixed. An equal volume of diluted CrCl3 solution was added dropwise with constant agitation. After 5 minutes the reaction was stopped by addition of 0.5 ml PBS/1% IgG-free BSA. Cells were subsequently washed and stored in EAS45 buffer. 1

ml aliquots from each sample were examined under light microscopy for aggregation. Samples were assayed for coating density and uniformity by flow cytometry. Appropriate ratios of protein to CrCl3 were determined empirically in a grid-design assay. While increasing levels of CrCl3 consistently increased the coating levels, this also increased the degree of cell aggregation. Increasing amounts of protein decreased aggregation, but did not necessarily increase the coating densities. In fact, excessive amounts of protein quenched the CrCl3 reaction completely.

Biotinylation of RBC

Human red blood cells were purified from fresh human blood and kept in EAS45 for future use. Human RBCs were washed five times with PBS before biotinylation. Biotin-X-NHS was added to 10% RBC suspension at pH 9.0. After 30 minutes incubation at room temperature, the RBCs were washed five times by centrifugation with BSA/PBS (PBS containing 2 mg/ml BSA). Next, streptavidin (SA) was added to a 10% suspension of biotinylated-RBC (b-RBC) and, after 30 minutes incubation at room temperature, non-bound SA was removed by centrifugation. Then SA-b-RBCs were incubated with biotinylated monomeric pMHC for 1 hour at room temperature. Resulted RBCs were washed three times in PBS and stored in EAS45 buffer.

Site Density Determination

Site densities of proteins on red blood cells (IgG or pMHC), T cell (TCR, CD3 and CD8) and polystyrene microspheres (solubilized CD16 captured by 214.1 covalently coupled to microspheres) were determined by quantitative direct fluorescent immunoassay (QIFI) [119-121] using monoclonal antibody against those proteins. Samples were prepared for flow cytometry using the usual flow cytometry staining protocol. FITC or PE (depend on mAB used) microbeads standards were tested under the same instrument setting as other samples. The mean fluorescence intensities for each fraction of the standard as well as the sample were acquired. The fluorescence intensity standard curve was plotted and total protein number per cell was calculated from the standard curve with protein/fluorophore ratio of the antibody provided by manufacture.

Finally, site density was calculated by dividing total protein number per cell by surface area of a cell.

Micropipette Binding-frequency Assay

Two-dimensional kinetic rates of cells-expressing receptor interacting with RBC coated-ligand were measured by micropipette method developed in our lab [118]. Briefly, a microchamber filled with 3 ml of buffer plus 1% BSA, 5mM EDTA, 0.04% sodium azide was mounted on microscope (Axiovert 100, Oberkochan, Germany) every time prior to experiment. Following introduction of 1×10^3 receptor-expressing cells and 1×10^4 ligand-coated RBC to the chamber, a single receptor-expressing cell and a single red blood cell were respectively aspirated by two apposing micropipettes and aligned via micromanipulation. The red blood cell pipette was mounted to a computer-driven piezo translator, which moves the two cells into contact for a pre-determined area and duration. Upon the pipette retraction, the two cells either were immediately separated (i.e. no adhesion, scored 0) or remained bound with the red blood cell being elongated for a short time before being detached by force (i.e. adhesion, scored 1). This adhesion test cycle was then repeated on several pairs of cells for fifty times each to obtain an estimate mean adhesion probability for different contact duration which varies from 0.25 s to 16s.

Size Exclusion Chromatography

Monomeric and multimeric human IgG1 ligands were separated by gel filtration. 7.5 g Sephadex G-200 (Pharmacia, Piscataway, NJ) was swelled in 200 ml PBS/EDTA (containing 5 mM EDTA, pH=7.4) at 90°C for 5 hr and then cooled at 4°C overnight. The supernatant was decanted and the gel was resuspended in 150 ml PBS/EDTA and poured into a column (1.7 cm in diameter, 150 ml in volume). Column was rinsed with 300 ml PBS/EDTA between each run. After adding 5-20 mg IgG in 2 ml PBS/EDTA, the column was connected to a one-liter reservoir of PBS/EDTA. Setting the flow rate at 0.75 ml/min, the effluent was collected sequentially in fractions of 1.5 ml each. The optical density (OD) at 280 nm was measured to monitor the protein concentration in each fraction. Gel filtration standard which contains 2.5 mg thyroglobulin, 2.5 mg bovine

gamma globulin, 2.5 mg chicken ovalbumin, 1.25 mg equine myoglobin, and 0.25 mg viamin B_{12} was loaded separately from the sample and the same procedure was performed. Optical density value for each fraction was plotted against the fraction number for both the gel filtration standard and sample. Fractions correspond to monomeric IgG were identified and sample was collected from these fractions for later use.

Real Time Flow Cytometry

Association experiment

Five million cells (particles) were washed three times in 5 ml FACS buffer (RPMI, 1% IgG free BSA, 0.02% sodium azide). Resuspended cells in a FACS tube at a final concentration of 2.5 million/ml and mount the tube on the sample inlet valve. Started the timer when mixed the IgG with cells and take fluorescence histogram at different time point. The earliest time point can be at 10 second after sample mixing. The experiment will last for 12 minutes. Total 15 histograms were obtained from single test.

Dissociation experiment

The mixture left from association experiment was incubated for another 20 minutes and centrifuge to pallet. The supernatant was decanted and pallet was vortexed in residue medium and ready for dissociation experiment. 2 ml plain medium was added to disperse cell particles while started the timer. The earliest time point can be at 10 second after plain medium was added. The experiment will last for 12 minutes. Total 15 histograms were obtained from single test.

CHAPTER V

MEASURING LIGAND-BINDING PROPERTIES OF FCγ RECEPTOR III IN REAL-TIME FLOW CYTOMETRY

Introduction

FcγRIII interacting with IgG has lower affinity and faster kinetics compared to antibody/antigen reaction. Several groups have studied the affinity and kinetics of different FcγRIII isoforms using different methods. Below is a summary of kinetics and affinities for different CD16 interacting with different IgG using four different assays, surface plasmon resonance (SPR, 3D), competitive inhibition assay (CI, 3D), micropipette (MP, 3D), and fluorescent recovery after photobleach method (FRAP, 2D).

Table 5-1. Kinetics and affinity of 2D and 3D measurement for CD16 molecules

Parameter / Molecular System	Assay	k_r (s^{-1})	k_f ($\mu M^{-1}s^{-1}$)	K_a (μM^{-1})	References
e-sCD16A – hIgG	SPR	**0.00471**	**0.00651**	**1.39**	[122]
e-sCD16A – hIgG1	SPR	**0.00574**	**0.00818**	**1.41**	[122]
e-sCD16A – rIgG	SPR	**0.0186**	**0.01762**	**0.934**	[122]
p-sCD16B^{NA2} – hIgG1(aglycosylation)	SPR	**0.98**	**0.54**	**0.556±0.04**	[123]
p-sCD16B^{NA2} – hIgG1(aglycosylation)	SPR	**0.00193±0.0002**	**0.00210±0.0003**	**1.1±0.2**	[124]
e-sCD16B^{NA2} – hIgG1	SPR	**0.00098±0.0003**	**0.00113±0.0003**	**1.3±0.6**	[124]
CD16A^{TM} – hIgG	CI	–	–	**0.25**	[25]
CD16A^{TM} – rIgG	CI	–	–	**0.93**	[25]
CD16A^{TM} – mIgG2a	CI	–	–	**0.41**	[25]
CD16A^{GPI} – hIgG	CI	–	–	**2.1**	[25]
CD16A^{GPI} – rIgG	CI	–	–	**6.3**	[25]
CD16A^{GPI} – mIgG2a	CI	–	–	**0.11**	[25]
CD16B^{NA1} – hIgG	CI	–	–	**0.032**	[25]
CD16B^{NA1} – rIgG	CI	–	–	**0.033**	[25]
CD16B^{NA2} – hIgG	CI	–	–	**0.019**	[25]
CD16B^{NA2} – rIgG	CI	–	–	**0.028**	[25]

Table 5-1 continued

Parameter / Molecular System	Assay	k_r(s^{-1})	AcK_f ($10^{-6}\mu m^4 s^{-1}$)	AcK_a ($10^{-6}\mu m^4$)	
$CD16A^{TM}$ – hIgG	MP	**0.34**	**0.25**	**0.74**	[25]
$CD16A^{TM}$ – rIgG	MP	**0.24**	**0.58**	**2.4**	[25]
$CD16A^{TM}$ – mIgG2a	MP	**0.31**	**2.4**	**7.6**	[25]
$CD16A^{GPI}$ – hIgG	MP	**0.42**	**0.77**	**1.8**	[25]
$CD16A^{GPI}$ – rIgG	MP	**0.17**	**0.70**	**4.1**	[25]
$CD16A^{GPI}$ – mIgG2a	MP	**0.54**	**0.59**	**1.1**	[25]
$CD16B^{NA2}$ – hIgG1	MP	**0.64**	**0.24**	**0.38**	[125]
		k_r(s^{-1})	K_f ($\mu m^2 s^{-1}$)	K_a (μm^2)	
$CD16A^{GPI}$ – rIgG	FRAP	**0.0024**	**0.000667**	**0.278**	(Tolentino et al.)
$CD16B^{NA2}$ – rIgG	FRAP	**0.0113**	**0.00124**	**0.110**	(Tolentino et al.)

From the table above, one can see several discrepancies in the existing data. First, there is a thousand fold difference on dissociation rate constant between four methods, provided the units are the same even in different 2D and 3D measurements. The half-lives acquired from micropipette are a few seconds, while SPR and FRAP measurement tends to get slower dissociation rate constant. Secondly, one can notice that due to the nature of a different method, the affinity and association rate constant acquired from three methods have different units. Thirdly, there is also a discrepancy within the same method SPR. For the same molecular pair $sCD16B^{NA2}$-hIgG1, two groups obtained two dissociation rate constants, that differed a thousand fold, regardless the similar dissociation constant they obtained.

One may also notice that two different $sCD16B^{NA2}$ were compared in SPR experiments. One was synthesized by prokaryotic cell ($p\text{-}sCD16B^{NA2}$), which was glycosylated, and another was synthesized by eucaryotic cell, which was aglycosylated. More consistent comparison of dissociation constant is among micropipette measurement, competitive inhibition assay and fluorescent recovery after photobleach method because all these three assays used CHO cell expressed CD16 molecules.

Therefore, developing a new 3D method that measures both affinity and kinetics and uses receptors reside in their native enviroment, cell membrane, is necessary.

This aim was designed to develop a real-time flow cytometry method that satisfying above requirements. Two protocols were developed, association and dissociation, and their application on $CD16a^{TM}$, $CD16b^{NA2}$ were compared along. In this project, real-time flow cytometry was also used in studying temperature effect on ligand binding.

Results

1. Size exclusion chromatography was used to separate monomeric IgG from aggregated IgG.

To ensure monomeric ligand binding, size exclusion chromatography was used to separate monomeric hIgG1 from aggregated IgG. A mixture of five molecular weight markers, ranging from 1.35 to 670 kD, was used as a calibration standard for size exclusion columns. The mixture includes vitamin B_{12} and myoglobin, which are visible when eluting from glass and can be used to ensure that the column is properly packed and the sample is eluting evenly. Elution was collected at 1.5ml per fraction. The optical density (OD) at 280 nm was measured to monitor the protein concentration in each fraction. Sample was loaded separately from standard and optical density value for each fraction was plotted against the fraction number for both the gel filtration standard and sample. Fractions correspond to monomeric IgG were identified and sample was collected from these fractions for later use.

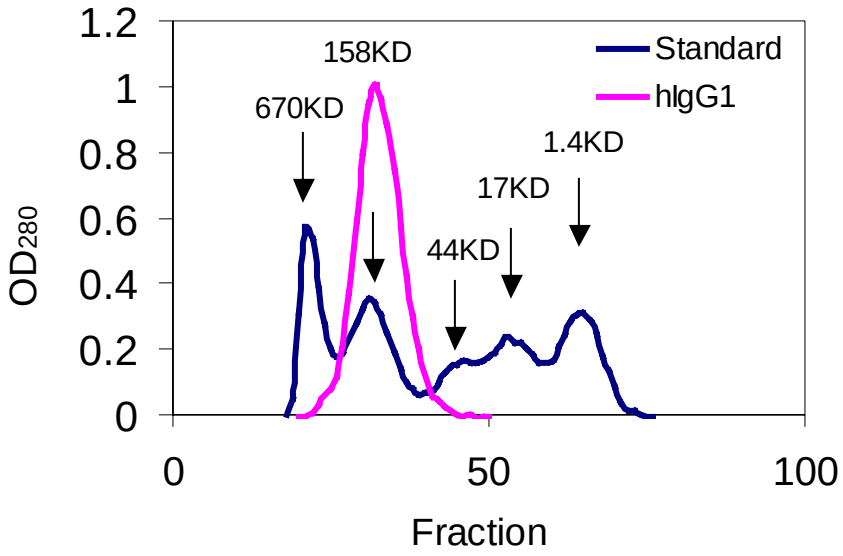

Figure 5-1. Size exclusion chromatography of standard and hIgG1. Arrows indicate molecular weight for 5 components of the standard, thyroglobulin 670 KD, bovine gamma-globulin 158 KD, chichen ovalbumin 44 KD, equine myoglobin 17 KD, vatamin B_{12} 1.3KD.

2. Real-time flowy cytometry: association experiment

Association experiment was designed to examine CHO CD16a^{TM} and CHO CD16b^{NA2} interaction with hIgG1 in real-time. During experiment, 2.5 million CD16 expressing cells were mixed with FITC-labeled hIgG1 for a designated concentration and meanwhile timer was started to record 0 time point. The mixture was immediately inserted to sample inlet valve of the flow cytometry and a histogram was taken every 15 second during the first 2 minutes, then every 30 seconds for the next 2 minutes and at a larger interval as indicated on the figure till 16 minutes. At lease 15 histograms were acquired for each interaction course and several different ligand concentrations were tried for each CD16 interaction with hIgG1. Because of the low affinity of CD16 to hIgG1, high concentration of ligand is required to saturate the receptor. Therefore, background control is needed for each ligand concentration that has been tried. In this case, CHO cells tranfected with CD59 molecule was used. CD59 is known not to interact with hIgG1 and this tranfection cell line is better than plain CHO cell in keeping the system consistent as all other cells tested are tranfected with different CD16s. Figure 5-2 show mean FI increases with increasing interaction time and finally reaches equilibrium when

CHO CD16a™ interaction with hIgG1. Total of 4 different ligand concentrations were tested, open symbols denote mean FI of background controls and solid symbols denote total mean FI of a sample. Noted that for higher ligand concentration, mean FI of a background is higher than mean FI of a total binding for a low ligand concentration, which show the necessity to having background control for each ligand concentration that tested.

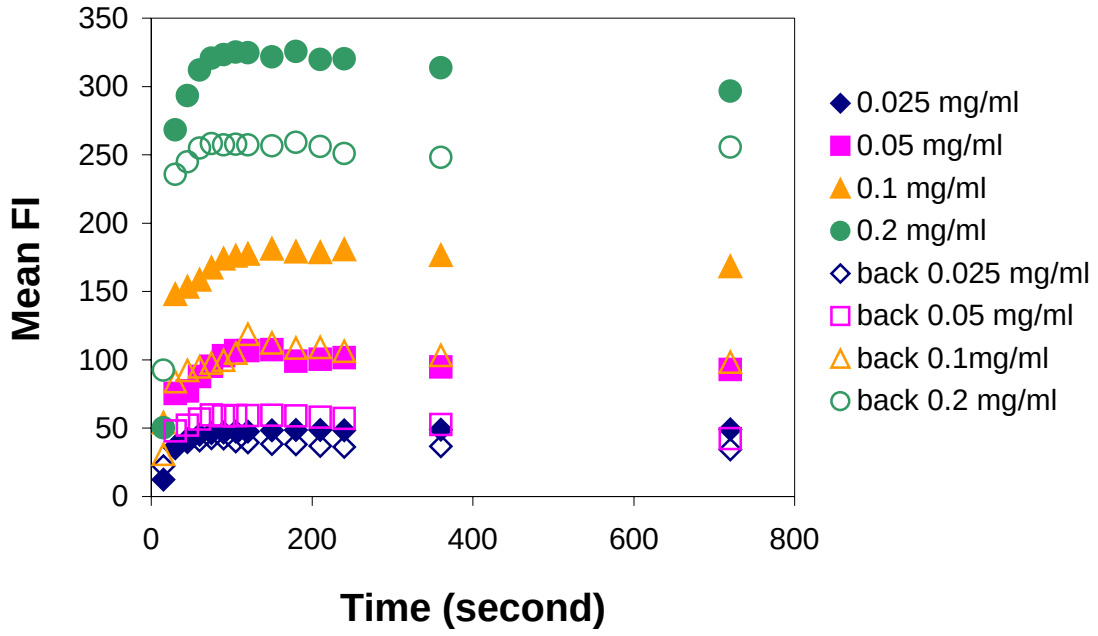

Figure 5-2. Mean fluorescent intensity (FI) vs interaction time curve for CHO CD16a™ interacting with hIgG1 at 0°C, association phase. Open symbols are background. Solid symbols are total binding.

3. Real-time flow cytometry: dissociation experiment

The dissociation experiment was design to monitoring the dissociation of hIgG1 from CD16 after their interaction reaches equilibrium. Therefore, in the experiment, half of the sample was used in the association experiment phase; the remaining half was allowed to incubate for another 20 minutes and then centrifuge to pellet. The supernatant was decanted and pallet was vortexed in residue medium and ready for dissociation experiment. 2 ml of plain media was added to already dispersed cells while timer was started. The mixture was immediately inserted to sample inlet valve of the flow cytometry and again a histogram was taken every 15 second during the first 2 minutes,

then every 30 seconds for the next 2 minutes and at a larger interval as indicated on the figure till 16 minutes. At lease 15 histograms were acquired for each interaction course and several different ligand concentrations were tried for each CD16 interaction with hIgG1 and same thing for background control. Noted that during dissociation, there is a fast dissociation phase before 4 minutes and a slower dissociation phase after 4 minutes. This could results from rebinding of the ligand to receptor and is taken into consideration in model fitting later.

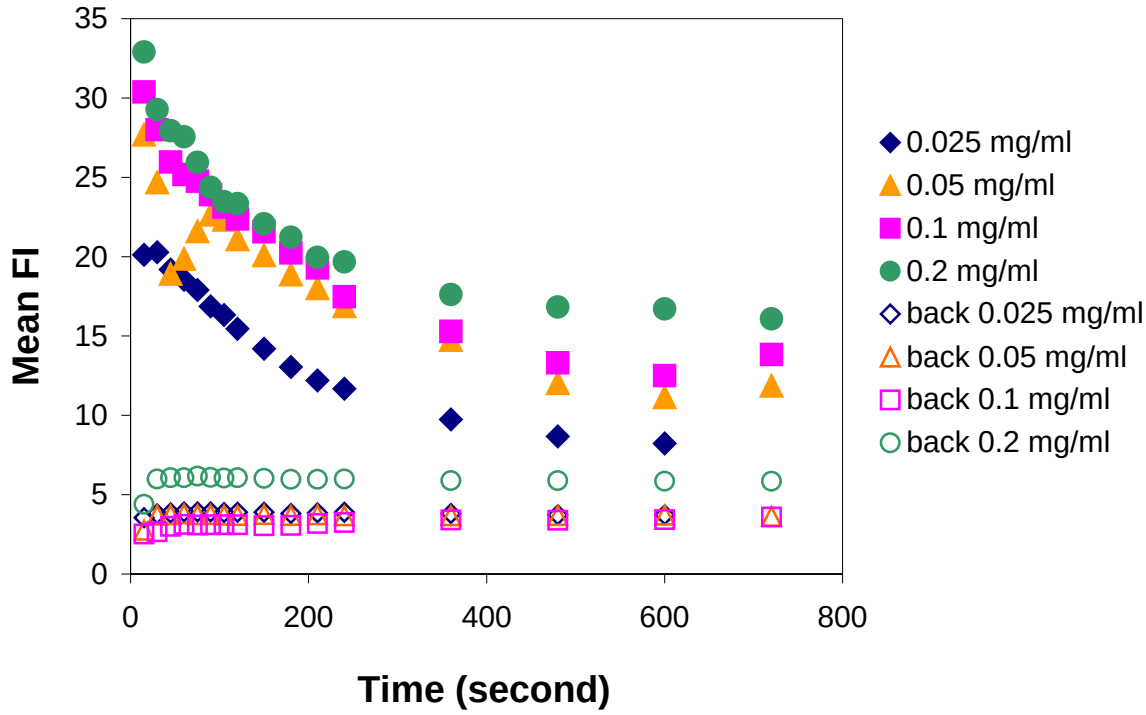

Figure 5-3. Mean fluorescent intensity (FI) vs interaction time curve for CHO CD16a^{TM} interacting with hIgG1 at 0°C, dissociation phase. Open symbols are background. Solid symbols are total binding.

4. Models for data fitting.

The association reaction can be modeled as monovalent receptor-ligand interaction where R, L and C are the concentration of free receptor, available ligand and receptor/ligand complex,

$$R + L \underset{k_r}{\overset{k_f}{\rightleftharpoons}} C \qquad \text{Eqn. 4-1}$$

where k_f is the association rate constant and k_r is the dissociation rate constant. The rate equation is

$$\frac{dC}{dt} = k_f RL - k_r C \qquad \text{Eqn. 4-2}$$

For the case of no ligand depletion and no change in total receptor concentration (R_T = constant), Equation 4-2 simplifies to:

$$\frac{dC}{dt} = k_f [R_T - C]L_0 - k_r C \qquad \text{Eqn. 4-3}$$

Equation 4-3 can be solved to give a general solution:

$$C(t) = C_0 \exp\{-(k_f L_0 + k_r)t\} + (\frac{k_f L_0 R_T}{k_f L_0 + k_r})[1 - \exp\{-(k_f L_0 + k_r)t\}] \qquad \text{Eqn. 4-4}$$

where L_0 is the initial ligand concentration and R_T is total receptor concentration. Background binding can be modeled as in Equation 4-5,

$$\frac{dB}{dt} = k_{fn} L - k_{rn} B \qquad \text{Eqn. 4-5}$$

where B is the amount of non-specifically-bound ligand. The terms $k_{fn}L$ and $k_{rn}B$ describe the non-specific cell surface association and dissociation events. The corresponding rate constants characterizing non-specific ligand interaction with the cell surface are k_{fn} and k_{rn}. Solve equation 4-5 and assuming L is large compared to B, we get

$$B = k_{fn} L(1 - e^{-k_{rn}t}) \qquad \text{Eqn. 4-6}$$

after fitting the background, it can be subtracted from total binding of each experiment. Figure 5-4a shows an example of the background fitting using equation 4-6 and a curve fitting using equation 4-4 for CHO CD16b^{NA2} interacting with hIgG1 at 0°C. The models fit both background and data well. Fitting reviews an initial fast increase phase and an equilibrium phase after 100 second. CHO CD16a^{TM} interaction with hIgG1 was similarly fitted and yielded parameters are listed in Table 4-2.

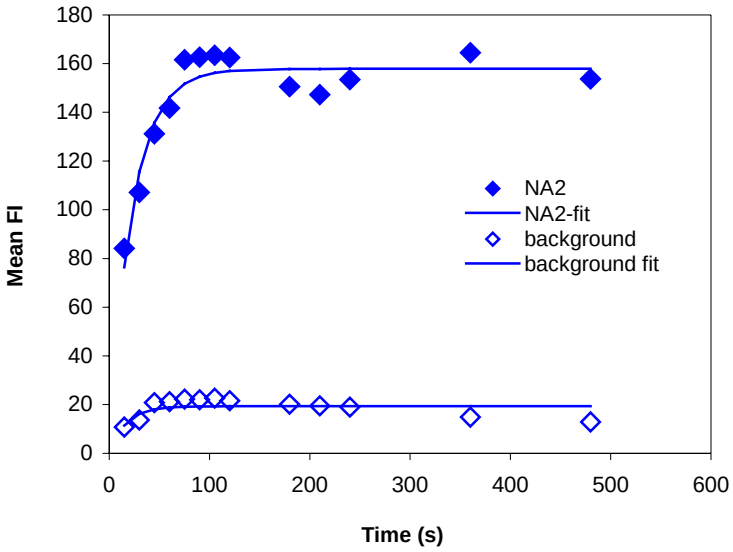

Figure 5-4a. Curving fitting of association experiment of CHO CD16b^{NA2} interacting with hIgG1 at 0°C.

Table 5-2. Kinetic rates and equilibrium dissociation constant of CD16 expressing on CHO cell binding to HigG1 at 0°C.			
Receptor	k_{on} ($M^{-1}s^{-1}$)	k_{off} (s^{-1})	K_d (M)
CD16a^{TM}	$(1.81 \pm 0.34) \times 10^4$	0.0038 ± 0.0005	$(2.09 \pm 0.30) \times 10^{-7}$
CD16b^{NA2}	$(2.55 \pm 0.47) \times 10^3$	0.0245 ± 0.0014	$(8.72 \pm 0.21) \times 10^{-6}$

Besides fitting association experiment, dissociation experiment was also fitted by modeling dissociation with following reaction scheme when association can be neglected during the initial phase of dissociation.

$$R + L \xleftarrow{k_r} C \qquad \text{Eqn. 4-7}$$

where k_r is the dissociation rate constant and the rate equation can be written as

$$\frac{dC}{dt} = -k_r C \qquad \text{Eqn. 4-8}$$

Equation 4-8 can be solved to give a general solution:

$$C(t) = C_0 e^{-k_r t} \qquad \text{Eqn. 4-9}$$

and above formula can be transferred to a linear equation:

$$\ln(C/C0) = -k_r t \qquad \text{Eqn. 4-10}$$

When applied equation 4-6 to fit background in dissociation experiment of CHO CD16b^{NA2} interaction with hIgG1 and equation 4-10 to fit data, both models give a nice fit. However, the resulted dissociation rate constant is smaller than the one acquired from fitting association experiment, 0.0040 s^{-1} compared to 0.0245 s^{-1}. It is possible that the fast dissociation phase was missed and only slower phase was captured during experiment.

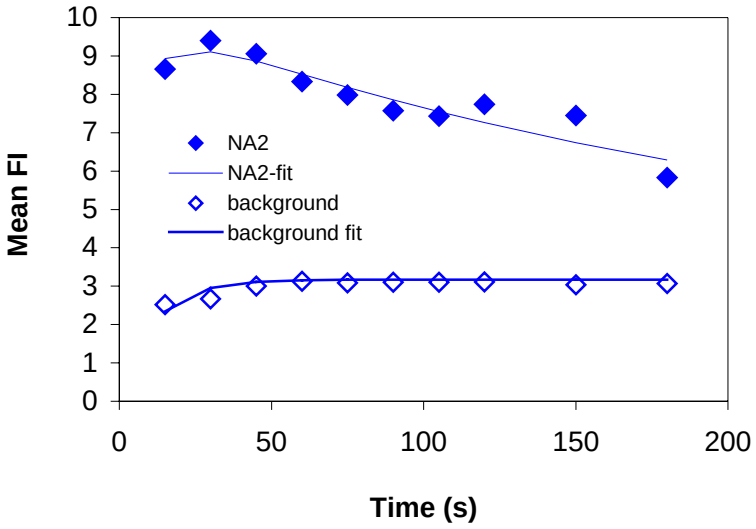

Figure 5-4b. Curving fitting of dissociation experiment of CHO CD16b^{NA2} interacting with hIgG1 at 0°C.

5. Temperature effect on CHO CD16a^{TM} binding to hIgG1.

Temperature is an important factor that affect affinity and kinetics of receptor – ligand binding. We are here to show that real-time flow cytometry is capable of measuring affinity and kinetics under different temperature. CHO CD16a^{TM} was used as a model system and its interaction with hIgG1 under 4 different temperatures was investigated. A homemade water reservoir with constant temperature was used to incubate the reaction tube throughout experiment. The parameters were extrapolated from fitting association experiments and listed in table 2. This experiment reveals differences in binding parameter under different reaction temperatures. Especially for dissociation constant, it increases with increasing temperature as shown in figure 5-5.

Table 5-3. Kinetic rates and equilibrium dissociation constant of CD16a^{TM} expressing on CHO cell binding to HigG1 at different temperature.			
Temperature	k_{on} ($M^{-1}s^{-1}$)	k_{off} (s^{-1})	K_d (M)
0 ^oC	$(1.81 \pm 0.34) \times 10^4$	0.0038 ± 0.0005	$(2.09 \pm 0.30) \times 10^{-7}$
15 ^oC	$(2.88 \pm 0.44) \times 10^4$	0.0136 ± 0.0024	$(4.71 \pm 1.10) \times 10^{-7}$
20 ^oC	$(3.90 \pm 0.55) \times 10^3$	0.0514 ± 0.0019	$(1.32 \pm 0.20) \times 10^{-5}$
37 ^oC	$(9.72 \pm 0.30) \times 10^2$	0.0138 ± 0.0026	$(1.42 \pm 0.27) \times 10^{-5}$

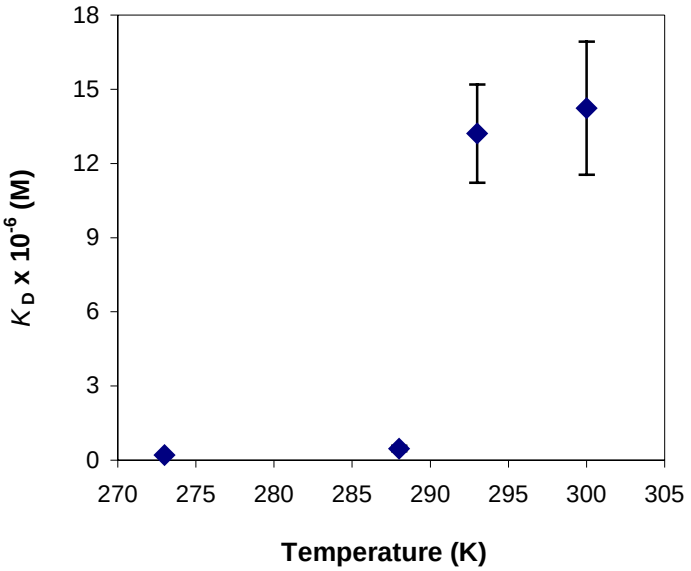

Figure 5-5. Relation between dissociation constant and temperature.

Discussion

In this aim, a real-time flow cytometry protocol was developed to measure binding affinity and kinetics of low affinity FcγR, CD16. This method was applied to CHO CD16a^{TM} and CHO CD16b^{NA2}. The resulted parameters were well within the range of previous reported value [25]. Both the association experiment and dissociation experiment were modeled and the results show that dissociation experiment tends to yield a slower k_r compared to k_r that is yield from association. This could be that in dissociation experiment, the mean FI dropped from several hundreds to several tens of reading within first 15 second. Part of this dropping is resulted from non-specific binding that washed away by fresh media, but part of this dropping is due to fast dissociation phase. On the other hand, association well captures this fast interaction phase. The data

showed that there is clearly a fast association phase followed by equilibrium binding (Figure 5-4a).

An important binding property reveal by this experiment is the unusual relation between dissociation constant and temperature (Figure 5-5). It was first noted by Maenaka et al. that unlike FcγRIIa or FcγRIIb, FcγRIIIb exihibite increased Gibbes Free Energy (Figure 5-6, third panel), ΔG°, when the temperature increased [123]. $\Delta G°$ can be calculated from the K_d; $\Delta G° = R \times T \times \ln(Kd/C)$, where R is 1.987×10^{-3} kcal•mol^{-1}K^{-1}; K_d is expressed as mol•L^{-1}; and C is 1 mol•L^{-1} (therefore making K_d/C dimensionless, as required). Our data show a similar trend if converted K_d to $\Delta G°$ following above equation. The reason for this difference in free energy existing among FcγRs is not known and it is thought to relate to structure differences among FcγRs.

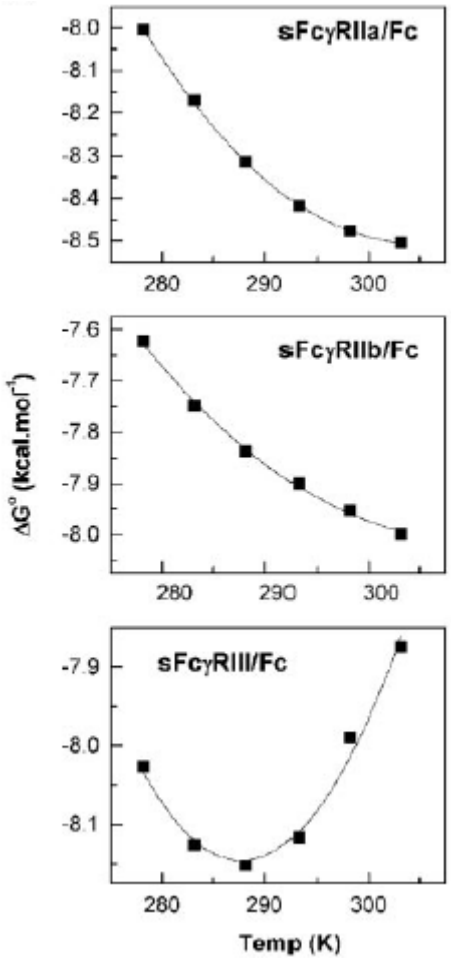

Figure 5-6. Gibbes free energy changes in relation with increased temperature for several FcγRs (adapted from Maenaka, K., et al., J. Biol. Chem., 2001).

CHAPTER VI

QUANTIFYING THE EFFECTS OF MEMBRANE ANCHOR AND GLYCOSYLATION OF FCγ RECEPTOR III ON LIGAND BINDING AFFINITY AND KINETICS

Introduction

In this study, we applied three different methods to solubilize CD16 (sCD16), which gave three different anchor lengths:

1, CD16 expressing-cell lysate (lysate), which results in soluble CD16 with full length in anchor, be it transmembrane or GPI (Figure 6-1a).

2, Phosphatidylinositol-specific phospholipase C (PIPLC) treatment, which truncates diacyleglacerol from the GPI anchor to release the CD16 (figure 6-1b), resulting in a shorter anchor attached to the extracellular domain (figure 6-1a).

3, CD16 spontaneously shed from cell membrane (shedding), which preserves the extracellular portion of the molecule but have no anchor at all (figure 6-1a).

$CD16a^{TM}$, $CD16a^{GPI}$ and $CD16b^{NA2}$ were solubilized according to the above three methods. The resulting soluble CD16s were captured by a mAb that covalently attached to microspheres. Kinetics and affinities of these CD16s interacting with hIgG1 and mouse IgG2a were measured. Not only do the results support our previous findings, but they also demonstrate that a conformational change on receptor anchor can affect ligand binding as well. These effects can be inversed upon using another ligand.

We also tested how glycosylation of the receptor affect ligand binding. Tunicamycin, a widely used N-glycosylation inhibitor, was added to culture medium to generate aglycosylated CHO CD16 isoforms. Glycosylation effect was also tested on soluble CD16, CD16aIg chimera (CD16aIg), by adding tunicamycin to CD16aIg secreting CHO cell culture. The resulting cell surface CD16s and CD16Ig were tested using micropipette adhesion assay and the affinities so acquired were compared with glycosylated molecules.

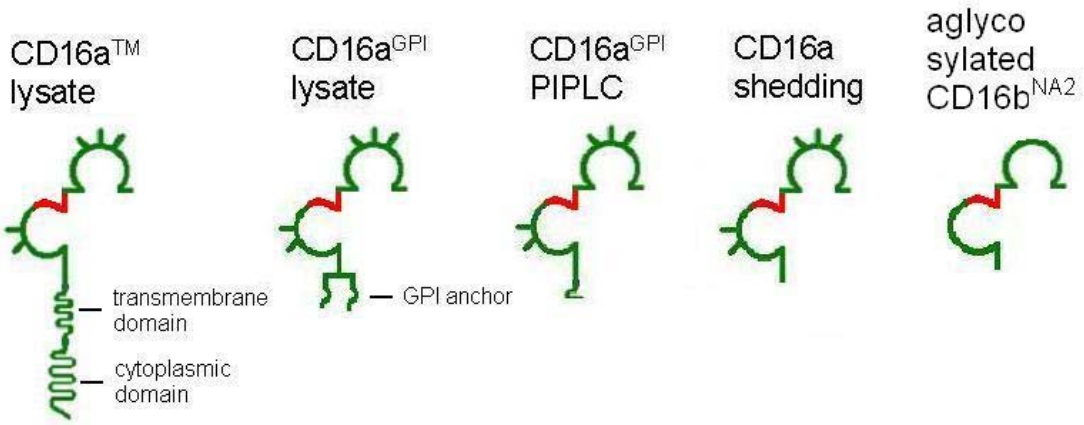

Figure 6-1a. Schematic drawings of different soluble CD16s.

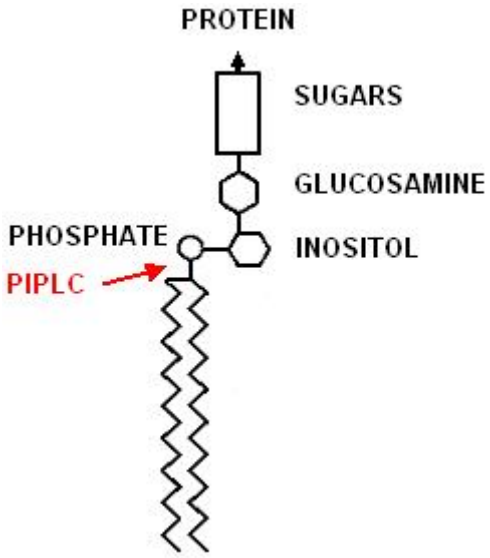

Figure 6-1b. Schematic drawing of GPI anchor and PIPLC cleavage site.

Results

1. Release of membrane CD16s (mCD16s) by three solubilization methods and their coating on microspheres.

The cell expressing CD16 molecules were released from membrane by lysing the cell, using PIPLC to cleavage diacyleglacerol off a GPI anchor (PIPLC) or by spontaneous shedding in a serum free media (shed). After PIPLC treatment or shedding, cells were stained for their surface expression of CD16 and the surpernatant was used to

incubate 214.1 coated microspheres. Figure 6-2 shows the decrease expression of surface CD16s after these treatments and the capture of sCD16 by 214.1 on microspheres.

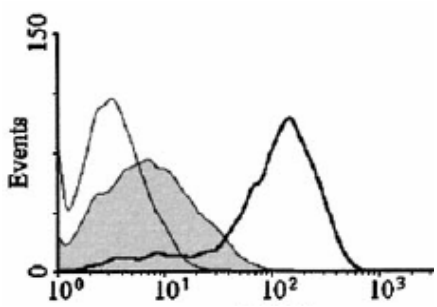

Figure 6-2a. FACS comparison of CHO CD16a^{GPI} before and after PIPLC. Thin line, background; thick line, CD16 expression before PIPLC; grey area, CD16 expression after PIPLC.

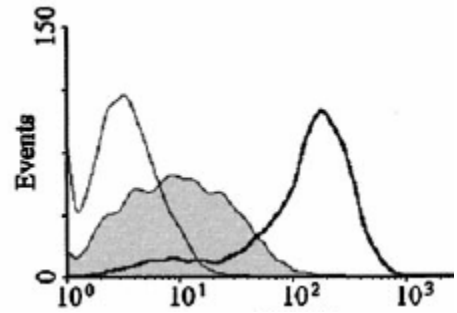

Figure 6-2b. FACS comparison of CHO CD16a^{GPI} before and after shedding. Thin line, background; thick line, CD16 expression before shedding; grey area, CD16 expression after shedding.

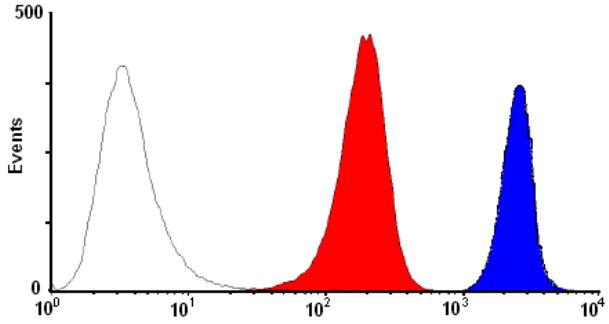

Figure 6-2c. FACS of solubilized CD16 captured by 214.1. Thin line, background; red area, CD16a^{GPI} shedding captured by 214.1 beads; blue area, CD16a^{GPI} PIPLC captured by 214.1 beads.

2. Microsphere-reconstituted CD16bs (mrCD16s) bind specifically to RBC-bound IgG

Binding specificity of mrCD16s coated on microspheres and IgG coated on RBC was tested using micropipette adhesion frequency assay (figure 6-3). Micospheres coated with BSA showed minimum binding to RBC-bound IgG. RBCs underwent the same procedure without adding IgG also showed minimum binding to mrCD16s. mrCD16a^{TM} show an average of 54% of adhesion probability with standard deviation of 13% estimated from 5 pairs of cells and beads tested 100 times each. Incubation of mrCD16s-coated microspheres with a function-blocking anti-CD16 monoclonal antibody CLBFcgran1 (10 mg/ml, 30 min, 4 °C) suppressed the binding to background level.

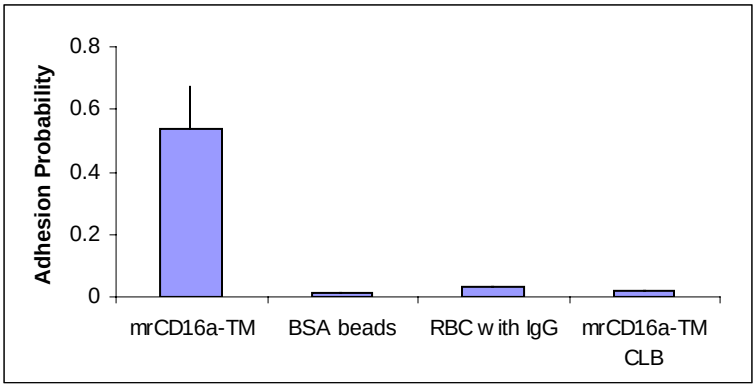

Figure 6-3. Specificity test of mrCD16 interacts with RBC.

3. Both mCD16a^{GPI} and sCD16a^{GPI} (lysate) bind hIgG with a higher affinity than CD16a^{TM}

CD16a^{TM} and CD16a^{GPI} lysates were generated and captured by 214.1 coated microspheres. Kinetics and affinity of these CD16s interacting with hIgG1 coated on RBC were measured by micropipette adhesion frequency assay. In this experiment, seven contact time points were chosen ranging from as short as 0.5 s to as long as 16 s. 5 pairs of cells were tested for each time point and 100 adhesion repeats were done for each cell pair to calculate adhesion frequency. Resulted adhesion frequency is total adhesion frequency (P_t), which has to be normalized into specific adhesion frequency (P_a) by removing nonspecific adhesion frequency (P_n) using Eqs. (5-1), [126].

$$P_a = (P_t - P_n)/(1-P_n) \quad (5\text{-}1)$$

resulted P_a was then fitted by Eqs. (2) [118] to retrieve affinity and kinetics information.

$$P_a = 1 - \exp\{-m_r m_l \eta A_c K_a^\circ [1 - \exp\{-k_{off}^\circ t\}]\} \quad (5\text{-}2)$$

These kinetics and affinities were plotted in comparison with kinetics and affinity of mCD16 interacting with hIgG [25]. sCD16a^{GPI} from lysate binds hIgG with a higher affinity than sCD16a^{TM} from lysate, just like the previous results with cell surface CD16a^{GPI} and CD16a^{TM} (figure 6-3a). Both sCD16a^{TM} and sCD16a^{GPI} from lysate have higher affinities than their respective membrane counterparts. This is likely because microspheres have a smoother surface compared to the CHO cells membrane, which results in a different fractional true contact area, η. Kinetics measurement from micropipette adhesion assay also reveals that despite the difference in fractional true contact area, the reverse rate constants (off-rate, k_r) of these four CD16s interacting with their ligand are quite comparable (figure 6-4b). Then the differences in affinity between CD16a^{GPI} and CD16a^{TM} come from forward rate constant (on-rate, k_f) (figure 6-4c).

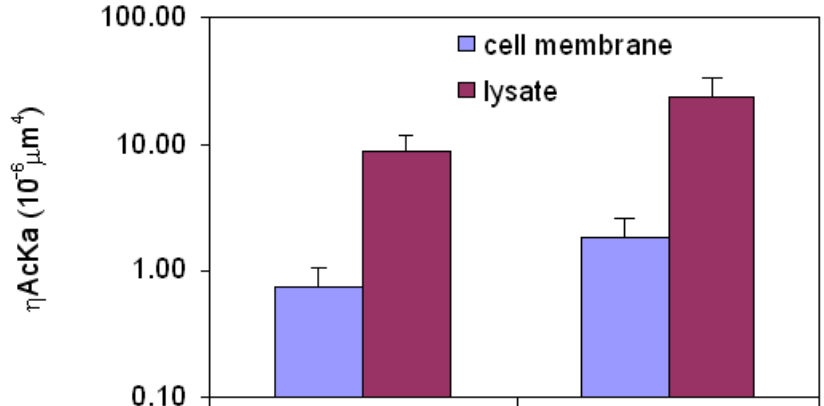

	CD16aTM	CD16aGPI
cell membrane	0.74 ± 0.30	1.80 ± 0.70
lysate	8.66 ± 2.91	24.06 ± 8.05

Figure 6-4a. Affinity comparison between CD16 lysate and CHO CD16. η = fractional true contact area.

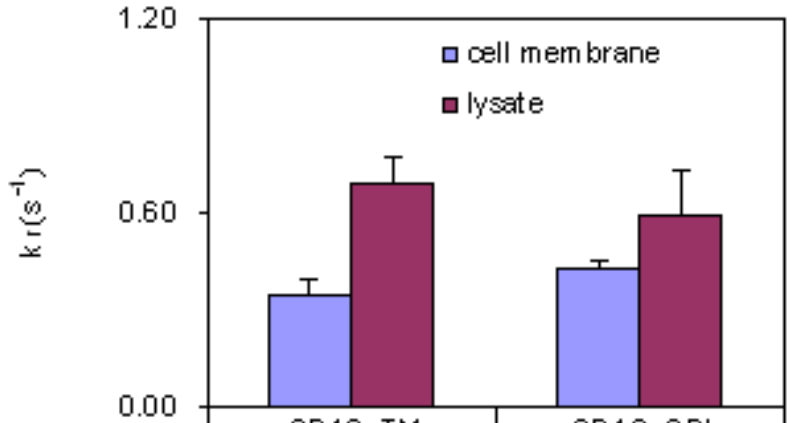

	CD16aTM	CD16aGPI
cell membrane	0.34 ±0.05	0.42 ±0.02
lysate	0.69 ±0.08	0.60 ±0.14

Figure 6-4b. Reverse rate constant comparison between CD16 lysate and CHO CD16.

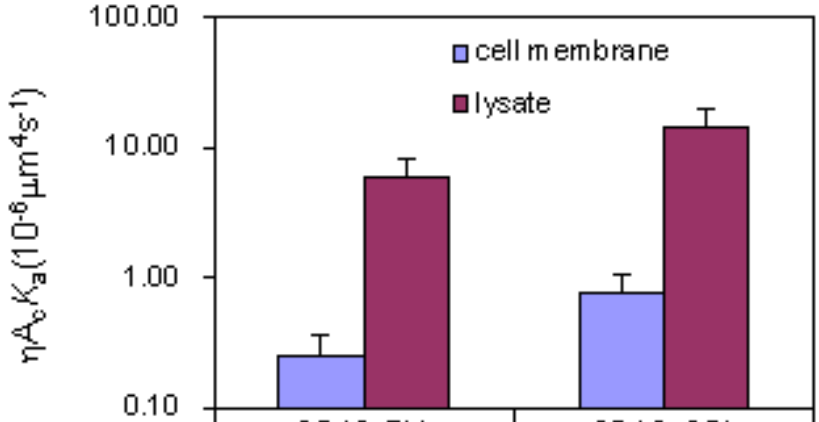

	CD16aTM	CD16aGPI
cell membrane	0.25 ±0.11	0.77 ±0.29
lysate	5.99 ±2.12	14.32 ±5.85

Figure 6-4 c. Forward rate constant comparison between CD16 lysate and CHO CD16. η = fractional true contact area.

4. Anchoring length of a molecule affects ligand-binding affinity.

Lysing the cells, PIPLC enzymatic cleavage and shedding were used to solubilize CD16a-GPI and CD16b[NA2]. Resulted molecules differ from their anchor lengths: lysing the cells allows the molecule to retain it's original GPI anchor, PIPLC cleavages part of

the GPI anchor; spontaneous shedding is the action of metalloproteinases bound to the cell membrane, resulting in molecules with no GPI anchor. Micropipette adhesion assay was applied to measure affinity of these molecules at a contact time long enough for the interaction to reach equilibrium. Previous kinetics measurements of mCD16 and sCD16 revealed that interactions between CD16 and hIgG1 had reach equilibrium at 8 second contact regardless of the ligands used. Adhesion frequencies were measured at 8 second contact time and normalized using equation 5-1. Affinities were then estimated from equation 5-3, which is a transformation of equation 5-2 when the interaction reaches equilibrium, contact time t approaching infinity.

$$A_c K_a^\circ = -\mathrm{Ln}\,(1 - P_a) / m_r m_l \qquad (5\text{-}3)$$

Progressive shorterning of the anchor length of $CD16a^{GPI}$ resulted in a progressive increase in its affinity for hIgG1 (figure 6-5 middle panel). The same result was seen with $CD16b^{NA2}$, which is also a GPI anchored molecule (Figure 6-5 left panel). Further confirmation was obtained using $CD16a^{TM}$, the anchor length of which can be changed by using cell lysate (full transmembrane anchor) and by shedding (no membrane anchor). The polypeptide transmembrane anchor resists PIPLC cleavage so only two anchor lengths were obtained. Affinity measurements show that $CD16a^{TM}$-lysate has a much higher affinity then $CD16a^{TM}$-shedding (Figure 6-5 left panel). Since the only difference between $CD16a^{TM}$ and $CD16a^{GPI}$ is in their anchor, these two molecules should have identical structure once they both became soluble by shedding and their affinity to hIgG1 should be the same. Our measurements show $CD16a^{TM}$-shedding and $CD16a^{GPI}$-shedding have respective affinity of $0.17 \pm 0.10 \times 10^{-6}$ μm^4 and $0.38 \pm 0.10 \times 10^{-6}$ μm^4, which are not statistically significantly different ($p = 0.0925$, Student t-test). Student's t-test has been used to compare two means at a time and the p values were indicated on the figure for every pair of test. All p values are reasonably small, confirming that, for all three CD16 molecules ($CD16a^{TM}$, $CD16a^{GPI}$, and $CD16a^{NA2}$), the lysate form has a significantly higher affinity for hIgG1 than the PIPLC cleavaged (wherever available), which in turn has a higher affinity for hIgG1 than the shedded form.

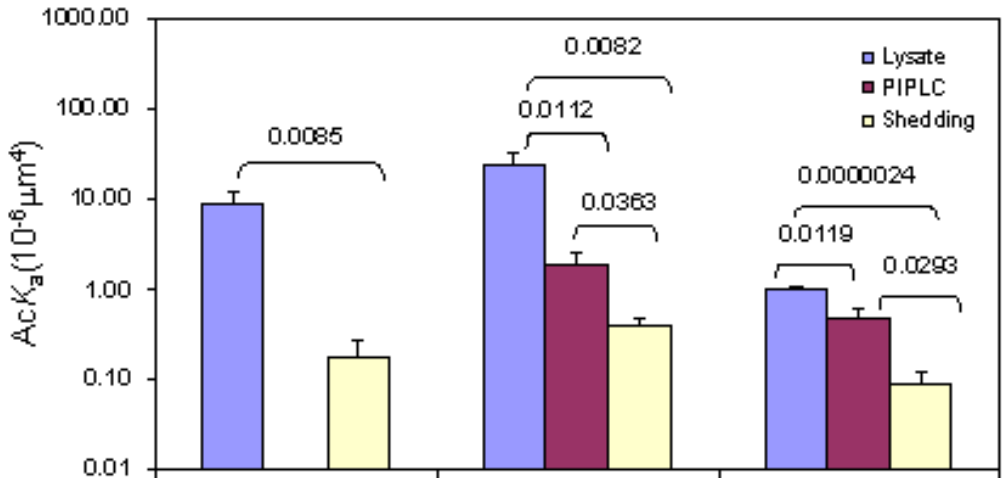

	CD16aTM	CD16aGPI	CD16bNA2
Lysate	8.66 ± 2.91	24.06 ± 8.05	0.96 ± 0.12
PIPLC		1.87 ± 0.62	0.46 ± 0.14
Shedding	0.17 ± 0.10	0.38 ± 0.10	0.09 ± 0.03

Figure 6-5. Affinity comparison of CD16 shedding, lysate and PIPLC binding to human IgG1 at 8 seconds.

5. The trend of anchoring effect on ligand binding was inversed when ligand was changed from hIgG1 to mouse IgG2a.

Previously we found that membrane CD16a^{GPI} binds to hIgG better than CD16a^{TM}. However, when ligand was switched from hIgG to mouse IgG2a, CD16a-TM binds better than CD16a^{GPI} (Chesla et al., 2000). In this study, ligand was switched from hIgG1 to mIgG2a and affinities were acquired as described in the preceding section. It is eveident that both CD16a^{TM}-shedding and CD16a^{TM}-lysate bind better than their CD16a^{GPI} counterparts (Figure 6-6 left and middle panels), consistent with our previous results (Chesla et al., 2000). Interestingly, the correlation between CD16a anchor length and its affinity for ligand is inversed when ligand changed from hIgG1 to mIgG2a for all membrane isoforms of CD16 (CD16a^{TM}, CD16a^{GPI}, and CD16a^{NA2}), such that the lysate form with the full anchor binds with the lowest affinity, the shedded form with no anchor binds with the highest affinity, and the PIPLC cleaved form (for CD16a^{GPI} and CD16a^{NA2} only) with part of the GPI anchor binds with intermediate affinity (figure 6-6). Again, Student's t-test has been used to compare two means at a time and the p values were indicated on the figure for every pair of test. All p values are reasonably small,

confirming that, for all three CD16 molecules (CD16a^{TM}, CD16a^{GPI}, and CD16a^{NA2}), the shedded form has a significantly higher affinity for mIgG2a than the PIPLC cleaved form, which in turn has a higher affinity for mIgG2a than the lysate form.

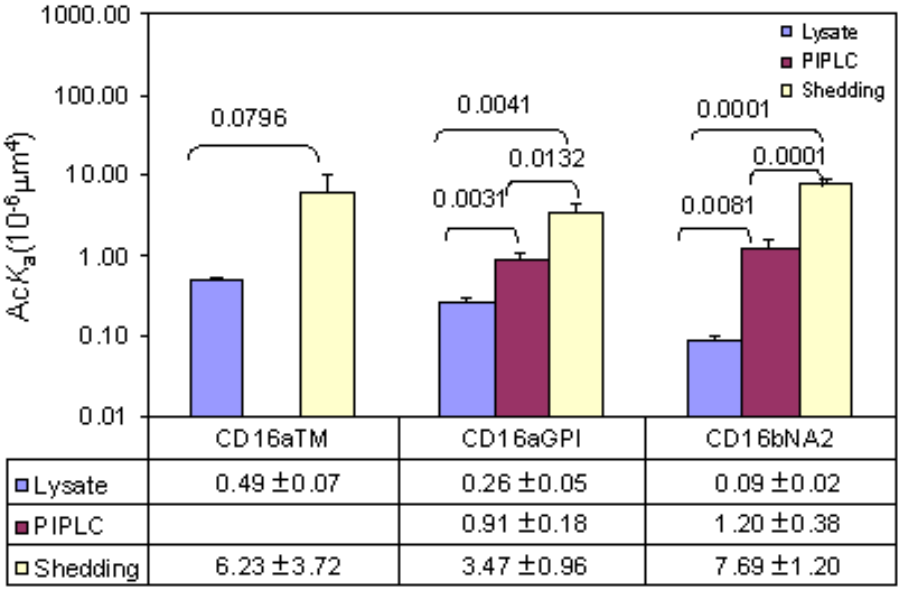

	CD16aTM	CD16aGPI	CD16bNA2
Lysate	0.49 ±0.07	0.26 ±0.05	0.09 ±0.02
PIPLC		0.91 ±0.18	1.20 ±0.38
Shedding	6.23 ±3.72	3.47 ±0.96	7.69 ±1.20

Figure 6-6. Affinity comparison of CD16 shedding, lysate and PIPLC binding to mouse IgG2a at 8 seconds.

6. Glycosylation of a receptor affects ligand binding properties.

In order to investigate the effect of receptor glycosylation on ligand binding properties, we compared affinity and kinetics of CHO CD16 interacting with hIgG1 with aglycosylated CHO CD16. In this experiment, tunicamycin, a widely used N-glycosylation inhibitor, was added to culture medium for 40 hr. This does not affect CD16 expression significantly as revealed by FACS (data not shown). All three CD16 cell lines were cultured in the same way and resulted cells were washed and then put into test chamber. Affinities and kinetics were estimated as previously described. Figure 6-7 a and b show affinity and reverse rate constant of CD16 transfected CHO cells treated with tunicamycin in this study in comparison with previously published data on the same CHO cells without the treatment [25, 125]. All three CHO CD16s that are treated with tunicamycin exhibit higher affinity for hIgG1 then untreated controls. In contrast to

affinity, tunicamycin does not have dramatic effect on k_r. Reverse rate constant for all three CD16 is about 1 s^{-1}.

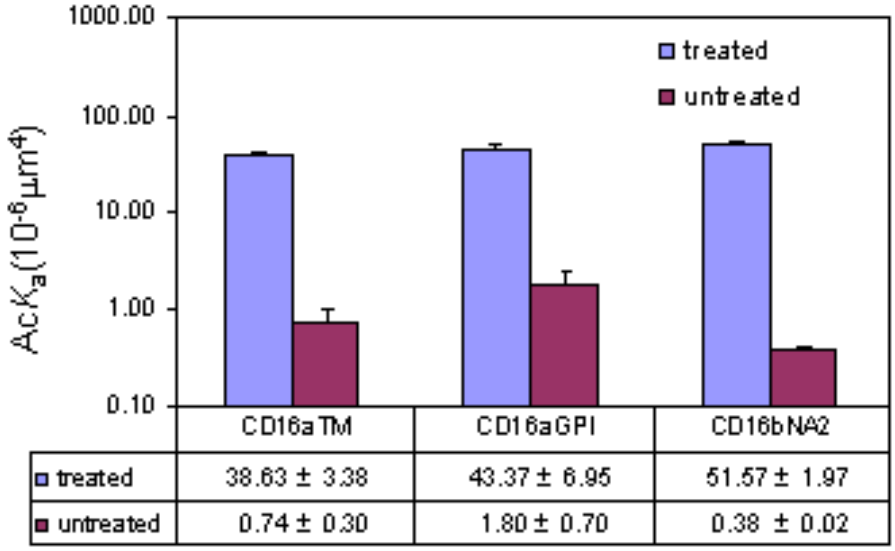

Figure 6-7a. Affinity comparison of CHO CD16 treated or untreated with tunicamycin.

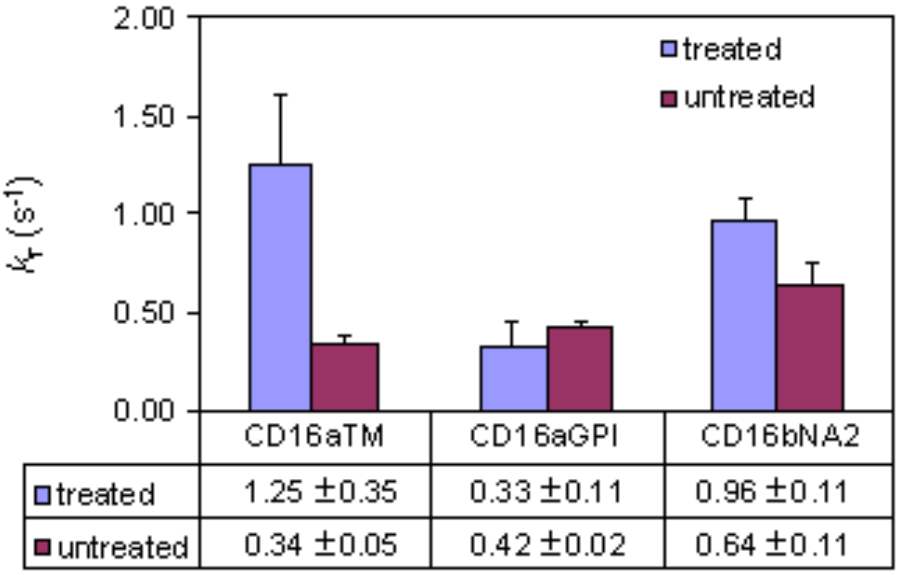

Figure 6-7b. Reverse rate constant comparison of CHO CD16 treated or untreated with tunicamycin.

Discussion

Our goal was to determine how the membrane anchor and glycosylation of CD16 affect its ligand binding. Previous studies have shown that CHO cell CD16a^{GPI} had a 3-fold higher affinity for hIgG than CHO cell CD16a^{TM} (Fig. 5-4). Since the extracellular domains of CD16a^{GPI} and CD16a^{TM} are identical, which are also identical to the CD16a portion of the sCD16a-Ig chimera, these data suggest the GPI anchor as the likely cause for the affinity difference. This work tested this hypothesis by comparing CD16 with full anchor and with various truncations in the anchor. We showed such structural variations near the membrane anchor affect the global conformation of CD16, which propagates to the ligand binding site, thereby affecting ligand binding affinity (Fig. 5-5, 6). Our data also provide another example for long range propagation of conformational changes that result in differences in ligand binding affinity. Similar examples have been demonstrated in integrins where such conformational changes are related to inside-out as well as outside-in signaling [127]. Yet another example is the bacterial FimH receptor for carbohydrates where structural variations distal to the binding site affect the mechanical properties of the interaction [128]. Apart from anchoring effect, we also show that glycosylation will dramatically inhibit ligand binding by 100 folds. Previously, Galon et al. have studied the affinity and kinetics of the interaction between human IgG1 and two soluble forms of CD16 (sCD16) corresponding to the 188 N-terminal amino acids of the extracellular region of the receptor using SPR, a glycosylated one made in eucaryotic cells (euc.sCD16) and an aglycosylated one (proc.sCD16) made in Escherichia coli.. Their results show that hIgG1 bound to immobilized euc.sCD16 with an affinity constant of 1.3×10^6 M^{-1} and the affinity constant of proc.sCD16 for human IgG1 was in the same range, 1.1×10^6 M^{-1} [124]. It is hard to believe that such a small difference in affinity between glycosylated and glycosylated CD16 would account for the huge difference observed in vivo study [22]. We also compared affinities between a glycosylated and an aglycosylated CD16aIg chimera binding to hIgG1. Aglycosylated CD16aIg chimera was obtained by culturing chimera secreting cells in medium supplemented with tunicamycin. Surprisingly, these two have similar affinity, $\sim 5.37 \times 10^{-6}$ μm^4. Further investigation reveals that in the culture supernantant of CD16aIg chimera, a significant portion of

aglycosylated CD16aIg is present as shown in western blot (Fig 5-8). So, if the aglycosylated form of CD16 indeed has about 100 folds higher affinity for hIgG1 than the glycosylated form as show for cell expressed CD16s, then the significant portion of aglycosylated CD16aIg chimera present in tunicamycin negative culture medium could dominant the binding and it could be the reason that the affinities we measured of these two CD16aIg chimera are similar. Separation of these two forms of CD16aIg chimera is underway using Lectin, which are capable of binding glycoproteins. Further investigation is needed to study the affinity on two purified populations to clarify this issue.

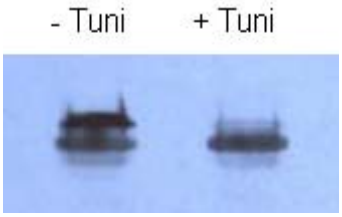

Figure 6-8. Western blot of cell culture supernant with or with tunicamycin at reducing condition. Tuni – tunicamycin.

In vivo, CD16 alleles have different affinities towards monomeric IgG and immune complex. This is an important regulator in selectively activating some cells but not all cells that express CD16. More importantly, same CD16 encoded by the same gene could undergo differential cell type-specific glycosylation as suggested by Edberg and Drescher [22, 23]. This 20 to 100 folds increase in affinity shown in current study could be an extreme case as tunicamycin inhibits all N-glycosylation. However, this broad range change in affinity could offer more subtleness in regulating cell activation. In human, monomeric IgG is about 20 mg/ml in plasma and this is not sufficient for low affinity CD16 to bind and trigger cell activation. However, cells that express higher affinity CD16 could be activated even at this IgG concentration.

CHAPTER VII

DISSECTING SIGNALING INDEPENDENT TCR-PMHC BINDING KINETICS

Introduction

Similar to the interactions of FcγRIII with IgG, TCR/pMHC interaction is also of low affinity and mediates weak adhesion. Their affinity and kinetics are important determinants of T cell antigen recognition. However, those measurements were not available until the merge of SPR. SPR measurements require that both receptor and ligand be purified and isolated from the cell membrane and one of them immobilized on the sensor chip while the other flowing in fluid phase. Recent experiments have shown that activated T cells react to pMHC better than naïve T cells. This difference could result from differential organization of TCRs on activated T cells and on naïve T cells. Micropipette adhesion frequency assay measures kinetics with receptors residing in their native environment, thereby allowing us to explore this difference.

In this aim, T cells from two clones of transgenic TCR mice were tested, 2C and F5. Naïve and activated 2C T cells were provided by Dr. Jonathan Schneck of the Johns Hopkins University. Spleen of F5 transgenic mice were provided by Dr. Suryaprakash Sambhara of CDC. Naïve T cells from F5 transgenic mice were purified using negative selection methods and maintained in complete medium supplemented with IL-2 for subsequent use. Portion of these naïve cells were activated with macrophages harvested from Tap knockout mice at a ratio 1:2. Macrophages were preloaded with agonist peptide for one hour at room temperature and excess peptide was washed away before addition of T cells. Either naïve or activated T cells were tested in the micropipette experiments for adhesion with RBCs coated with pMHC. For testing of F5 T cells, RBCs were biotinylated and incubated with streptavidin. After wash, four different pMHC monomers (agonist, partial agonist, antagonist and null) the C termini of which were tagged with a biotin (provided by the NIH Tetramer Facility at Emory University) were added separately to the RBCs. For testing of 2C T cells, a goat anti-mouse secondary antibody was first immobilized onto RBC surface using chromium chloride method. Then, pMHC

dimer incorporated with cognate or noncognate peptpide was added to RBC separately. Site densities of pMHCs as well as TCR were quantified by flow cytometry.

Using the above systems, we made the first in situ 2D affinity and kinetics measurement of TCR interacting with peptide-MHC. For the F5 TCR, eight sets of affinity and kinetics data were collected and compared, including TCR on both activated T cells and naïve T cells interacting with four different pMHC. For 2C TCR, four sets of affinity and kinetics data were collected and compared, including TCR on both activated T cells and naïve T cells interacting with either cognate or noncognate pMHC. Results show that TCR on activated T cell has a higher affinity for pMHC. Though they trigger different biological outcomes, agonist pMHC and antagonist pMHC exhibit similar affinity and kinetics for TCR under the conditions tested.

Results

1. T cells bind specifically and stably to pMHC coated RBC.

Specificity of TCR binding to pMHC was tested using RBC coated with pMHC or irrelevant protein or uncoated RBC interacting with naïve T cells. As can be seen in figure 7-1a, agonist-pMHC coated RBC showed a 26% adhesion frequency. The other two kinds of RBC showed <1% adhesion frequency, suggesting that biotinylated RBC has a clean background in the micropipette adhesion assay. In order to eliminate potential interaction between LFA-1 expressed on T cell and ICAM-3 expressed on RBC, 5mM of EDTA was added to chamber buffer to see whether the adhesion frequency can be reduced. Results showed that T cell-RBC adhesion frequencies remained unchanged, confirming that the adhesion observed is not mediated by integrin and its ligand (Fig 6-1b). Nevertheless, EDTA was used in all the experiments presented in this Chapter to eliminate any potential divalent cation dependent interactions, including integrins, selectins, and cadherins. TCR has been known to rapidly internalize once in contact with ligand. To prevent TCR internalization, 0.04% sodium azide was added to the media in all the experiments presented in this Chapter, as it did not change the binding frequency as shown in figure 7-1b. The running frequency is plotted against the adhesion test cycle to test if the adhesion functionality changes during the time of assay. Results showed that the running frequency fluctuated initially due to small sample size, but then became

stabilized as the test cycles increased, indicating that TCR was not internalized by T cell after interacting with pMHC nor pMHC been extracted off from the RBC membrane (figure 7-1c).

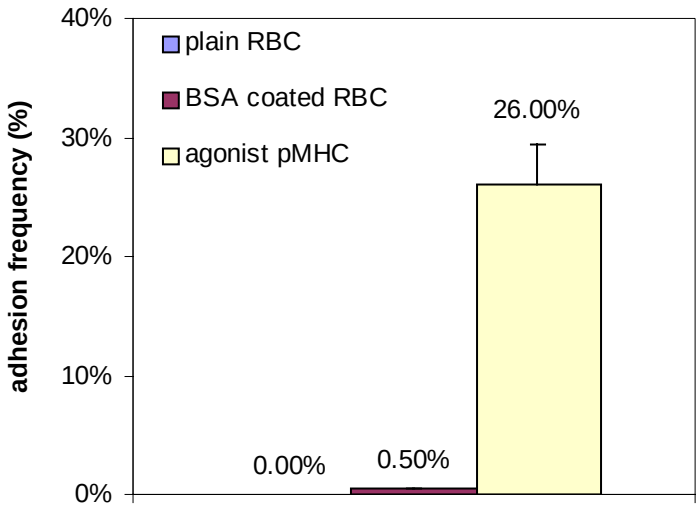

Figure 7-1a. Specificity test of naïve T cell interacting with RBC coated with different molecules.

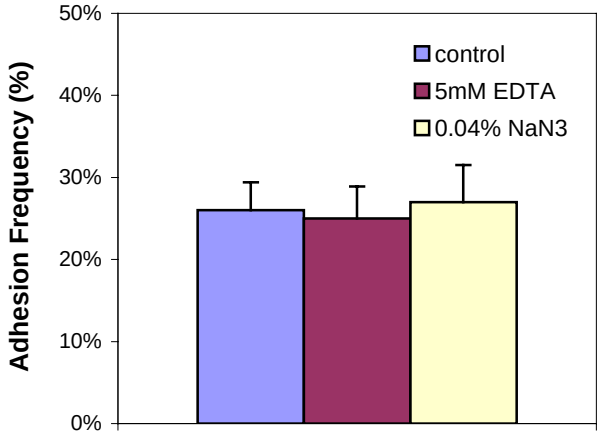

Figure 7-1b. Adhesion frequency of naïve T cells interacting with agonist-MHC coated RBCs without and with EDTA or NaN_3 in the media.

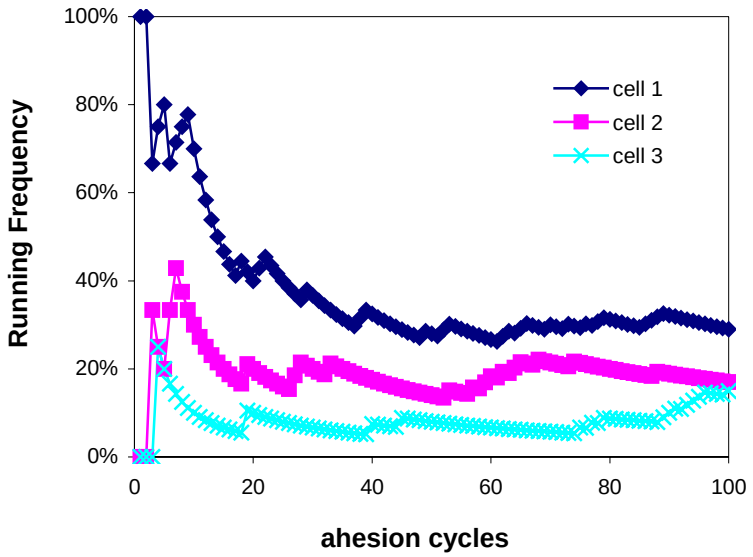

Figure 7-1c. Running frequency of naïve T cells interact with agonist pMHC coated RBCs.

2. Activated T cells show higher adhesion frequencies for pMHC than naïve T cells for the same TCR and pMHC densities.

Naive and activated T cells were tested for adhesion with different pMHC bearing RBCs. Three individual experiments were performed for each T cell and pMHC combination. At least 30 pairs of cells were tested in each experiment in order to complete a whole binding curve, which are exemplified in Figures 6-2a. Each point on the figure represents mean ± s.e.m. of adhesion frequency estimated using 5 pairs of cells. For each pair of cell, 50 adhesion cycles were tested and adhesion score, either 0 for non-adhesion or 1 for adhesion, were recorded to calculate the adhesion frequency. Equation 5-2 was used to fit the binding curved both for naïve and activated T cells. It assumes that the kinetic mechanism is second-order forward, first-order reverse, single-step bimolecular monomeric binding. Resulted affinity and kinetics for F5 T cells were plotted in figure 7-2b and c. The binding of both naïve and activated T cells to RBC coated with null pMHC was similar to background level. Therefore the affinity cannot be estimated. By comparison, activated T cells have a higher affinity than naïve T cells for all other three pMHCs. A possible explanation maybe that TCR may be better organized, for example, forming dimmer, on activated than on naïve T cells. The results also show that partial agonist pMHC has a much lower affinity than agonist pMHC, which

correlated to their biological function, as partial agonist is not as potent as agonist in stimulating T cell activation. However, antagonist pMHC, which does not elicit T cell activation by itself and antagonize the agonist effect when both peptides are presented by antigen presenting cells (APC), has a comparable affinity for TCR on both naïve and activated T cells (Figure 7-2b).

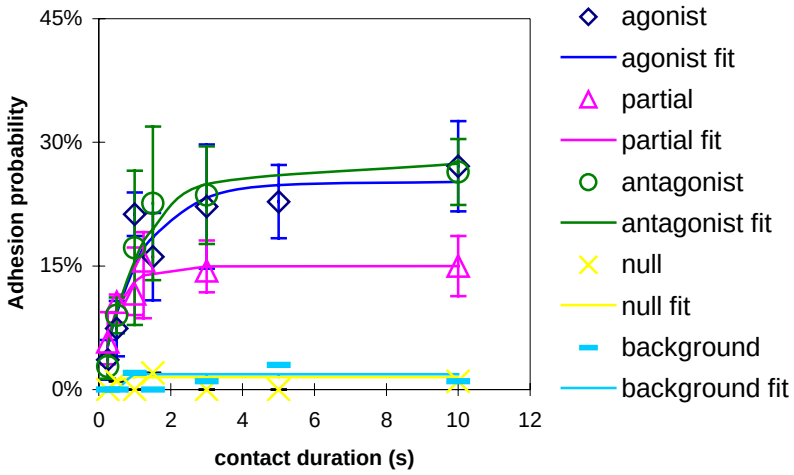

Figure 7-2a. Comparison between measured (points) and fitted (curves) adhesion frequencies between naïve F5 CTL and RBC coated without (background) or with MHC complexed with the indicated peptides.

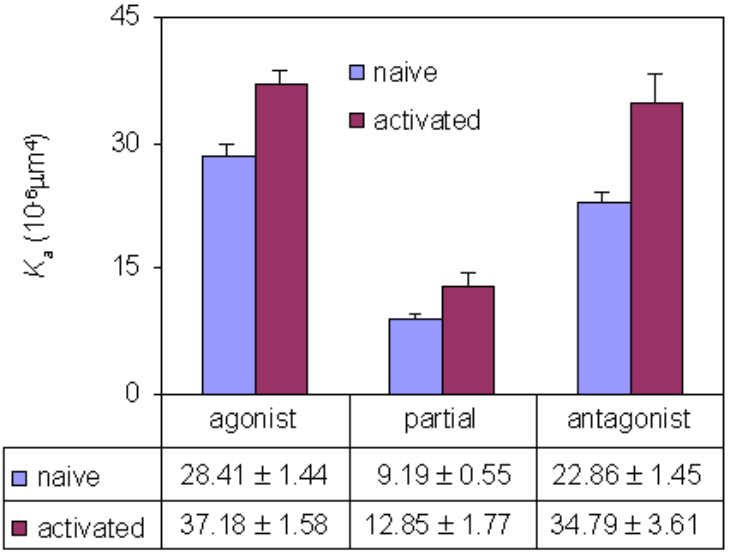

	agonist	partial	antagonist
naive	28.41 ± 1.44	9.19 ± 0.55	22.86 ± 1.45
activated	37.18 ± 1.58	12.85 ± 1.77	34.79 ± 3.61

Figure 7-2b. Affinity comparison between naïve and activated F5 T cells interacting with different pMHCs.

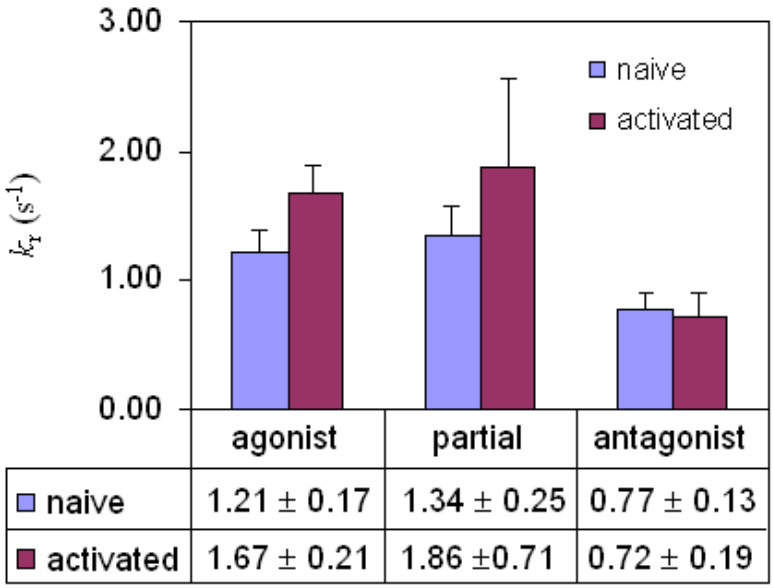

	agonist	partial	antagonist
naive	1.21 ± 0.17	1.34 ± 0.25	0.77 ± 0.13
activated	1.67 ± 0.21	1.86 ±0.71	0.72 ± 0.19

Figure 7-2c. Reverse rate constant comparison between naïve and activated T cells interacting with different pMHCs.

Another important kinetic parameter estimated from fitting the adhesion frequency data in figure 7-2a is the dissociation rate constant, k_r, which measures how fast a bond between a receptor and a ligand dissociates or the reciprocal lifetime of a bond. In the case of TCR/pMHC interaction, the dissociation rate constants measured in this study are faster than some other weak adhesion measured in micropipette, e.g. CD16 (~ 0.5 s, [25, 118]). The results indicate that both naive and activated F5 T cell has comparable dissociation rate constants for all three pMHCs. This fast dissociation may allow TCR to quickly scan hundreds and thousands of pMHC presented on APC surface to find agonist pMHC to lunch an activation process.

3. CD8 did not contribute to T cell adhesion with pMHC-coated RBC.

We have shown that integrins do not participate in the measured adhesions of T cells, which depend on pMHC. However, it is still possible that TCR-pMHC interaction triggers the recruitment of other adhesion molecules that mediate the measured adhesions. CD8 also can interact with pMHC through a different epitope (figure 3-3). To assess the CD8 contribution to adhesion, we used two CD8 blocking antibodies, 53-6.7 (BD Pharmingen, CA) and 5H10 (Caltag, CA) to blocking any CD8 mediate adhesion. The first antibody has been reported to inhibit the CD8 dependent tyrosine

phosphorylation events in CTL [129] and second antibody has been reported to block CD8. Results with F5 TCR indicated that adhesion frequencies between naïve T cells and agonist-pMHC coated RBCs remained unchanged when T cells were incubated with as high as 10ug/ml of these two antibodies, which was also present in the chamber media. In next Chapter, CD8 will be shown to participate in the strong adhesion observed in isotonic condition. Hypotonic condition seems to disrupt the association of CD8 to TCR through an unknown mechanism so that TCR-pMHC engagement could not upregulate CD8 dependent binding of pMHC. This CD8 related upregulation of adhesion is further studied in next result section.

Besides CD8 blocking experiments, binding to null-pMHC was no higher than background level even at the highest possible pMHC coating density. The other three pMHCs all gave adhesion frequencies significantly higher than the background level. If the CD8 binding to pMHC was independent of TCR, it would have shown some signal when T cells were allowed to interact with null-pMHC-coated RBCs. However, the result shows that null-pMHC cannot elicit any adhesion, indicating that CD8/pMHC interaction, if any, is too weak to be detected by micropipette. Since the micropipette assay is sensitive enough to detect adhesion mediated by as low as a single receptor-ligand bond and since no CD8/pMHC interaction can be detected at respective CD8 and pMHC densities as high as 400 and 800 μm^{-2}, the affinity of CD8/pMHC binding must be less then 6.30×10^{-8} μm^4.

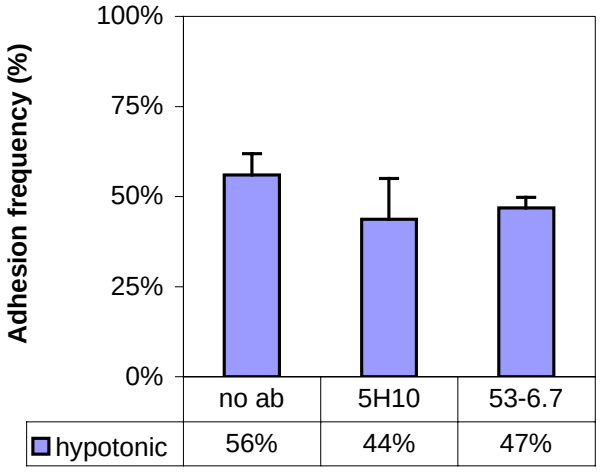

Figure 7-3. Adhesion frequency between naïve T cell and agonist-MHC coated RBC at 8 second contact in the presence or absence of two CD8 blocking antibodies.

4. TCR blocking antibody affects binding to agonist and antagonist pMHC differently

In order to test the specificity of TCR/pMHC interaction and dissect the role of CD8 in TCR mediated adhesion, Fab of a TCR $V_\beta 11$ blocking antibody (RR3-15) was tested for its ability to block TCR/pMHC interaction using naïve F5 T cells. At 25μg/ml concentration, it completely blocked the TCR interactions with partial and antagonist pMHC. However, it only reduced the adhesion frequency mediated by TCR and agonist pMHC by 35%. Increasing the antibody concentration to 50μg/ml further reduced adhesion frequency by 78% (Fig. 6-4a). Both antibody concentrations were repeated for agonist pMHC and resulted binding curves were fitted together with the binding curve that no blocking antibody was added. Equation 5-2 was modified by taking into account the effect of concentration, c, and 3D binding affinity of blocking mAb, $K_{a,3D}$.

$$P_a = 1 - \exp\{-\frac{1}{1 + cK_{a,3D}} m_r m_l A_c K_a{}^0 [1 - \exp\{-k_{off}{}^0 t)]\} \qquad (6\text{-}1)$$

Results show that at mAb concentrations of 25 and 50 μg/ml, respectively 86% and 92% of TCRs were effectively blocked (Fig 6-4b). The best-fit parameters resulted in a 2D effective affinity, $A_c K_a = 34.8 \times 10^{-6}$ μm^4, reverse rate constant $k_r = 0.82$ s^{-1}, and the 3D binding affinity of blocking mAb, $K_{a,\,3D} = 1.20 \times 10^7$ M^{-1}.

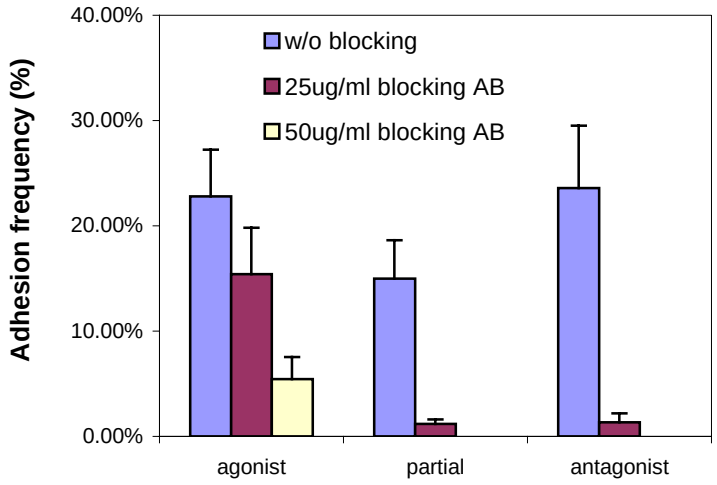

Figure 7-4a. Blockade by Fab of anti-TCR Vb11 mAb RR3-15 was more effective for binding of partial pMHC and antagonist pMHC than agonist pMHC.

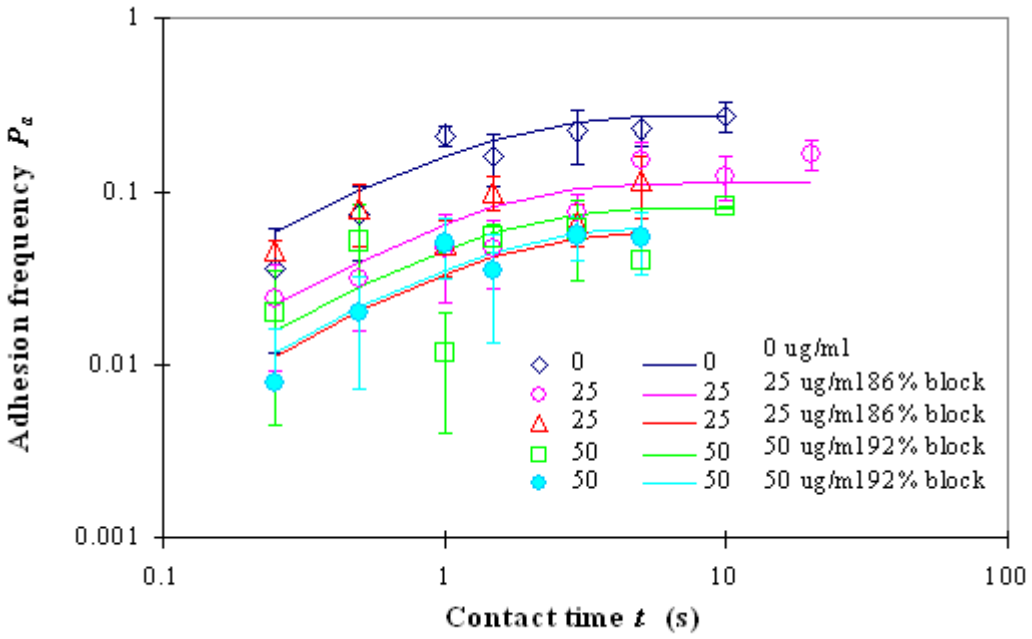

Figure 7-4b. Global fits of adhesion frequency data of naïve T cells interacting with agonist pMHC without or with different concentrations of blocking mAb.

5. Confirmation of key results using 2C TCR.

Naive and activated T cells from another clone of transgenic TCR, 2C, were also tested for adhesion with cognate and noncognate pMHC bearing RBCs. Each T cell and pMHC combination was test once by using at least 30 pairs of cells in each experiment in order to complete a whole binding curve. Resulted affinity and kinetics were plotted in figure 7-5a and b, which show that activated T cells have a higher affinity than naïve T cells for both the cognate and noncognate pMHCs, confirming our observation with the F5 TCR. The results also show that noncognate pMHC, which does not elicit T cell activation by itself had a comparable affinity for TCR as cognate pMHC for both naïve and activated T cells (Figure 7-5a).

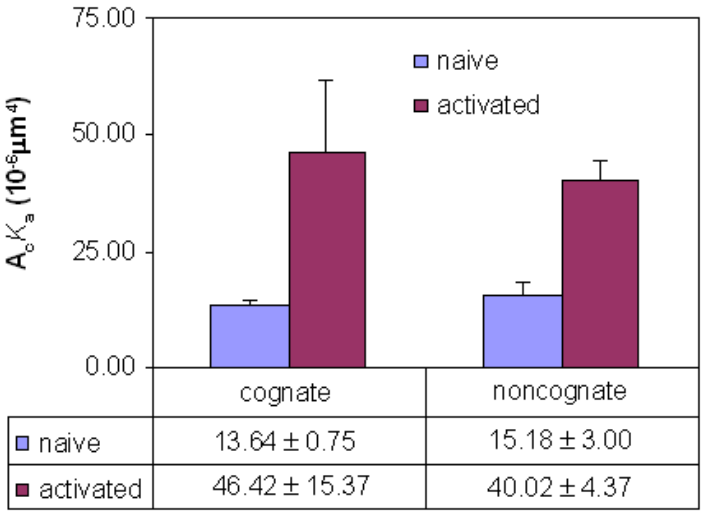

	cognate	noncognate
naive	13.64 ± 0.75	15.18 ± 3.00
activated	46.42 ± 15.37	40.02 ± 4.37

Figure 7-5a. Affinity comparison between naïve and activated 2C T cells interacting with cognate and noncognate pMHCs fitted using monomeric model.

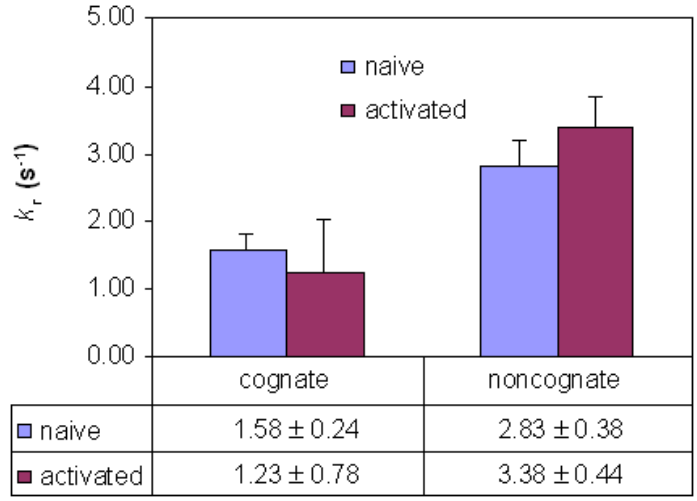

	cognate	noncognate
naive	1.58 ± 0.24	2.83 ± 0.38
activated	1.23 ± 0.78	3.38 ± 0.44

Figure 7-5b. Reverse rate constant comparison between naïve and activated 2C T cells interacting with cognate and noncognate pMHCs fitted using monomeric model.

The TCR-pMHC dissociation rate constants, k_r, are comparable for naïve and activated 2C T cells. However, noncognate pMHC had faster dissociation rate constants for TCR on both naive and activated T cells. Compared with previous F5 data, the k_r value for cognate pMHC is in the same range of agonist pMHC and k_r value for noncognate pMHC is higher than all three pMHC in the F5 system.

Discussion

We measured adhesion frequencies between TCR from naïve or activated mouse CTL and RBC coated with four pMHC known to elicit distinct activation states (Figs. 1E and 2). The measured dependence of adhesion frequency on contact duration as well as on densities of TCR and pMHC enabled reliable estimates of kinetic and affinity constants for the agonist, partial agonist, and antagonist pMHC (Figs. 2 and 3), which represent the first in situ 2D kinetic measurements of this kind. For both naïve and activated CTL, adhesion frequencies were reduced to the background level (< 0.02%) when the null peptide was used, suggesting their much lower affinities. Thus, the component of CD8-pMHC interaction that is independent of pMHC-TCR interaction and independent of the peptide could not be stronger than the interaction of TCR with null pMHC, which was undetectable event at CD8 and pMHC densities as high as 400 and 800 μm^{-2}. The agonist and antagonist pMHC had similar affinities for TCR, which were higher than that of partial agonist pMHC. The off-rate of partial agonist pMHC dissociating from TCR was faster than agonist pMHC, which was similar to antagonist pMHC.

The binding affinity of TCR from activated CTL showed trends similar to those from naïve CTL but shifted towards higher values relative to those from naïve CTL in two transgenic T cell clones, suggesting that activated T cells better organize their TCR on the cell surface for more effective binding. This is consistent with previous report that activated T cells have an enhanced ability to cross-link TCR. The off-rates of TCR from activated CTL appeared similar for agonist, partial agonist, and antagonist peptides.

Frequencies of adhesion between naïve CTL and RBC coated with agonist pMHC were comparable with those coated with antagonist pMHC and were only < 2-fold higher than those coated with partial agonist pMHC in the absence of anti-TCR blocking mAb RR3-15 (Fig. 4). However, in the presence of mAb RR3-15 the adhesion frequencies for partial agonist and antagonist pMHC were reduced to much greater extent than those for agonist pMHC, even when the mAb concentration used in the agonist pMHC experiment was twice of that used in the partial agonist and antagonist pMHC experiments (Fig. 5). This suggests that the detail interactions and structure in the contact surface between TCR and agonist pMHC might be different from those between TCR and partial agonist

and antagonist pMHC. This raises the question of whether there are other determinants of TCR discrimination in addition to kinetics and affinity.

The lack of TCR kinetic and affinity differences between agonist (or cognate) and antagonist (or noncognate) pMHC was quite surprising and puzzling, as differences have been found by other cell adhesion assays. One may question whether the assay and/or the experimental conditions are adequate. However, the micropipette adhesion frequency assay performed in hypotonic medium condition has been successfully used to measure the kinetics of ligand and antibody binding of Fcγ receptors, selectins, and integrins. The conditions include hypotonic media to swell the RBC to nearly spherical shape when captured by micropipette, addition of EDTA to inhibit divalent cation dependent adhesion pathways, and addition of sodium azide to inhibit energy dependent active processes. While these conditions suppress T cell signaling, they should not be any worse than the conditions used in the SPR experiments. In subsequent experiment (Chapter 7, below), we found that, under physiological conditions agonist pMHC, but not antagonis pMHC, induce a signaling dependent strong adhesion to T cell that includes a major contribution from CD8. To examine whether the difference in medium osmorality also impact 2D kinetic measurements of adhesion mediated by other receptor-ligand interactions, $CD16a^{GPI}$ on CHO cells, PSGL-1 on HL-60 cells, and LFA-1 on both K562 cells and naïve F5 T cells were tested with their respective ligands coated on RBC either in hypotonic medium or isotonic medium. No differences were observed in the adhesion frequency measured in hypotonic and isotonic medium using the same batch of cells (Figure 7-6). This suggested that the medium effect is specific for TCR, which is capable of converting weak adhesion into strong adhesion by signaling to recruit CD8. It is possible that TCR has a different membrane association property, for example association with lipid rafts, which is sensitive to hypotonic treatment. This is further investigated in the next Chapter.

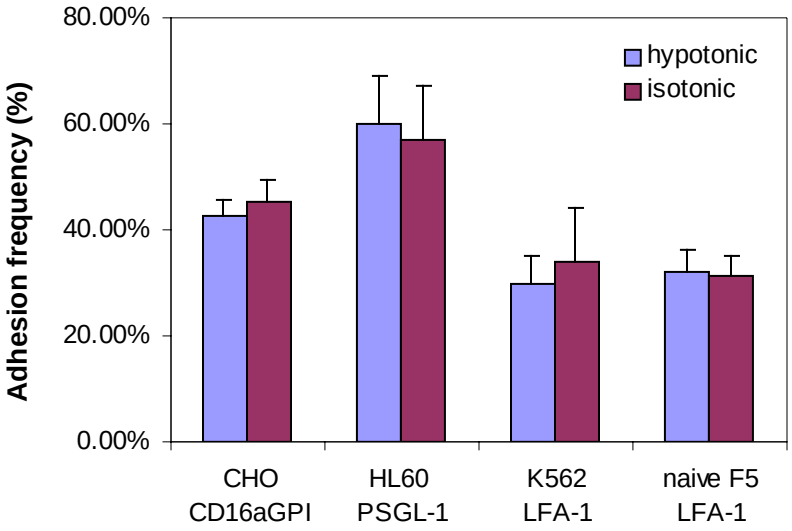

Figure 7-6. Adhesion frequency comparison for $CD16a^{GPI}$ on CHO cells, PSGL-1 on HL-60 cells, and LFA-1 on both K562 cells and naïve F5 T cells interacting with their respective ligands coated on RBC, hIgG1, P-selectin, ICAM-1.

CHAPTER VIII

INVESTIGATING TCR-TRIGGERED SIGNALING-DEPENDENT RAPID TRANSITION TO CD8-MEDIATED STRONG ADHESION

Introduction

Upon engagement of pMHC, TCR recognizes different antigenic peptides incorporated in the MHC and generates distinct signals. Together with its coreceptor and other accessory molecules, they orchestrate different responses. Over the past several years, significant advances have been made in elucidating the molecular details of signaling cascades triggered by TCR engagement. Recent discovery of immunological synapse and application of different fluorescent microscopic technologies have brought us colorful and live pictures of what are happening on the T cell/APC contact. However, due to the insufficient temporal resolution of these techniques, events that happen in the first several seconds immediately after the T cell makes contact with an APC is still not well defined. We previously noticed that T cells develop strong adhesion for agonist pMHC coated RBC, which is different from the weak adhesion we saw in the affinity and kinetics measurements (see Chapter VI). In this Chapter, we continue to explore this transition from weak adhesion to strong adhesion. We took advantage of the micropipette adhesion assay, which allows us to measure adhesions developed within very brief contacts between a T cell and a pMHC decorated RBC. Results obtained under physiological conditions show that T cells develop aggravated adhesion for agonist-pMHC on RBC but not for other pMHCs. We further show that, this change in adhesion mode happens around 0.75 second after TCR in contact with pMHC and can be completely blocked by anti-CD8 antibody. It can also be reduced by inhibiting protein tyrosine kinase (PTK) activation, disrupting membrane rafts, and dissolving actin cytoskeleton. Tetramer binding experiment showed that the same inhibitors that effectively blocked CD8 up regulated strong adhesion in micropipette experiment failed to block soluble tetramer binding in fluid phase.

Results

1. Naïve T cell developed strong adhesion to RBC coated with agonist but not antagonist pMHC.

During TCR affinity and kinetics measurements, it was noticed that in rare cases, T cells developed very strong adhesions for agonist pMHC coated RBC, which were very different from the weak adhesions commonly seen in the assay. Instead of isolated point attachments that could be easily dissociated by a low aspiration pressure of few millimeters of water height, which is characteristic of the weak adhesion, the RBC formed a large continuous area of adhesion with the T cell that could not be separated by a much higher level of aspiration pressure. While such strong adhesions were rarely seen when the experiment was performed in hypotonic media, they occurred in every single test with every pair of cells tested when the chamber solution was changed to isotonic medium. In order to assess the strong adhesion more efficiently, a population assay, rosetting, was adapted. In short, naïve T cells were mixed with pMHC coated RBC at a ratio of 1:100 and the mixture was gently spin and cell pallet was incubated for indicated period of times. Then the fraction of T cells that formed rosettes with RBC and the distribution of rosette size (i.e., the number of RBC per T cell) were enumerated under a microscope by observing a total of one hundred T cells per condition per experiment. As shown in figure 8-1a, among the four pMHCs tested agonist pMHC has the highest percentage of rosette, partial agonist pMHC has a much lower percentage of rosettes, and no rosette was formed between T cells and other two pMHCs. These results are in sharp contrast to the data obtained in the preceding chapter but consistent with the expected ability for TCR to discriminate different types of antigen peptides. In both cases of agonist and partial agonist pMHC, the rosette percentage increased with increasing incubation time. Rosette percentage also increased with increasing pMHC site density, as expected from the law of mass action. At a coating site density of 250 sites/μm^2, which is twelve times more than that used in figure 8-1a, almost all T cells form rosette even at the shortest incubation time allowed, 2 minute (figure 8-1b). To rule out any effects of pH fluctuation in the medium, metabolic dependent adhesion mechanisms, and possible integrin participation, rosetting was performed in three different media: L-15 buffered with 5mM HEPES and 1% BSA, PBS with 0.05% NaN_3, and L-15 buffered with 5mM

HEPES, 1% BSA and 5mM EDTA. As shown in Figure 8-1c, no difference was observed among all conditions tested, which confirmed that the strong adhesion mode depended on TCR-antigenic peptide-MHC recognition and was not an artifact of medium nor did it involve integrin binding.

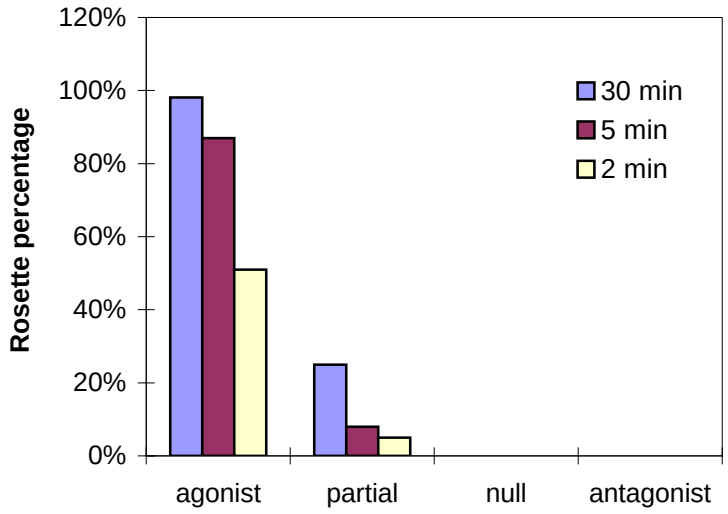

Figure 8-1a. Percentages of naïve T cells rosetted with RBC coated with the indicated pMHC for three incubation times: 30, 5, and 2 minutes. pMHC site density was 20 sites/μm^2.

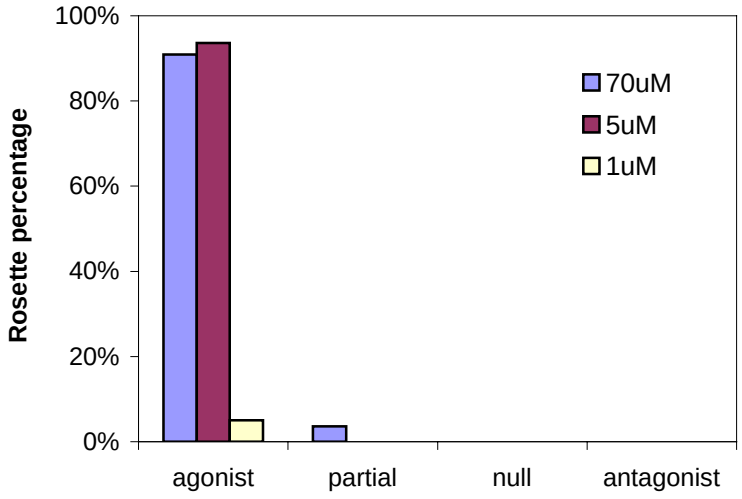

Figure 8-1b. Percentage of naïve T cells rosetted with RBC coated with indicated pMHC at three different site densities for 2 minutes incubation. Site densities were, 70μM - 250 sites/μm^2, 5μM - 20 sites/μm^2, 1μM - 3 sites/μm^2.

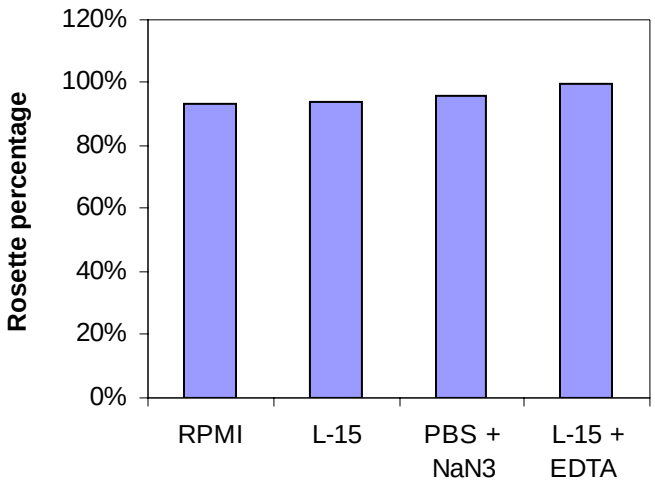

Figure 8-1c. Percentage of naïve T cells rosetted with pMHC-RBC in different media for 30 minutes.

2. The strong adhesion mode is mediated by T cell surface molecules interacting with agonist pMHC only.

We have shown that T cells will develop strong adhesion for agonist pMHC coated RBC that is independent of integrins. However, RBC expresses many proteins on its surface in addition to the pMHC coated, including those that have not been identified and those the ligands for which were not yet known. To rule out any possible contributions from other molecules, streptavidin coated polystyrene beads were used to present pMHC to repeat the above experiment. Similar to the previous observation, agonist pMHC again resulted in a high percentage of rosettes, whereas null and antagonist pMHC did not promote rosette formation (Figure 8-2a). In order to test whether adhesion would increase upon introducing another ligand for T cell surface proteins, silica beads coated with biotinylated lipid bilayer were used in lieu of streptavidin coated polystyrene beads, which, after incubation with streptavidin, allowed coating of biotin tagged pMHC and GPI anchored ICAM-1, a known ligand for LFA-1 on T cell (ICAM-1 liposome was provided by Tim Tolentino). Figure 8-2b and c show rosette percentages between T cells and silica beads before and after addition of ICAM-1. As shown on the figures, agonist pMHC had a significant percentage of rosette formed before addition of ICAM-1, where antagonist formed about the same rosette percentage of null pMHC, which was the background level. Upon addition of ICAM-1, the rosette

percentage reached 100% for agonist and significant increases were observed for null and antagonist pMHC. Together with the above results, we show that the strong adhesion mode is mediated only by pMHC binding of T cell surface proteins, which can discriminate agonist from antagonist peptide.

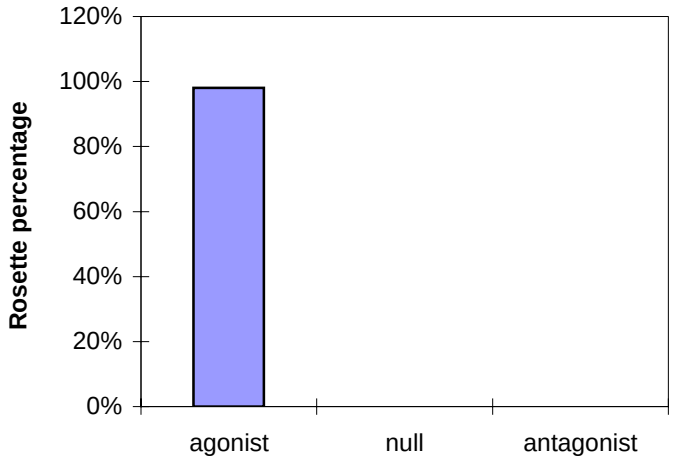

Figure 8-2a. Rosette percentage of naïve T cells incubated with pMHC coated polystyrene beads for 30 minutes.

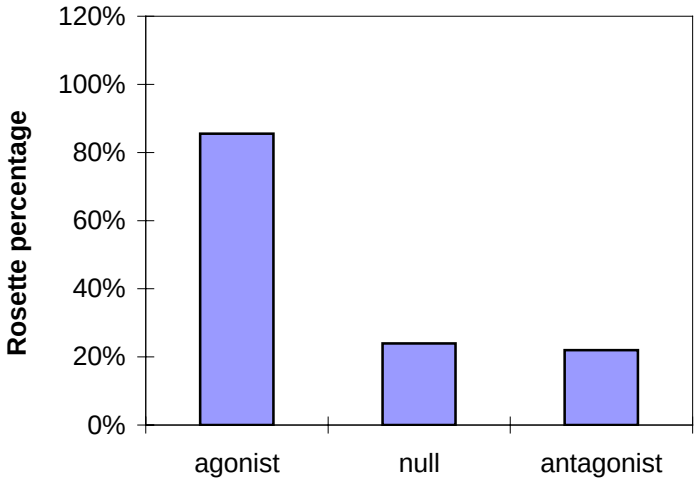

Figure 8-2b. Rosette percentage of naïve T cells incubated with pMHC coated on 1% biotin lipid coated silica beads for 30 minutes.

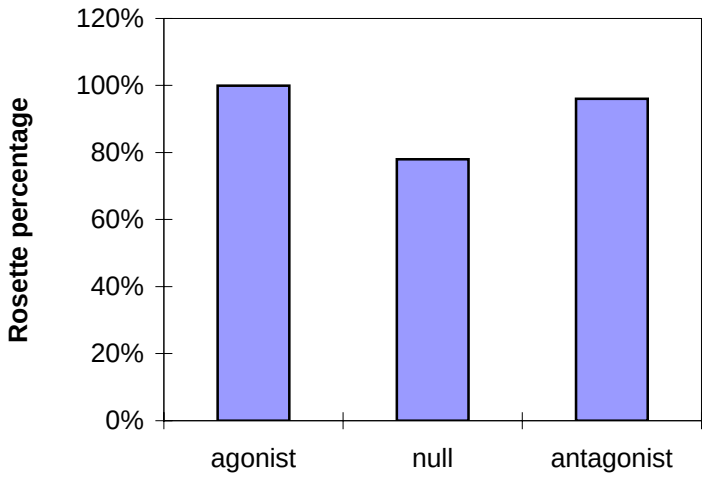

Figure 8-2c. Rosette percentage of naïve T cells incubated with pMHC and ICAM-1 coated on 1% biotin lipid coated silica beads for 30 minutes.

3. Quantify the effects of inhibitors on the strength of the strong adhesions.

In order to quantify the adhesion strength between a T cell and an agonist pMHC coated RBC, a micropipette adhesion strength experiment was designed. In this experiment, a micropipette of 3 μm inner diameter at the mouth was used to aspirate a T cell and the suction pressure was adjusted to 5 mm of H_2O height. A T cell and a RBC were placed into contact for a minute and the pipette holding the T cell was then pulled away with a speed of ~1 μm/s. If the adhesion between the two cells was strong enough, i.e., exceeding 350 pN (= $\pi/4 \times 3\ (\mu m)^2$ 5 mm H_2O), the T cell would be pulled off from its holding pipette. The percentage of pull-off is plotted in figure 8-3. Without any inhibitors, 75% of the T cells developed sufficient adhesion strength for them to be pulled off from the pipette, indicating their adhesion for agonist pMHC coated RBC exceeded 350 pN, an order of magnitude higher than the typical strength of a single bond at the range of loading rates used (20 pN/s). Previous results have shown that this adhesion up-regulation is mediated by T cell surface molecules interacting with pMHC only. To assess the contribution from CD8, another CTL surface protein that can bind MHC beside TCR, T cells were preincubated with CD8 blocking antibody, CT-CD8α. Incubation with CT-CD8α resulted a 7.5-folds reduction in the pull-off rate to a level similar to that when blocked by soluble agonist pMHC tetramer (Figure 8-3 second and third column), indicating that CD8 participates in this strong adhesion upon TCR antigenic peptide

recognition. Inhibitors to actin polymerization, latrunculin A (2 μM), and membrane rafts, Methyl-β-cyclodextrin (30 mM), were then tested. They were found to reduce the pull-off rate to levels comparable to those treated with the anti-CD8 blocking antibody and soluble agonist pMHC tetramer, suggesting that the strong adhesion mode is actin dependent and associated with membrane rafts. Three inhibitors targeted different components of signaling pathway were also tested and found to reduce the pull-off rate by almost half. Genistein, a broad PTK inhibitor, seemed to reduce the pull-off rate slightly more than PP2, an inhibitor to Src family of protein tyrosine kinases, and wortmannin, a PI3K inhibitor.

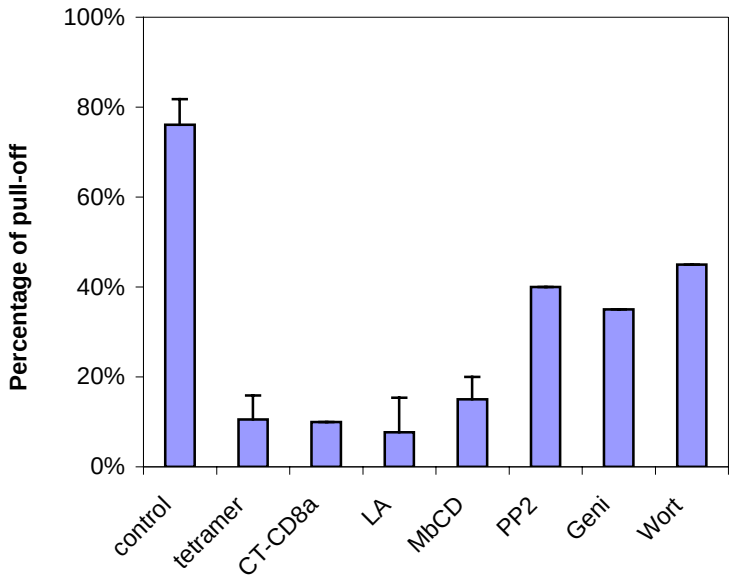

Figure 8-3. Various inhibitors affect the adhesion strength between a naïve T cell and an agonist pMHC coated polystyrene bead. Tetramer – soluble agonist pMHC tetramer, LA – latrunculin A, MbCD – Methyl-β-cyclodextrin, Geni – genisterin, Wort – wortmannin.

4. Monitoring the adhesion mode change within the first ten seconds of TCR/pMHC recognition.

We have shown in previous chapter that in hypotonic medium TCR bound to agonist and antagonist pMHC weakly with similarly low affinities and that CD8 did not contribute to binding of T cells to pMHC coated RBC. In isotonic medium, however, agonist, but not antagonist, pMHC induced strong adhesion to T cells that includes a significant contribution of CD8 and can be inhibited by disruption of actin cytoskeleton, membrane rafts, as well as tyrosine and lipid phosphorylation. Therefore, there must be a

TCR triggered, signaling required transition from CD8 independent weak adhesion to CD8 dependent strong adhesion. Here, we take advantage of micropipette adhesion assay to explore initial adhesion within the first 10 second of a T cell in contact with pMHC. Similar to previous kinetic measurement, a T cell and a pMHC coated RBC was held respectively by two glass micropipettes. They were put into contact for a predetermined amount of time as indicated on Figure 8-4a before one pipette was retracted to separate the two cells. This experiment was done in isotonic medium, in which the T cell would adhere to the RBC with a large area of continuous attachment if it was coated with as high a site density of agonist pMHC as those used in the previous kinetic measurement in hypotonic medium. Therefore the site densities were lowed by 1-2 orders of magnitude so that even at the longest contact time, 10 second, the resulted adhesion would still remain isolated point attachments mediated by single bonds between a TCR (and/or a CD8) and a pMHC. RBC coated with 12 sites/μm^2 of agonist pMHC was used to generate the binding curves in figure 8-4a and b from two different experiments. Each point in the figures represents a mean ± s.e.m. of adhesion frequency estimated from 5 pairs of cells with 50 repeated contacts each pair. The contact times were chosen to have 0.25 s increment for the first 2 seconds to provide better temporal resolution. Both experiments obtained sigmoidal binding curves. The initial adhesion was low but remained stable for the first few contact times. Between 0.5-1 second, the adhesion frequency suddenly jumped to a much higher level and then stayed at that plateau level for the longest contact time tested (5 and 8 s). While the binding curves from the two experiments exhibit the same sigmoidal shape, their stable states (i.e., the two plateaus) and perhaps the transition from the initial to the final state, show different levels and time (Figure 8-4a, b). The higher plateau levels and earlier transition of the binding curve shown in Figure 8-4b correlates with the higher site densities of TCR and CD8 (80 and 668 μm^{-2}, respectively) from the T cells used than those used to generate the binding curve shown in Figure 8-4a (74 and 530 μm^{-2}, respectively). The same batch of RBCs coated with the same density of agonist pMHC was used in these two experiments.

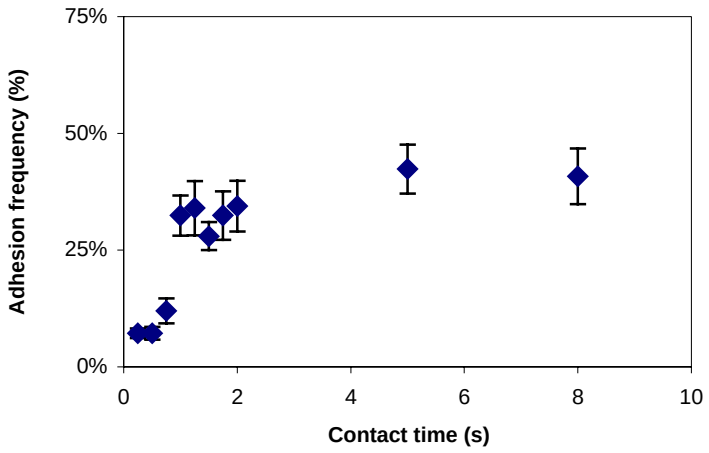

Figure 8-4a. Adhesion frequency between T cell and agonist pMHC coated RBC in isotonic media. The site densities of TCR and CD8 were 74 and 530 μm^{-2}, respectively.

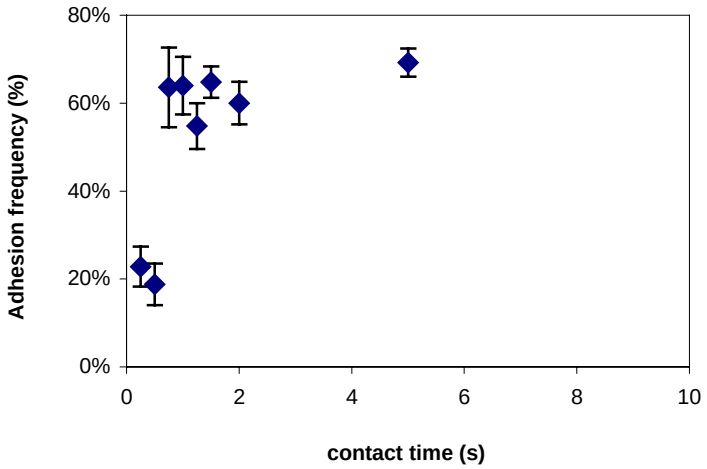

Figure 8-4b. Adhesion frequency between T cell and agonist pMHC coated RBC in isotonic media. The site densities of TCR and CD8 were 80 and 668 μm^{-2}, respectively.

5. The adhesion mode change is affected by anti-CD8 blocking antibody and other inhibitors.

We have observed a new type of binding curves that are quite different from the typical binding curves observed from the previously kinetic measurement using the same adhesion frequency assay. Instead of a simple convex curve that can be well fitted by the exponential Eq. 5-2, the nearly step-function type of sigmoidal curve cannot be described by the kinetic mechanism of second-order forward, first-order reverse, single step bimolecular reaction to form monomeric bonds. A more complex kinetic mechanism is

required, with multiple binders contributing to two different stable phases in the binding curve, a lower frequency phase and a higher frequency phase with the rapid transition around 0.75 second. We would like to further examine what factors might regulate the various features of such binding curve. From previous experiment, we know that anti-CD8 blocking antibody and several inhibitors are able to inhibit the strong adhesion between T cell and agonist pMHC coated RBC. We therefore tested their effects on the high plateau level of the binding curve using a single contact time point of 5 second. The anti-CD8 blocking antibody, CT-CD8α, completely blocked adhesion - the detected ~1% background was the same as TCR interaction with null pMHC. Genistein and latrunculin A also reduced adhesion partly. These findings suggest that there is an up-regulation of CD8/pMHC interaction upon TCR antigenic peptide recognition. Without it, the adhesion remains at low level. However, 1% of adhesion frequency after CT-CD8α blocking is significant lower than the adhesion frequency at the initial phase showed in figure 8-4a and b. This suggests that there is probably already some synergistic effect between TCR and CD8 at that initial phase. However, due to temporal resolution, we could not observe the transition. Later, as contact time increase, there is second increase in adhesion frequency. Together, these results suggesting that there are probably multiple steps from simple TCR/agonist pMHC interaction to evolve into massive adhesion, and current resolution only allows us to dissect two steps. When other two CD8 blocking antibodies that we used in previous chapter were tested again in isotonic condition, we found that 53-6.7 was still not able to block the adhesion where 5H10 could (figure 8-5b). We concluded that 53-6.7 does not interfere with CD8 binding. CT-CD8α has been shown to have a binding epitope located on CDR2 loop of the CD8α [130], therefore it interferes with CD8 binding. 5H10 probably has a similar binding epitope as CT-CD8α.

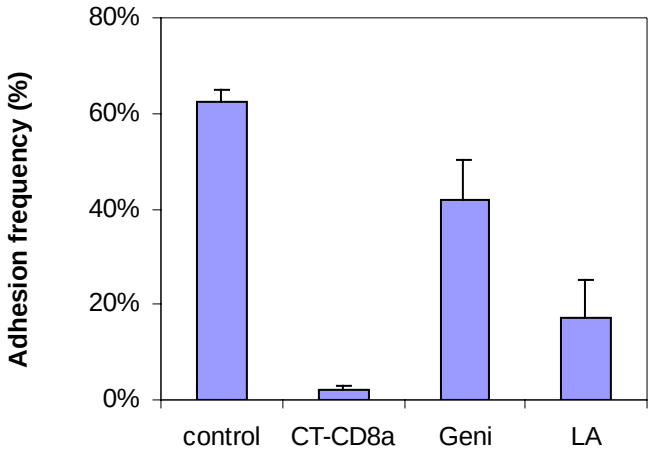

Figure 8-5a. Various inhibitors affect the adhesion frequency between naïve T cells and agonist pMHC coated RBC at contact time 5 second. Geni – genistein, LA – latrunculin A.

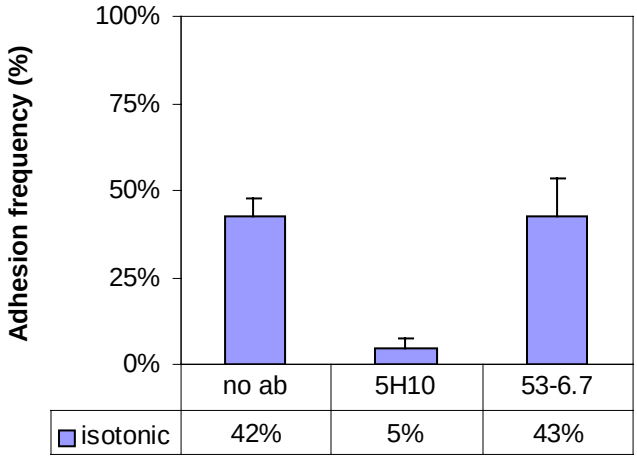

Figure 8-5b. Adhesion comparison of T cell interacting with pMHC with or with CD8 blocking antibodies at contact time 5 second.

6. Antagonist pMHC also show synergistic effect with CD8 binding.

We have shown that antagonist pMHC is not able to promote strong adhesion at a site density 30 times of the agonist pMHC which generates strong adhesion. It is therefore concluded that there is only weak adhesion between T cell and antagonist pMHC. However, when we repeated the adhesion frequency test using RBC coated with 600 sites/μm^2 antagonist pMHC by high temporal resolution of 0.25 s contact time for the first 2 seconds, we observed the same sigmoidal curve as in section 4 (figure 8-6a). Subsequent blocking experiment shows that CT-CD8α antibody completely blocked the

second phase adhesion at 5 s to the level of the first phase adhesion at 0.25 s, which is the same for background level (figure 8-6b). We therefore conclude that although antagonist pMHC is not able to promote massive adhesion, it shows synergistic effect with CD8 binding.

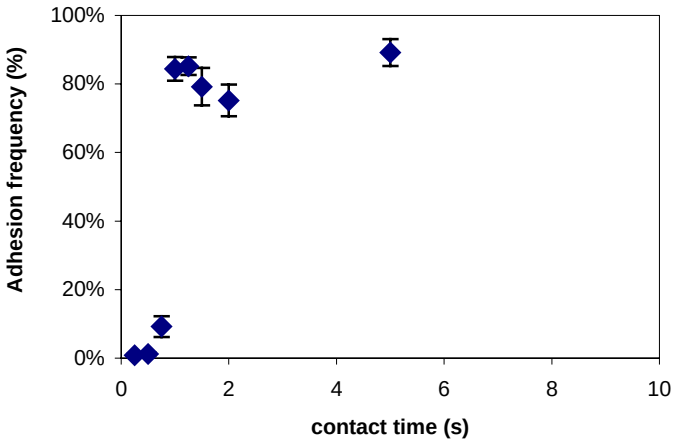

Figure 8-6a. Adhesion frequency between T cell and antagonist pMHC coated RBC at a site density 30 times of agonist coating in isotonic media.

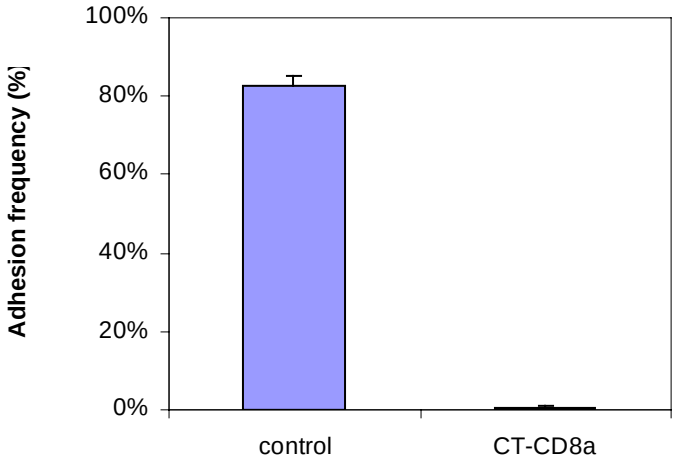

Figure 8-6b. CD8 blocking antibody, CT-CD8α, reduce adhesion frequency between naïve T cells and antagonist pMHC coated RBC to background level.

7. Tetramer binding was not affected by inhibitors.

By linking 4 pMHC monomers on one streptavidin molecule, tetramer pMHC has a higher avidity and a significant slower dissociation rate than monomers in binding to TCR. It has become a useful tool for staining T cell based on TCR antigenic specificity,

especially in identifying peripheral T cells. It has also been used to evaluate the role of coreceptors CD4 and CD8 in TCR/pMHC binding, from which controversial results were obtained.

To further test the hypothesis that engagement of TCR with agonist pMHC triggers actin cytoskeleton- and membrane raft-dependent signaling that results in upregulation of CD8 binding to pMHC, we analyze tetramer pMHC binding to T cells using flow cytometry in the absence or presence of anti-CD8 mAbs and other inhibitors over four decades of tetramer concentrations, ranging from 0.001 μg/ml to 10 μg/ml. For blocking experiments, Latrunculin A, methyl-β-cyclodextrin, Wortmannin and two CD8 blocking antibodies, 5H10 and CT-CD8α, were added to T cells prior of adding tetramer. For each inhibitor, two different incubation conditions were tested, 0°C with sodium azide to prevent receptor internalization or 25°C without sodium azide. Null pMHC tetramer was used as background control for every agonist pMHC tetramer concentration used. A set of phycoerytherin (PE) fluorescent calibration beads was used for each experiment to convert mean fluorescent intensity into number of PE molecules bound per cell (PEBC). Surprisingly, none of the inhibitors tested significantly reduced the tetramer binding and tetramer binding was not affected by possible receptor internalization as there was no difference between the binding curves acquired at 0°C with sodium azide and the ones acquired at 25°C without sodium azide (figure 8-7 a-e). Thus, the transition to strong adhesion observed when pMHC was presented by a surface does not occur when T cells bind to tetramer in solution.

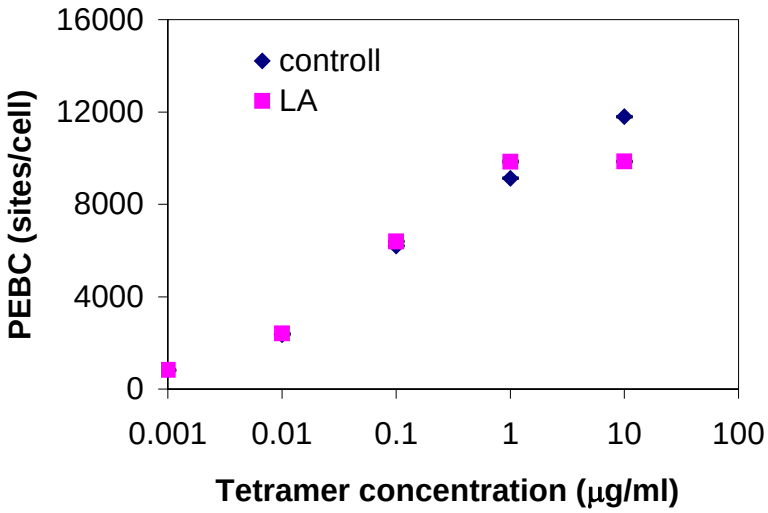

Figure 8-7a. Lack of effect of Latrunculin A on agonist pMHC tetramer binding to naïve F5 T cells at 0°C.

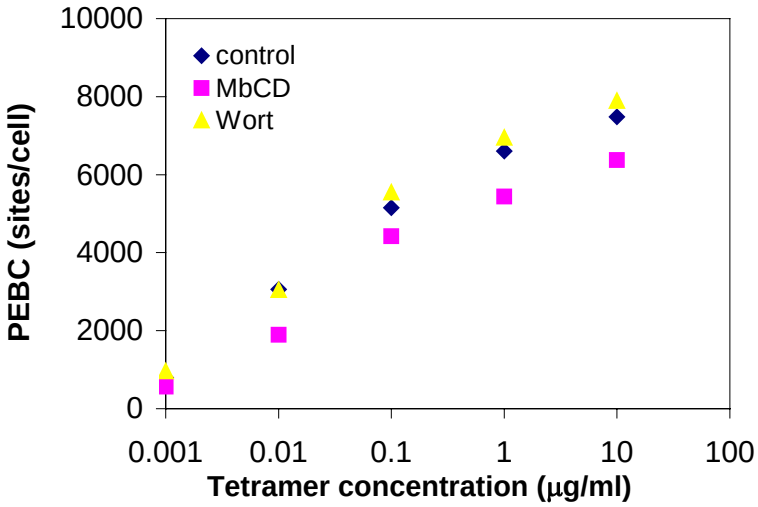

Figure 8-7b. Lack of effects of methyl-β-cyclodextrin and wortmannin on agonist pMHC tetramer binding to naïve F5 T cells at 0°C.

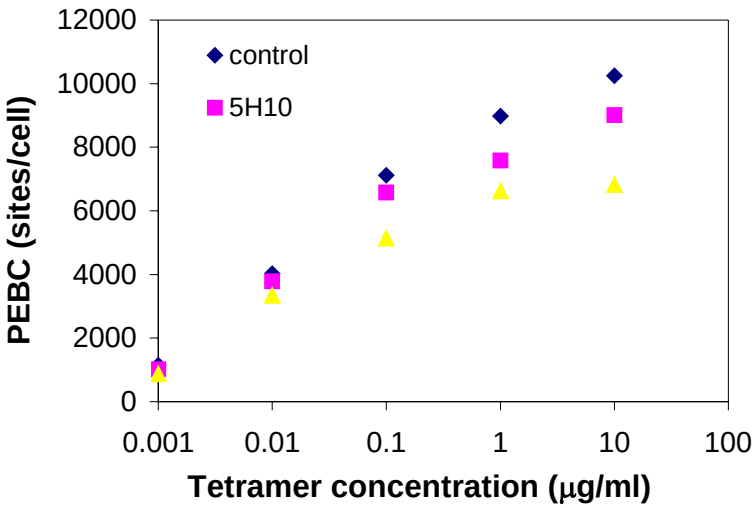

Figure 8-7c. Lack of effects of CD8 blocking antibodies, 5H10 and CT-CD8α, on agonist pMHC tetramer binding to naïve F5 T cells at 0°C.

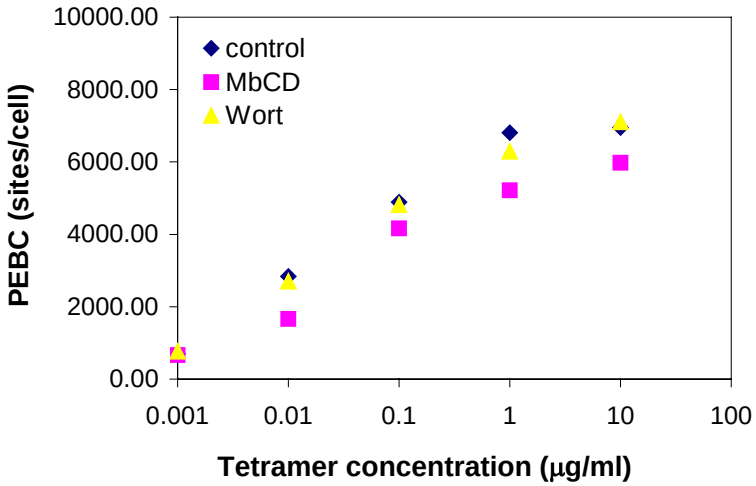

Figure 8-7d. Lack of effects of methyl-β-cyclodextrin and wortmannin on agonist pMHC tetramer binding to naïve F5 T cells at 25°C.

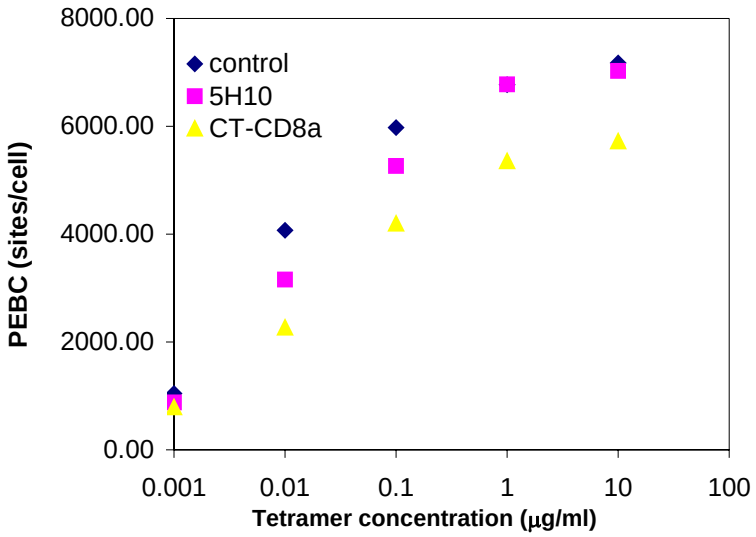

Figure 8-7e. Lack of effects of CD8 blocking antibodies, 5H10 and CT-CD8α, on agonist pMHC tetramer binding to naïve F5 T cells at 25°C.

Discussion

Upon engagement to pMHC, TCR recognize different antigenic peptides that incorporated to MHC and generate distinct signal. Together with its coreceptor and other accessory molecules, they will orchestrate different response to antigen. In contrast to the kinetic and affinity data obtained in hypotonic media (preceding chapter), which are at odds with this conceptual framework, results from both micropipette and resetting experiments performed in isotonic media are consistent with this framework. In physiological conditions, T cells develop strong adhesion for agonist-MHC on RBC but not to null or antagonist pMHCs. This adhesion is mediated by TCR-CD8/pMHC only and is independent of other molecules. The change in adhesion mode happens around 0.75 second after TCR in contact with pMHC and can be completely blocked by CD8 blocking antibody and can be reduced by inhibiting protein tyrosine kinase (PTK) activation, disrupting actin polymerization, and dissolving membrane rafts.

CD8 as a coreceptor has been shown to be important in T cell activation by coupling TCR/CD3 to raft-associated Lck [108, 129, 131], although the exact mechanism is still not clear. Early kinetic studies using SPR reveal controversial result about cooperative binding between TCR and CD8 to pMHC. It was first shown that CD8

enhances formation of stable TCR/MHC I complexes by reducing off rate [106]. Later, Wyer et al. show that TCR and CD8αα bind pMHC independently [105]. However, many experiments involving T cell clones or transgenic T cells seam to support the idea that CD8 facilitate ligand recognition [116, 117, 132]. Mescher's group has shown that upon the addition of anti-TCR mAb in solution (fluid-phase), where only bivalent cross-linking of the TCR is presumed to occur, CTL are stimulated to undergo CD8-dependent adhesion to class I MHC. CTL binding to irrelevant class I MHC could also be achieved by this TCR cross-linking method and can be blocked by CD8 antibody too [111]. Furthermore, the TCR-dependent activation of CD8 requires protein tyrosine phosphorylation, as shown by the ability of herbimycin A and genistein to inhibit triggered adhesion to class I MHC [114]. Recently the same group used wortmannin, a potent PI3 kinase inhibitor, blocks TCR-signaled activation of CD8-mediated adhesion to class I MHC protein [115]. They suggested that activation of fyn-associated PI3K is downstream of TCR-dependent activation of PTK in the signaling pathway that leads to up-regulation of CD8-dependent adhesion.

However, our results reveal a more complicated mechanism. We observed massive adhesion occur only on agonist pMHC not null or antagonist pMHC and CD8 blocking antibody can effectively block this massive adhesion (figure 8-1a, 7-2a and b). Other disruption agents can also affect this, like genistein, latrunculin A and methyl-β-cyclodextrin (figure 8-3). This massive adhesion developed at a very short time – within the shortest 2 min time resolvable by the resetting experiment and also seen in 1 min in the micropipette pull-off experiment. This is much shorter than what Mescher group observed (30 minute to 2 hour) and at a higher percentage than they reported (nearly 100% for resetting and 75% for micropipette compared to 20%) (figure 8-1a and figure 8-3). Antagonist is not capable of mediating CD8 up-regulated strong adhesion (7-1a, 7-2a and b). However, when we examined the initial contact between T cells and antagonist pMHC coated RBCs using micropipette adhesion frequency assay, we noticed that the binding curve exhibit a sigmoidal shape with threshold around 0.75 second (figure 8-6a). Consequent CD8 blocking antibody experiment showed that this increase in adhesion probably is mediated by CD8 (figure 8-6b). Therefore, antagonist is also capable of CD8 cooperative binding but not developing this weak adhesion into a strong adhesion. On the

other hand, initial contact test between T cells and agonist pMHC coated RBCs revealed that adhesion followed a stepwise increase with a threshold around 0.75 second and possible another before 0.25 second, which exceeds our temporal resolution (figure 8-4a and b). This initial weak adhesion could eventually developed into a strong adhesion if enough contact time between a T cell and an agonist coated RBC was allowed (figure 8-1a).

In studying the mechanism of TCR dependent CD8 up-regulated adhesion, Mescher's group suggested that activation of fyn-associated PI3K is downstream of TCR-dependent activation of PTK in the signaling pathway that leads to up-regulation of CD8-dependent adhesion [114, 115]. In collaboration with Dr. Sambhara from CDC, we showed that only agonist was capable of activation PI3K not antagonist, yet in short contact time, which no one were able to examine before, they both were able to mediate CD8 binding (figure 8-8). Therefore, other signal pathway must play a role in this initial CD8 cooperative binding.

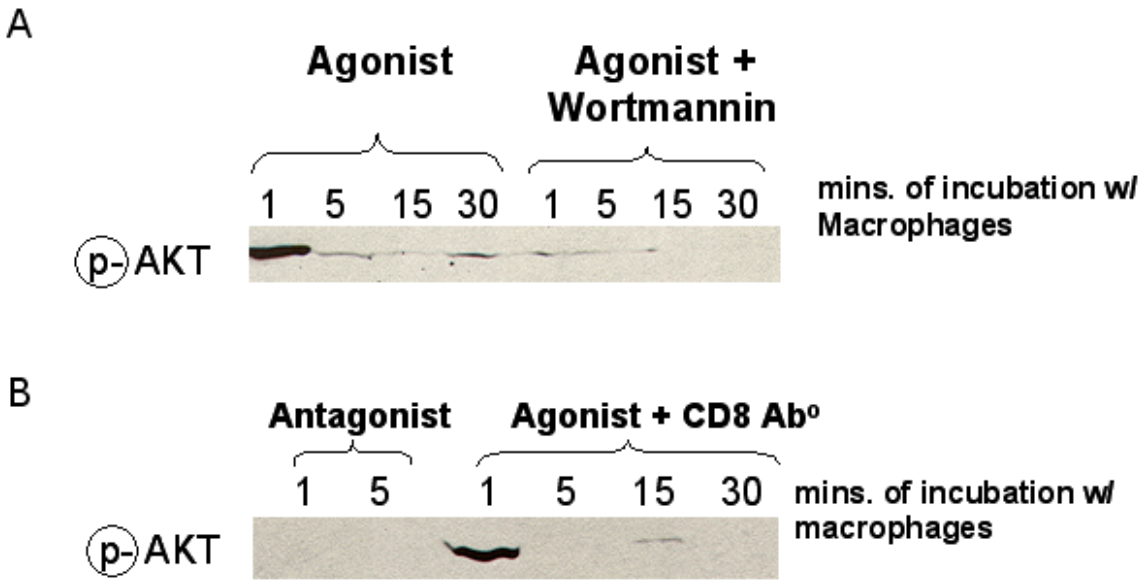

Figure 8-8. Western blot of phosphorylated Akt (common marker for PI3K activation) on SDS-page loaded with whole T cell lysates after incubated with different peptide load macrophages for indicated time. (Courtesy of Dr. Karen Hill-Williams from Dr. Sambhara's lab in CDC.)

Tetramer pMHCs have been applied to study the interaction among TCR, coreceptor and pMHC and controversial results have been shown regarding the role of coreceptors. Using class II MHC dimmer, similar to tetramer in enhancing avidity and reducing off rate between TCR and MHC, Hamad et al found that CD4 does not play any significant role in stabilizing pMHC-TCR interaction as it fails to enhance binding of dimeric pMHC to specific T cells or influence pMHC-TCR dissociation rate or TCR downregulation [133]. Using either $CD4^+$ and $CD4^-$ T cell clones or CD4 blocking antibody, two groups have separately shown that CD4 is important in IL-2 secretion or pH change due to T cell activation. However, neither group noticed any change in tetramer binding, indicating that CD4 is not important in pMHC binding yet is necessary in T cell activation possibly through a another mechanism [134, 135]. Recently, Daniels et al. showed that CD8 is not only important in T cell activation but also TCR-pMHC tetramer binding [136]. Using engineered pMHC mutant tetramers that retain faithful interactions with cognate TCR but bind CD8 with either reduced or enhanced affinities, Wooldridge et al. showed that pMHC/CD8 interaction can significantly affect the decay of soluble pMHC from the CTL surface. When using CD8 blocking reagents to study the role of CD8, different groups used different blocking antibodies with different incubation temperature and conditions, which made it very difficult to assessment the results. For example, some researchers showed that antibody 53-6.7 enhanced tetramer binding [130]. However, we showed in previous chapter that this antibody did not have any inhibitory effect in micropipette experiment performed in hypotonic media. Two other anti-CD8 antibodies, 5H10 and CT-CD8α, inhibited binding completely in rosetting and micropipette pull-off experiments performed in isotonic media. In tetramer binding experiments performed in isotonic media, we selectively used some of the inhibitors that were shown potent in inhibiting pMHC binding to TCR and tested their effects on tetramer binding systematically. Interestingly, they failed to block tetramer binding in all cases. To rule out the possibility of TCR internalization after the application of inhibitors, site densities measured by flow cytometry with or without inhibitors were compared in figure 8-9, which show no differences. These results confirmed our observation that CD8 did not facility TCR/pMHC binding when tetramer ligand was used.

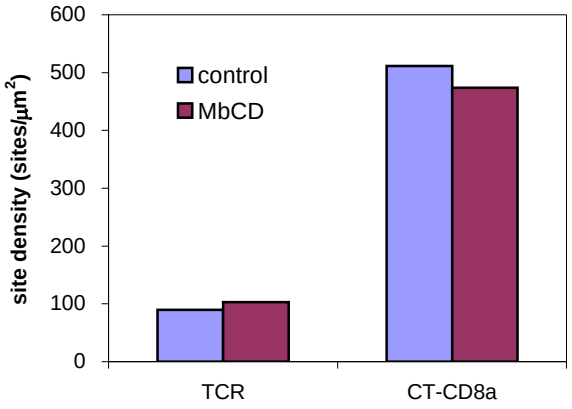

Figure 8-9a. Site density comparison of TCR and CD8 (stained with CT-CD8α) with or without adding methyl-β-cyclodextrin.

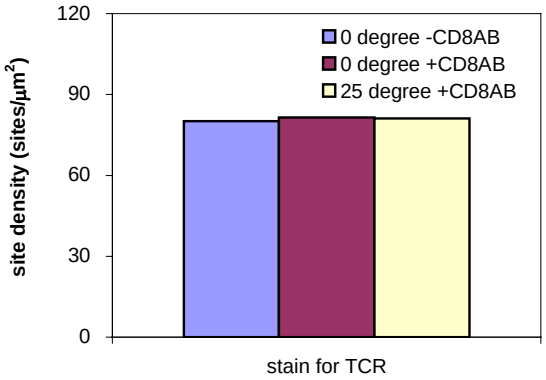

Figure 8-9b. Site density comparison of TCR with or with CD8 blocking antibody (CT-CD8α) at different temperature, 0°C with sodium azide to prevent receptor internalization or 25°C degree without sodium azide.

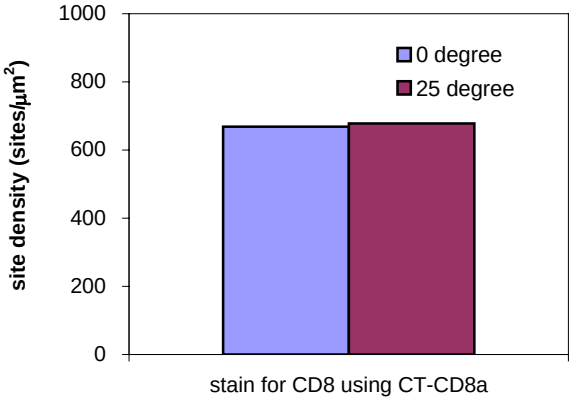

Figure 8-9c. Site density comparison of CD8 (stained with CT-CD8α) at different temperature, 0°C with sodium azide to prevent receptor internalization or 25°C degree without sodium azide.

CHAPTER IX

SUMMARY AND RECOMMENDATION FOR FUTURE STUDIES

Introduction

Early kinetics studies of CD16 and TCR interacting with respective ligands revealed some unexpected features of binding properties. The quest for investigating part of these features was outlined in the specific aims stated in chapter I, leaving new venues of investigation for future study.

Ligand binding properties of CD16

Ligand binding properties of CD16 has been intensively studies by us and many other groups using various forms of CD16 and assays. Existing data revealed some interesting findings. Our lab has previously showed that CHO CD16a^{TM} and CHO CD16a^{GPI} have different affinity and kinetics for the same ligand, IgG, despite that fact that they have exactly the same extracellular domain, and the effect is reversed for IgG from different species. It was suggested that receptor membrane anchor causes this effect by altering the receptor conformation. We have now expanded this observation from CD16a to CD16b. We have shown a correlation between affinity and molecule anchor length, and depending on the ligand species such correlation can be either positive or negative. We have also shown that glycosylation is important in regulating binding affinity, raising question for some data generated using only the extracellular domain of an aglycosylated receptor: Are they really measure the intrinsic affinity and kinetics of a receptor ligand binding?

The real-time flow cytometry methods developed in this thesis is most suitable to study binding of cell membrane receptors to soluble ligands, as in the case of CD16 and soluble hIgG1 binding. It allows us to mesure ligand binding affinity and kinetics in the native environment of the receptor. Other 3D assays may have to compromise the native environment of the molecules. Recently, this method has been applied to study TCR organization on cell membrane using dimeric pMHC-Ig. Results revealed that TCR on

activated T cells were preferably organized in dimeric form whereas TCR on naïve T cell were preferably organized in monomeric form. Real-time flow cytometry can also be modified by adding competition binding into the assay, which may be more robust in measuring some other molecular interactions.

Our results suggeste a probable long range conformational change upon anchor truncation and indicate the effects of glycans. Molecular simulation may provide a power tool to simulate the possible conformational changes and glycan binding since no crystal structures for the membrane anchors and for glycorsylated CD16 are available yet.

The ability to regulate affinity the receptor anchor and glycosylation could be important in ligand binding and signaling transduction as suggested by some of in vivo studies. The exact mechanism of how outside signal of ligand binding is converted into inside signal and how CD16 expressing cells are able to discriminate different isotypes of IgG remain unknown. Not only is membrane anchor important in regulating ligand binding as we showed here, but it is also important in association with ITAM containing signaling chains, like γ and ζ chains for CD16a^{TM}. What is more important is how GPI anchored molecule generates signals. It is believed that they do so by associating with other signaling motif containing Fcγ receptors, like CD32a^{TM}. How ligand binding leads to molecular association and vice versa and how association generates signal are not known.

2D and 3D kinetics

Most of the data reported in this thesis were generated by micropipette adhesion frequency assay. This assay measures receptor ligand binding on two apposing membranes and evaluates 2D kinetics parameters using a probabilistic model. Another method for 2D kinetic measurement is fluorescent recovery after photo bleach (FRAP). In this method, a receptor expressing cell is placed on a glass-supported lipid bilayer, which replaces one cell membrane in the micropipette assay. It measures kinetics in a diffusion coupled reaction process and also results in 2D kinetics parameters. In SPR and real-time flow cytometry measurements, one of the binding partners is placed in solution. Molecules in 2D and 3D bind with different association rate constants and affinities, move with different degrees of freedom, and change different amount of entropy upon

binding [137]. From Table 4-1, one can see that there exist many discrepancies between 2D and 3D measurements. At present, there is no established method to convert affinity and kinetic parameters acquired from 3D to 2D measurements because not until recently have 2D parameters become experimentally measurable [118]. To solve this problem, two different measurements, 2D and 3D, on exactly the same molecule, including molecular anchor and glycosylation, are necessary.

TCR antigenic pMHC recognition

T cells can discriminate antigen peptides from other peptides that differ as little as a single amino acid and launch very distinct responses toward APC. How do T cells fulfill this is still poorly understood. Several models have been proposed, which deal with various aspects of T cell discrimination, including affinity model [87], conformational change model [88, 89], dimerization or oligomerization model [90, 91], kinetic proof-reading [92] or kinetic discrimination model [93], kinetic/segregation model [94, 95] and peptide stability model, etc. So far no direct evidence has been found to support the conformational change model. For the dimerization model, several groups have shown that crosslinked pMHC can induce TCR dimerization or oligomerization [135, 138]. However, discrepant results have been reported on soluble TCR oligomerization studies: Baker et al. [96] cannot reproduce the result published by Reich et al [90]. Further more, no evidence has been obtained to support the notion of TCR dimerization or oligomerization on cell membrane upon binding of pMHC. Recently emerged peptide stability model highlights the interaction between peptide and MHC as an important factor in determining the outcome of T cell-APC contact. In this model, partial agonist can be generated through changing peptide affinity for MHC [97]. Other models suggest that discrimination may be based on the parameter(s) of the TCR-pMHC interaction. The general approach is to measure parameter(s) of the same TCR interacting with the same MHC that is complexed with several peptides known to trigger different T cell responses and examine the correlation (or the lack thereof) between the parameter values and the levels of T cell activation. The affinity model argues that TCR-pMHC binding affinity is the key parameter that regulates the TCR activation. It is difficult to explain how small variations in affinity among the different pMHCs interacting with the same TCR may

give rise to a wide range of variations in cellular responses. Kinetic proof-reading and kinetic discrimination models suggested that kinetics, especially the dissociation rate constant, is the key regulator. Through a serial signal transduction kinetic scheme, moderate differences in off-rates of TCR/pMHC interactions can be amplified to sufficient large to give rise to a threshold-type of response curve for T cell activation. The kinetic/segregation model further extends the kinetic proof-reading or kinetic discrimination model. It proposes that the segregation induced by kinetic difference between TCR and different pMHC is the determinant for TCR triggering. The mechanism of T cell discrimination and the initiating mechanism of T cell signaling may be related. Segregation by size of the TCR-pMHC bond, which excludes phosphotases such as CD45 (check out whether this statement is true), has been suggested as a mechanism for T cell signaling and also for discrimination.

All these arguments are focused on the affinity and kinetics of TCR binding to peptide-MHC. Because the experimental data for off-rates of TCR-pMHC are most available and correlate with T cell activation, the kinetic proof-reading model has been the most popular model so far. Though there are a few outliers in the correlation between half-life and potency to trigger T cell activation, it can be corrected if enthalpy is used. Considerations of other requirements for T cell discrimination also place constraints on the above models, for example, the positive and negative selections that determine the T cell repertoire, the substantial differences in the densities of self-peptides and antigen peptides, etc.

In our experiments, antigenic discrimination can be detected at the level of 2D binding between T cells and surfaces (RBC, polystyrene and silica beads) that are functionalized with pMHC only and be assayed by adhesion experiments (micropipette adhesion frequency test, pull-off test, and rosetting). Contributions from selectins, integrins, cadherins and other molecules are excluded through control experiments where either EDTA was used to inhibit cation-dependent adhesion or RBCs were replaced by polystyrene or silica beads. Thus, pMHC is sufficient and other molecules from APC are not required for discrimination at the level of adhesion.

Antigenic discrimination has no less than two components. The first requires TCR binding to pMHC but not CD8 and the second requires both TCR and CD8 binding to

pMHC, hereafter referred to as CD8 independent and CD8 dependent binding and discrimination. In the present experiment, the participation of CD8 was blocked by incubating T cells with a CD8-blocking monoclonal antibody that bind to pMHC-binding epitope of the CD8. However, the antibody used is a full antibody and it may cause a possible crosslink of two CD8s by two Fab arms. Therefore, other means of inhibiting CD8, which will not introduce possible crosslink or steric hinder are worth checking. For example, using α3 domain mutants of pMHC-I complexes to suppress CD8 binding to MHC-I as suggested by Xu et al [139]. TCR binding precedes CD8 dependent binding. However, we do not know if CD8 only binds to the same pMHC that is engaged by TCR or an unengaged pMHC. In other experimental system, people have shown that activation of TCR by a monoclonal antibody could lead to CD8 binding to an irrelevant pMHC [114]. On naïve T5 T cell surface, the number of CD8 molecules exceeds TCR by 5 times. After TCR engagement, it is possible that CD8 bind to other pMHCs that are not engaged with TCR. A micropipette experiment with RBC presenting a mixed ratio of agonist and null pMHCs will allow us to investigate this.

The micropipette binding curve with high temporal resolution revealed a sigmoidal curve instead of a typical hyperbolic curve with a low binding frequency phase before 0.75 second contact time and to a high binding frequency phase after 1 second and stayed at that level. In an effort to dissect the regulatory mechanisms, various agents were tested for their ability to block the high binding frequency phase. Signaling inhibitors, latrunculin A and methyl-β-cyclodextrin had partial effects. However, CD8 blocking antibody completely blocked the high binding frequency down to background level, which suggested CD8 binding results in a much higher adhesion frequency than the TCR-pMHC binding. Unlike the TCR/pMHC interaction, which can be initiated as soon as the TCR is in physical contact with pMHC, CD8 binding has a ~1 second delay after which it binds with very rapid on- and off-rates. The combined effect of these two levels of binding is a sigmoidal binding curve. What are the kinetic mechanisms for the component interactions and for the overall reaction? And what are the kinetic rate and binding affinity constants for those? A simple two-step model can be constructed. The first step is TCR binding, which follows second-order forward, first-order reverse kinetic mechanism. The second step is CD8 binding, which requires no less than 0.75 second

TCR engagement to activate. Once activated, however, it binds with very rapid kinetics. Several parameters of interest can be determined by adding some experiments to the data already obtained: a) the binding affinities of TCR for agonist and antagonist pMHC in the CD8 independent binding and the difference between the two values, b) the putative upregulated binding affinities of CD8 for agonist and antagonist pMHC (assuming that the TCR binding is additive to the upregulated CD8 binding) and the difference between the two values, c) test the hypothesis that TCR binding is additive to the CD8 binding by measuring the adhesion frequenies corresponding to two different sets of densities of TCR and CD8, and d) determine whether or not the recruitment of CD8 in the second step amplifies the discrimination signal. The data obtained in this thesis suggest that T cells interacted with either agonist pMHC or antagonist pMHC displayed a sigmoidal binding curve. Mechanisms for upregulation of the CD8-dependent adhesion in the second phase of the sigmoidal binding curve may include conformational change that increases CD8 affinity or change in membrane organization that increases CD8 avidity. Since CD8-binding to null pMHC is undeteactable and to agonist pMHC follows after TCR binding, the CD8 binding must be induced by the TCR binding, which may involve inside-out signaling that changes CD8 and/or the cell membrane organization. Questions such as what triggers the transition from CD8-independent binding to CD8-dependent binding, how this transition is regulated, and how the parameters measured above correlate with the potency for different peptides to trigger T cell activation, need to be answered before we fully understand this phenomenon.

The present results showed the CD8 dependent adhesion to agonist pMHC can be reduced by treatment with lutrunculin A, methyl-β-cyclodextrin, PP2, genisterin, wortmanin, but not by EDTA etc (spell out all items in the etc). It would be interesting to see if CD8 dependent adhesions to partial agonist and antagonist pMHCs are also regulated by the same treatments and what the signaling mechanisms that result in the up-regulation of CD8 binding are, and how the discriminatory signals (differences in the parameters of binding to MHC complexed with different peptides) are affected by these agents.

The CD8-dependent component of discrimination is eliminated and the CD8-independent component of discrimination is greatly suppressed by hypotonic medium.

The apparent affinity of TCR for agonist pMHC is substantially reduced. More micropipette experiments on partial agonist and antagonist pMHC in isotonic medium will allow us to compare the differences of apparent affinities under isotonic and hypotonic condition. We still do not know the mechanisms for the effects of the hypotonic medium. Compared to the experiments that conducted in isotonic medium with varies inhibitors, hypotonic medium had effect similar to latrunculin A and methyl-β-cyclodextrin on agonist. It is possible that hypotonic medium disrupt the proper TCR membrane organization so that when interacting with agonist pMHC, TCRs cannot aggregate and send out signal as usual. It will be ideal if we could test soluble TCR under micropipette to compare kinetic parameters with hypotonic data. It will allow us to determine if the kinetic parameters measured under hypotonic medium is intrinsic parameters. CD8 seems not to participate in binding in hypotonic medium, as several CD8 blocking antibodies did not decrease binding probability for agonist. More experiments on CD8 blocking need to be done on partial agonist and antagonist binding.

The long-term binding of agonist pMHC tetramer to T cells analyzed by flow cytometry is CD8 independent and nonresponsive to lutrunculin A, methyl-β-cyclodextrin, and wortmanin. These data point out the inadequacy of using SPR data to understand the mechanism of T cell discrimination. The flow cytometry experiment uses T cells so it is more physiological than the BIAcore experiment that uses purified TCR, CD8, and pMHC. Yet flow cytometry experiment fails to detect the CD8 dependent binding and the regulatory effects of lutrunculin A, methyl-β-cyclodextrin, and wortmanin. It can therefore be concluded that CD8 dependent binding and the regulatory effects of lutrunculin A, methyl-β-cyclodextrin, and wortmanin cannot be revealed by SPR. The micropipette experiments are more adequate because a) very strong signals for discrimination (orders of magnitude differences) can be detected, b) at least two levels of discrimination (CD8 independent and CD8 dependent) can be dissected, c) the discrimination signals can be manipulated by treatments with hypotonic media and several regulatory agents, and d) the molecules reside in their native environment and all ingredients in the T cell are intact. Therefore, the reason why flow cytometry experiment did not detect CD8 dependent binding could be that surface presentation of pMHC is required to trigger CD8 depend binding. Although in the flow cytometry experiment, null

pMHC tetramer showed mean fluorescence intensity a little higher than T cells without incubation with any tetramer therefore was treated as background, it is necessary to perform flow cytometry experiment on partial agonist and antagonist pMHC tetramer to see if the flow cytometry experiment detect discrimination with similar levels of signal as in micorpipette experiment that performed in isotonic medium. In micropipette experiment, inhibitors such as lutrunculin A, methyl-β-cyclodextrin, and wortmanin only regulated the CD8 dependent binding. More micropipette experiments, where those inhibitors are present together with CD8 blocking antibody, are needed to investigate if they have any effect on CD8 independent binding.

REFERENCES

1. Daeron, M., *Fc receptor biology.* Annu Rev Immunol, 1997. **15**: p. 203-34.

2. Ravetch, J.V., *Fc receptors: rubor redux.* Cell, 1994. **78**(4): p. 553-60.

3. Ravetch, J.V., *Fc receptors.* Curr Opin Immunol, 1997. **9**(1): p. 121-5.

4. Kimberly, R.P., J.E. Salmon, and J.C. Edberg, *Receptors for immunoglobulin G. Molecular diversity and implications for disease.* Arthritis Rheum, 1995. **38**(3): p. 306-14.

5. Sandor, M. and R.G. Lynch, *The biology and pathology of Fc receptors.* J Clin Immunol, 1993. **13**(4): p. 237-46.

6. Indik, Z.K., et al., *Structure/function relationships of Fc gamma receptors in phagocytosis.* Semin Immunol, 1995. **7**(1): p. 45-54.

7. Gergely, J. and G. Sarmay, *Fc gamma RII-mediated regulation of human B cells.* Scand J Immunol, 1996. **44**(1): p. 1-10.

8. Moretta, A., et al., *Activating receptors and coreceptors involved in human natural killer cell-mediated cytolysis.* Annu Rev Immunol, 2001. **19**: p. 197-223.

9. Sanchez-Mejorada, G. and C. Rosales, *Signal transduction by immunoglobulin Fc receptors.* J Leukoc Biol, 1998. **63**(5): p. 521-33.

10. Ravetch, J.V. and S. Bolland, *IgG Fc receptors.* Annu Rev Immunol, 2001. **19**: p. 275-90.

11. Anderson, P., et al., *Fc gamma receptor type III (CD16) is included in the zeta NK receptor complex expressed by human natural killer cells.* Proc Natl Acad Sci U S A, 1990. **87**(6): p. 2274-8.

12. Kimberly, R.P., et al., *The glycosyl phosphatidylinositol-linked Fc gamma RIIIPMN mediates transmembrane signaling events distinct from Fc gamma RII.* J Exp Med, 1990. **171**(4): p. 1239-55.

13. Unkeless, J.C., et al., *Function of human Fc gamma RIIA and Fc gamma RIIIB.* Semin Immunol, 1995. **7**(1): p. 37-44.

14. Galon, J., et al., *Soluble Fcgamma receptor type III (FcgammaRIII, CD16) triggers cell activation through interaction with complement receptors.* J Immunol, 1996. **157**(3): p. 1184-92.

15. Gessner, J.E., et al., *The IgG Fc receptor family.* Ann Hematol, 1998. **76**(6): p. 231-48.

16. Hibbs, M.L., M. Tolvanen, and O. Carpen, *Membrane-proximal Ig-like domain of Fc gamma RIII (CD16) contains residues critical for ligand binding.* J Immunol, 1994. **152**(9): p. 4466-74.

17. Tamm, A., et al., *The IgG binding site of human FcgammaRIIIB receptor involves CC' and FG loops of the membrane-proximal domain.* J Biol Chem, 1996. **271**(7): p. 3659-66.

18. Tamm, A. and R.E. Schmidt, *The binding epitopes of human CD16 (Fc gamma RIII) monoclonal antibodies. Implications for ligand binding.* J Immunol, 1996. **157**(4): p. 1576-81.

19. Zhang, Y., et al., *Crystal structure of the extracellular domain of a human Fc gamma RIII.* Immunity, 2000. **13**(3): p. 387-95.

20. Sondermann, P., et al., *The 3.2-A crystal structure of the human IgG1 Fc fragment-Fc gammaRIII complex.* Nature, 2000. **406**(6793): p. 267-73.

21. Radaev, S., et al., *The structure of a human type III Fcgamma receptor in complex with Fc.* J Biol Chem, 2001. **276**(19): p. 16469-77.

22. Edberg, J.C. and R.P. Kimberly, *Cell type-specific glycoforms of Fc gamma RIIIa (CD16): differential ligand binding.* J Immunol, 1997. **159**(8): p. 3849-57.

23. Drescher, B., T. Witte, and R.E. Schmidt, *Glycosylation of FcgammaRIII in N163 as mechanism of regulating receptor affinity.* Immunology, 2003. **110**(3): p. 335-40.

24. Moody, A.M., et al., *Sialic acid capping of CD8beta core 1-O-glycans controls thymocyte-major histocompatibility complex class I interaction.* J Biol Chem, 2003. **278**(9): p. 7240-6.

25. Chesla, S.E., et al., *The membrane anchor influences ligand binding two-dimensional kinetic rates and three-dimensional affinity of FcgammaRIII (CD16).* J Biol Chem, 2000. **275**(14): p. 10235-46.

26. Kukulansky, T., S. Abramovitch, and N. Hollander, *Cleavage of the glycosylphosphatidylinositol anchor affects the reactivity of thy-1 with antibodies.* J Immunol, 1999. **162**(10): p. 5993-7.

27. Bjorkman, P.J. and W.P. Burmeister, *Structures of two classes of MHC molecules elucidated: crucial differences and similarities.* Curr Opin Struct Biol, 1994. **4**(6): p. 852-6.

28. Griesser, H. and T.W. Mak, *The T-cell receptor--structure, function, and clinical application.* Hematol Pathol, 1994. **8**(1-2): p. 1-23.

29. Weissman, A.M., et al., *Molecular cloning of the zeta chain of the T cell antigen receptor.* Science, 1988. **239**(4843): p. 1018-21.

30. Gao, G.F., et al., *Crystal structure of the complex between human CD8alpha(alpha) and HLA-A2.* Nature, 1997. **387**(6633): p. 630-4.

31. Kern, P.S., et al., *Structural basis of CD8 coreceptor function revealed by crystallographic analysis of a murine CD8alphaalpha ectodomain fragment in complex with H-2K^b.* Immunity, 1998. **9**(4): p. 519-30.

32. Gao, G.F. and B.K. Jakobsen, *Molecular interactions of coreceptor CD8 and MHC class I: the molecular basis for functional coordination with the T-cell receptor.* Immunol Today, 2000. **21**(12): p. 630-6.

33. Garboczi, D.N., et al., *Structure of the complex between human T-cell receptor, viral peptide and HLA-A2.* Nature, 1996. **384**(6605): p. 134-41.

34. Garcia, K.C., et al., *An alphabeta T cell receptor structure at 2.5 A and its orientation in the TCR-MHC complex.* Science, 1996. **274**(5285): p. 209-19.

35. Garcia, K.C., et al., *Structural basis of plasticity in T cell receptor recognition of a self peptide-MHC antigen.* Science, 1998. **279**(5354): p. 1166-72.

36. Teng, M.K., et al., *Identification of a common docking topology with substantial variation among different TCR-peptide-MHC complexes.* Curr Biol, 1998. **8**(7): p. 409-12.

37. Reinherz, E.L., et al., *The crystal structure of a T cell receptor in complex with peptide and MHC class II.* Science, 1999. **286**(5446): p. 1913-21.

38. Hennecke, J., A. Carfi, and D.C. Wiley, *Structure of a covalently stabilized complex of a human alphabeta T-cell receptor, influenza HA peptide and MHC class II molecule, HLA-DR1.* Embo J, 2000. **19**(21): p. 5611-24.

39. Davis, M.M. and P.J. Bjorkman, *T-cell antigen receptor genes and T-cell recognition.* Nature, 1988. **334**(6181): p. 395-402.

40. Jorgensen, J.L., et al., *Mapping T-cell receptor-peptide contacts by variant peptide immunization of single-chain transgenics.* Nature, 1992. **355**(6357): p. 224-30.

41. Sant'Angelo, D.B., et al., *The specificity and orientation of a TCR to its peptide-MHC class II ligands.* Immunity, 1996. **4**(4): p. 367-76.

42. Chang, H.C., et al., *Topology of T cell receptor-peptide/class I MHC interaction defined by charge reversal complementation and functional analysis.* J Mol Biol, 1997. **271**(2): p. 278-93.

43. Leahy, D.J., R. Axel, and W.A. Hendrickson, *Crystal structure of a soluble form of the human T cell coreceptor CD8 at 2.6 A resolution.* Cell, 1992. **68**(6): p. 1145-62.

44. Ryu, S.E., et al., *Crystal structure of an HIV-binding recombinant fragment of human CD4.* Nature, 1990. **348**(6300): p. 419-26.

45. Wang, J.H., et al., *Atomic structure of a fragment of human CD4 containing two immunoglobulin-like domains.* Nature, 1990. **348**(6300): p. 411-8.

46. Wu, H., P.D. Kwong, and W.A. Hendrickson, *Dimeric association and segmental variability in the structure of human CD4.* Nature, 1997. **387**(6632): p. 527-30.

47. Wang, J.H., et al., *Crystal structure of the human CD4 N-terminal two-domain fragment complexed to a class II MHC molecule.* Proc Natl Acad Sci U S A, 2001. **98**(19): p. 10799-804.

48. Acuto, O. and D. Cantrell, *T cell activation and the cytoskeleton.* Annu Rev Immunol, 2000. **18**: p. 165-84.

49. Lin, J. and A. Weiss, *T cell receptor signalling.* J Cell Sci, 2001. **114**(Pt 2): p. 243-4.

50. van Leeuwen, J.E. and L.E. Samelson, *T cell antigen-receptor signal transduction.* Curr Opin Immunol, 1999. **11**(3): p. 242-8.

51. Myung, P.S., N.J. Boerthe, and G.A. Koretzky, *Adapter proteins in lymphocyte antigen-receptor signaling.* Curr Opin Immunol, 2000. **12**(3): p. 256-66.

52. Zhang, W. and L.E. Samelson, *The role of membrane-associated adaptors in T cell receptor signalling.* Semin Immunol, 2000. **12**(1): p. 35-41.

53. Henning, S.W. and D.A. Cantrell, *GTPases in antigen receptor signalling.* Curr Opin Immunol, 1998. **10**(3): p. 322-9.

54. Gupta, S., et al., *The T-cell antigen receptor utilizes Lck, Raf-1, and MEK-1 for activating mitogen-activated protein kinase. Evidence for the existence of a second protein kinase C-dependent pathway in an Lck-negative Jurkat cell mutant.* J Biol Chem, 1994. **269**(25): p. 17349-57.

55. Rincon, M., et al., *Conference highlight: do T cells care about the mitogen-activated protein kinase signalling pathways?* Immunol Cell Biol, 2000. **78**(2): p. 166-75.

56. Ward, S.G., et al., *Regulation of D-3 phosphoinositides during T cell activation via the T cell antigen receptor/CD3 complex and CD2 antigens.* Eur J Immunol, 1992. **22**(1): p. 45-9.

57. Thompson, P.A., et al., *Identification of distinct populations of PI-3 kinase activity following T-cell activation.* Oncogene, 1992. **7**(4): p. 719-25.

58. Costello, P.S., M. Gallagher, and D.A. Cantrell, *Sustained and dynamic inositol lipid metabolism inside and outside the immunological synapse.* Nat Immunol, 2002. **3**(11): p. 1082-9.

59. Harriague, J. and G. Bismuth, *Imaging antigen-induced PI3K activation in T cells.* Nat Immunol, 2002. **3**(11): p. 1090-6.

60. Liu, Y., et al., *Regulation of protein kinase Ctheta function during T cell activation by Lck-mediated tyrosine phosphorylation.* J Biol Chem, 2000. **275**(5): p. 3603-9.

61. Altman, A. and M. Villalba, *Protein kinase C-theta (PKCtheta): it's all about location, location, location.* Immunol Rev, 2003. **192**: p. 53-63.

62. DiDonato, J.A., et al., *A cytokine-responsive IkappaB kinase that activates the transcription factor NF-kappaB.* Nature, 1997. **388**(6642): p. 548-54.

63. Regnier, C.H., et al., *Identification and characterization of an IkappaB kinase.* Cell, 1997. **90**(2): p. 373-83.

64. Mercurio, F., et al., *IkappaB kinase (IKK)-associated protein 1, a common component of the heterogeneous IKK complex.* Mol Cell Biol, 1999. **19**(2): p. 1526-38.

65. Rao, A., C. Luo, and P.G. Hogan, *Transcription factors of the NFAT family: regulation and function.* Annu Rev Immunol, 1997. **15**: p. 707-47.

66. Kurosaki, T. and S. Tsukada, *BLNK: connecting Syk and Btk to calcium signals.* Immunity, 2000. **12**(1): p. 1-5.

67. Berridge, M.J., M.D. Bootman, and P. Lipp, *Calcium--a life and death signal.* Nature, 1998. **395**(6703): p. 645-8.

68. Penninger, J.M. and G.R. Crabtree, *The actin cytoskeleton and lymphocyte activation.* Cell, 1999. **96**(1): p. 9-12.

69. Vanhaesebroeck, B., et al., *Synthesis and function of 3-phosphorylated inositol lipids.* Annu Rev Biochem, 2001. **70**: p. 535-602.

70. Vanhaesebroeck, B., et al., *Phosphoinositide 3-kinases: a conserved family of signal transducers.* Trends Biochem Sci, 1997. **22**(7): p. 267-72.

71. Hawkins, P.T., T.R. Jackson, and L.R. Stephens, *Platelet-derived growth factor stimulates synthesis of PtdIns(3,4,5)P3 by activating a PtdIns(4,5)P2 3-OH kinase.* Nature, 1992. **358**(6382): p. 157-9.

72. Rameh, L.E. and L.C. Cantley, *The role of phosphoinositide 3-kinase lipid products in cell function.* J Biol Chem, 1999. **274**(13): p. 8347-50.

73. Ward, S.G., et al., *Ligation of CD28 receptor by B7 induces formation of D-3 phosphoinositides in T lymphocytes independently of T cell receptor/CD3 activation.* Eur J Immunol, 1993. **23**(10): p. 2572-7.

74. Schneider, H., et al., *CTLA-4 binding to the lipid kinase phosphatidylinositol 3-kinase in T cells.* J Exp Med, 1995. **181**(1): p. 351-5.

75. Prasad, K.V., et al., *Phosphatidylinositol (PI) 3-kinase and PI 4-kinase binding to the CD4-p56lck complex: the p56lck SH3 domain binds to PI 3-kinase but not PI 4-kinase.* Mol Cell Biol, 1993. **13**(12): p. 7708-17.

76. Schaeffer, E.M. and P.L. Schwartzberg, *Tec family kinases in lymphocyte signaling and function.* Curr Opin Immunol, 2000. **12**(3): p. 282-8.

77. Yang, W.C., et al., *Tec kinase signaling in T cells is regulated by phosphatidylinositol 3-kinase and the Tec pleckstrin homology domain.* J Immunol, 2001. **166**(1): p. 387-95.

78. Reif, K. and D.A. Cantrell, *Networking Rho family GTPases in lymphocytes.* Immunity, 1998. **8**(4): p. 395-401.

79. Arrieumerlou, C., et al., *Involvement of phosphoinositide 3-kinase and Rac in membrane ruffling induced by IL-2 in T cells.* Eur J Immunol, 1998. **28**(6): p. 1877-85.

80. Parry, R.V., et al., *Ligation of the T cell co-stimulatory receptor CD28 activates the serine-threonine protein kinase protein kinase B.* Eur J Immunol, 1997. **27**(10): p. 2495-501.

81. Lafont, V., et al., *The T cell antigen receptor activates phosphatidylinositol 3-kinase-regulated serine kinases protein kinase B and ribosomal S6 kinase 1.* FEBS Lett, 2000. **486**(1): p. 38-42.

82. Kane, L.P., et al., *Akt provides the CD28 costimulatory signal for up-regulation of IL-2 and IFN-gamma but not TH2 cytokines.* Nat Immunol, 2001. **2**(1): p. 37-44.

83. Jameson, S.C. and M.J. Bevan, *T cell receptor antagonists and partial agonists.* Immunity, 1995. **2**(1): p. 1-11.

84. Harding, C.V. and E.R. Unanue, *Quantitation of antigen-presenting cell MHC class II/peptide complexes necessary for T-cell stimulation.* Nature, 1990. **346**(6284): p. 574-6.

85. Demotz, S., H.M. Grey, and A. Sette, *The minimal number of class II MHC-antigen complexes needed for T cell activation.* Science, 1990. **249**(4972): p. 1028-30.

86. Sykulev, Y., et al., *Evidence that a single peptide-MHC complex on a target cell can elicit a cytolytic T cell response.* Immunity, 1996. **4**(6): p. 565-71.

87. Matis, L.A., et al., *Magnitude of response of histocompatibility-restricted T-cell clones is a function of the product of the concentrations of antigen and Ia molecules.* Proc Natl Acad Sci U S A, 1983. **80**(19): p. 6019-23.

88. Janeway, C.A., Jr., et al., *Cross-linking and conformational change in T-cell receptors: role in activation and in repertoire selection.* Cold Spring Harb Symp Quant Biol, 1989. **54 Pt 2**: p. 657-66.

89. Mannie, M.D., *A unified model for T cell antigen recognition and thymic selection of the T cell repertoire.* J Theor Biol, 1991. **151**(2): p. 169-92.

90. Reich, Z., et al., *Ligand-specific oligomerization of T-cell receptor molecules.* Nature, 1997. **387**(6633): p. 617-20.

91. Alam, S.M., et al., *Qualitative and quantitative differences in T cell receptor binding of agonist and antagonist ligands.* Immunity, 1999. **10**(2): p. 227-37.

92. McKeithan, T.W., *Kinetic proofreading in T-cell receptor signal transduction.* Proc Natl Acad Sci U S A, 1995. **92**(11): p. 5042-6.

93. Rabinowitz, J.D., et al., *Kinetic discrimination in T-cell activation.* Proc Natl Acad Sci U S A, 1996. **93**(4): p. 1401-5.

94. Davis, S.J. and P.A. van der Merwe, *The structure and ligand interactions of CD2: implications for T-cell function.* Immunol Today, 1996. **17**(4): p. 177-87.

95. Shaw, A.S. and M.L. Dustin, *Making the T cell receptor go the distance: a topological view of T cell activation.* Immunity, 1997. **6**(4): p. 361-9.

96. Baker, B.M. and D.C. Wiley, *alpha beta T cell receptor ligand-specific oligomerization revisited.* Immunity, 2001. **14**(6): p. 681-92.

97. Ryan, K.R., et al., *Modification of peptide interaction with MHC creates TCR partial agonists.* Cell Immunol, 2004. **227**(1): p. 70-8.

98. Davis, S.J., et al., *CD2 and the nature of protein interactions mediating cell-cell recognition.* Immunol Rev, 1998. **163**: p. 217-36.

99. van der Merwe, P.A., *A subtle role for CD2 in T cell antigen recognition.* J Exp Med, 1999. **190**(10): p. 1371-4.

100. Somoza, C. and L.L. Lanier, *T-cell costimulation via CD28-CD80/CD86 and CD40-CD40 ligand interactions.* Res Immunol, 1995. **146**(3): p. 171-6.

101. Malissen, B., *Dancing the immunological two-step.* Science, 1999. **285**(5425): p. 207-8.

102. Norment, A.M., et al., *Cell-cell adhesion mediated by CD8 and MHC class I molecules.* Nature, 1988. **336**(6194): p. 79-81.

103. Salter, R.D., et al., *Polymorphism in the alpha 3 domain of HLA-A molecules affects binding to CD8.* Nature, 1989. **338**(6213): p. 345-7.

104. Salter, R.D., et al., *A binding site for the T-cell co-receptor CD8 on the alpha 3 domain of HLA-A2.* Nature, 1990. **345**(6270): p. 41-6.

105. Wyer, J.R., et al., *T cell receptor and coreceptor CD8 alphaalpha bind peptide-MHC independently and with distinct kinetics.* Immunity, 1999. **10**(2): p. 219-25.

106. Garcia, K.C., et al., *CD8 enhances formation of stable T-cell receptor/MHC class I molecule complexes.* Nature, 1996. **384**(6609): p. 577-81.

107. Kern, P., et al., *Expression, purification, and functional analysis of murine ectodomain fragments of CD8alphaalpha and CD8alphabeta dimers.* J Biol Chem, 1999. **274**(38): p. 27237-43.

108. Arcaro, A., et al., *CD8beta endows CD8 with efficient coreceptor function by coupling T cell receptor/CD3 to raft-associated CD8/p56(lck) complexes.* J Exp Med, 2001. **194**(10): p. 1485-95.

109. Moody, A.M., et al., *The CD8alphabeta co-receptor on double-positive thymocytes binds with differing affinities to the products of distinct class I MHC loci.* Eur J Immunol, 2001. **31**(9): p. 2791-9.

110. Davis, M.M., et al., *Ligand recognition by alpha beta T cell receptors.* Annu Rev Immunol, 1998. **16**: p. 523-44.

111. O'Rourke, A.M., J. Rogers, and M.F. Mescher, *Activated CD8 binding to class I protein mediated by the T-cell receptor results in signalling.* Nature, 1990. **346**(6280): p. 187-9.

112. O'Rourke, A.M., et al., *Cytoskeletal function in CD8- and T cell receptor-mediated interaction of cytotoxic T lymphocytes with class I protein.* J Exp Med, 1991. **173**(1): p. 241-9.

113. O'Rourke, A.M. and M.F. Mescher, *Signals for activation of CD8-dependent adhesion and costimulation in CTLs.* J Immunol, 1994. **152**(9): p. 4358-67.

114. O'Rourke, A.M. and M.F. Mescher, *Cytotoxic T-lymphocyte activation involves a cascade of signalling and adhesion events.* Nature, 1992. **358**(6383): p. 253-5.

115. Jensen, P.L. and M.F. Mescher, *Role of phosphoinositide 3-kinase in TCR-signaled regulation of CD8-mediated adhesion to class I MHC protein.* Eur J Immunol, 2001. **31**(12): p. 3612-21.

116. Luescher, I.F., et al., *CD8 modulation of T-cell antigen receptor-ligand interactions on living cytotoxic T lymphocytes.* Nature, 1995. **373**(6512): p. 353-6.

117. Delon, J., et al., *CD8 expression allows T cell signaling by monomeric peptide-MHC complexes.* Immunity, 1998. **9**(4): p. 467-73.

118. Chesla, S.E., P. Selvaraj, and C. Zhu, *Measuring two-dimensional receptor-ligand binding kinetics by micropipette.* Biophys J, 1998. **75**(3): p. 1553-72.

119. Poncelet, P. and P. Carayon, *Cytofluorometric quantification of cell-surface antigens by indirect immunofluorescence using monoclonal antibodies.* J Immunol Methods, 1985. **85**(1): p. 65-74.

120. Serke, S., A. van Lessen, and D. Huhn, *Quantitative fluorescence flow cytometry: a comparison of the three techniques for direct and indirect immunofluorescence.* Cytometry, 1998. **33**(2): p. 179-87.

121. Bikoue, A., et al., *Quantitative analysis of leukocyte membrane antigen expression: normal adult values.* Cytometry, 1996. **26**(2): p. 137-47.

122. Li, P., et al., *Affinity and kinetic analysis of Fcgamma receptor IIIa (CD16a) binding to IgG ligands.* Unpublished.

123. Maenaka, K., et al., *The human low affinity Fcgamma receptors IIa, IIb, and III bind IgG with fast kinetics and distinct thermodynamic properties.* J Biol Chem, 2001. **276**(48): p. 44898-904.

124. Galon, J., et al., *Affinity of the interaction between Fc gamma receptor type III (Fc gammaRIII) and monomeric human IgG subclasses. Role of Fc gammaRIII glycosylation.* Eur J Immunol, 1997. **27**(8): p. 1928-32.

125. Williams, T.E., P. Selvaraj, and C. Zhu, *Concurrent binding to multiple ligands: kinetic rates of CD16b for membrane-bound IgG1 and IgG2.* Biophys J, 2000. **79**(4): p. 1858-66.

126. Williams, T.E., et al., *Quantifying the impact of membrane microtopology on effective two-dimensional affinity.* J Biol Chem, 2001. **276**(16): p. 13283-8.

127. Lub, M., Y. van Kooyk, and C.G. Figdor, *Ins and outs of LFA-1.* Immunol Today, 1995. **16**(10): p. 479-83.

128. Schembri, M.A., E.V. Sokurenko, and P. Klemm, *Functional flexibility of the FimH adhesin: insights from a random mutant library.* Infect Immun, 2000. **68**(5): p. 2638-46.

129. Anel, A., et al., *T cell receptor and CD8-dependent tyrosine phosphorylation events in cytotoxic T lymphocytes: activation of p56lck by CD8 binding to class I protein.* Eur J Immunol, 1996. **26**(10): p. 2310-9.

130. Devine, L., et al., *Location of the epitope for an anti-CD8alpha antibody 53.6.7 which enhances CD8alpha-MHC class I interaction indicates antibody stabilization of a higher affinity CD8 conformation.* Immunol Lett, 2004. **93**(2-3): p. 123-30.

131. Doucey, M.A., et al., *CTL activation is induced by cross-linking of TCR/MHC-peptide-CD8/p56lck adducts in rafts.* Eur J Immunol, 2001. **31**(5): p. 1561-70.

132. Sewell, A.K., et al., *Antagonism of cytotoxic T-lymphocyte activation by soluble CD8.* Nat Med, 1999. **5**(4): p. 399-404.

133. Hamad, A.R., et al., *Potent T cell activation with dimeric peptide-major histocompatibility complex class II ligand: the role of CD4 coreceptor.* J Exp Med, 1998. **188**(9): p. 1633-40.

134. Crawford, F., et al., *Detection of antigen-specific T cells with multivalent soluble class II MHC covalent peptide complexes.* Immunity, 1998. **8**(6): p. 675-82.

135. Boniface, J.J., et al., *Initiation of signal transduction through the T cell receptor requires the multivalent engagement of peptide/MHC ligands [corrected].* Immunity, 1998. **9**(4): p. 459-66.

136. Daniels, M.A. and S.C. Jameson, *Critical role for CD8 in T cell receptor binding and activation by peptide/major histocompatibility complex multimers.* J Exp Med, 2000. **191**(2): p. 335-46.

137. Dustin, M.L., et al., *Identification of self through two-dimensional chemistry and synapses.* Annu Rev Cell Dev Biol, 2001. **17**: p. 133-57.

138. Cochran, J.R., T.O. Cameron, and L.J. Stern, *The relationship of MHC-peptide binding and T cell activation probed using chemically defined MHC class II oligomers.* Immunity, 2000. **12**(3): p. 241-50.

139. Xu, X.N., et al., *A novel approach to antigen-specific deletion of CTL with minimal cellular activation using alpha3 domain mutants of MHC class I/peptide complex.* Immunity, 2001. **14**(5): p. 591-602.

VITA

Ning Jiang was born on April 28, 1977 in Xi'an, China. At age 12, she and her family moved to Shanghai where she attended middle school and higher school. She received BA in Bioengineering in 1999 from Shanghai University, China. She was honored one of top one hundred students in university. Later that year, she entered graduate school at Georgia Institute of Technology. She is married to Jun Xiao and gave birth to their daughter, Amber, on September 20th, 2005.